UNIVERSIDADE FEDERAL DO PARÁ
INSTITUTO DE TECNOLOGIA
PROGRAMA DE PÓS-GRADUAÇÃO EM ENGENHARIA ELÉTRICA

GIANNI MASAKI TANAKA PORTELA

DISPOSITIVOS DE CONTROLE NÃO RECÍPROCOS BASEADOS EM CRISTAIS FOTÔNICOS PARA UTILIZAÇÃO NA FAIXA DE FREQUÊNCIAS ÓPTICA

TD 14 / 2015

UFPA / ITEC / PPGEE
Campus Universitário do Guamá
Belém-Pará-Brasil
2015

UNIVERSIDADE FEDERAL DO PARÁ
INSTITUTO DE TECNOLOGIA
PROGRAMA DE PÓS-GRADUAÇÃO EM ENGENHARIA ELÉTRICA

GIANNI MASAKI TANAKA PORTELA

DISPOSITIVOS DE CONTROLE NÃO RECÍPROCOS BASEADOS EM CRISTAIS FOTÔNICOS PARA UTILIZAÇÃO NA FAIXA DE FREQUÊNCIAS ÓPTICA

Tese submetida à Banca Examinadora do Programa de Pós-Graduação em Engenharia Elétrica da UFPA para a obtenção do Grau de Doutor em Engenharia Elétrica na área de Telecomunicações

UFPA / ITEC / PPGEE
Campus Universitário do Guamá
Belém-Pará-Brasil
2015

UNIVERSIDADE FEDERAL DO PARÁ
INSTITUTO DE TECNOLOGIA
PROGRAMA DE PÓS-GRADUAÇÃO EM ENGENHARIA ELÉTRICA

"DISPOSITIVOS DE CONTROLE NÃO RECÍPROCOS BASEADOS EM CRISTAIS FOTÔNICOS PARA UTILIZAÇÃO NA FAIXA DE FREQUÊNCIAS ÓPTICA"

AUTOR: **GIANNI MASAKI TANAKA PORTELA**

TESE DE DOUTORADO SUBMETIDA À BANCA EXAMINADORA APROVADA PELO COLEGIADO DO PROGRAMA DE PÓS-GRADUAÇÃO EM ENGENHARIA ELÉTRICA, SENDO JULGADA ADEQUADA PARA A OBTENÇÃO DO GRAU DE DOUTOR EM ENGENHARIA ELÉTRICA NA ÁREA DE TELECOMUNICAÇÕES.

APROVADA EM: 11/09/2015

BANCA EXAMINADORA:

_____
Prof. Dr. Victor Alexandrovich Dmitriev
(Orientador – PPGEE/UFPA)

_____
Prof. Dr. Rodrigo Melo e Silva de Oliveira
(Avaliador Interno – PPGEE/UFPA)
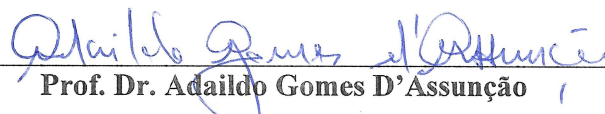
_____
Prof. Dr. Fabrício José Brito Barros
(Avaliador Externo ao Programa– CAMTUC/UFPA)

_____
Prof. Dr. Fabrício Queiroz Potiguar
(Avaliador Externo ao Programa – FACFIS/UFPA)

_____
Prof. Dr. Adaildo Gomes D'Assunção
(Avaliador Externo – UFRN)

_____
Prof. Dr. Licinius Dimitri Sá de Alcantara
(Avaliador Externo – UFRA)

VISTO:

_____
Prof. Dr. Evaldo Gonçalves Pelaes
(Coordenador do PPGEE/ITEC/UFPA)

AGRADECIMENTOS

SUMÁRIO

LISTA DE ILUSTRAÇÕES

RESUMO

O estudo da tecnologia de cristais fotônicos vem sendo realizado por muitos grupos de pesquisa, principalmente por conta das muitas aplicações práticas deles. Cristais fotônicos são estruturas constituídas por materiais com diferentes índices de refração, arranjados periodicamente em uma, duas ou três dimensões. Podem ser empregados na construção de dispositivos fotônicos passivos, para utilização em sistemas ópticos. Dispositivos baseados em cristais fotônicos têm dimensões reduzidas, quando comparados aqueles tradicionalmente empregados, favorecendo o aumento na densidade de integração de componentes de sistemas ópticos. Tendo como base a realização de estudos sobre os grupos de simetrias de várias configurações geométricas de cristais fotônicos e a execução de uma série de simulações computacionais, foram desenvolvidos oito dispositivos passivos inéditos, com novos princípios de operação. Cinco chaves, um circulador, um divisor de potência não recíproco e um dispositivo multifuncional foram projetados, com base na tecnologia de cristais fotônicos. Os dispositivos desenvolvidos podem ser utilizados, por exemplo, em computadores ópticos da próxima geração, bem como em sistemas de comunicações ópticas.

PALAVRAS-CHAVE: cristais fotônicos, chaves, circuladores, divisores de potência, dispositivos multifuncionais, sistemas ópticos integrados.

ABSTRACT

The study of the photonic crystals technology is being performed by many research groups, mostly because of their many practical applications. Photonic crystal structures are comprised by materials with different refractive indexes, periodically arranged in one, two or three dimensions. They can be employed in the construction of passive photonic devices, for use in optical systems. Photonic crystal based devices have reduced dimensions when compared to the traditionally employed ones, favoring an increase on the component integration density in optical systems. On the basis of studies related to the symmetry groups of several geometrical configurations of photonic crystals and by performing many computational simulations, eight unprecedented passive devices were developed, with new operating principles. Five switches, one circulator, one nonreciprocal power divider and one multifunctional device were designed, on the basis of photonic crystals technology. The designed devices can be used, for example, in the next generation optical computers, as well as in optical communication systems.

KEYWORDS: photonic crystals, switches, circulators, power dividers, multifunctional devices, integrated optical systems.

INTRODUÇÃO

O desenvolvimento da tecnologia baseada em estruturas conhecidas como cristais fotônicos (em inglês, *photonic crystals*) vem ocorrendo de forma bastante acelerada ao longo dos últimos anos. Vários grupos de pesquisa ao redor do mundo têm se dedicado ao estudo das propriedades de cristais fotônicos e dos modos de utilização dos mesmos nas mais diversas aplicações.

Basicamente, cristais fotônicos são estruturas concebidas pelo homem e são caracterizados por possuírem uma distribuição espacial periódica de materiais com diferentes índices de refração [1]. Esta periodicidade está associada à existência de uma faixa de frequências proibida, conhecida como *photonic band gap*. De modo geral, quanto maior o contraste dielétrico entre os diferentes materiais que compõem um cristal fotônico, maior o *photonic band gap* do mesmo.

Ondas eletromagnéticas com frequência localizada no intervalo correspondente ao *photonic band gap* de um determinado cristal fotônico não podem se propagar ao longo do mesmo. Neste caso, elas são completamente refletidas pelo cristal [2].

Uma série de analogias pode ser feita entre tais cristais e os materiais semicondutores, amplamente empregados, por exemplo, na microeletrônica [3]. Nestes últimos, há uma variação periódica do potencial eletrônico, que por sua vez está associada à existência de bandas de energia proibidas para os elétrons.

A tecnologia de cristais fotônicos pode ser empregada nos mais diversos sistemas. Neste trabalho, foi dada atenção especial às aplicações desta tecnologia em sistemas de comunicações ópticas com alta densidade de integração de componentes. Um dos principais modos de utilização da tecnologia de cristais fotônicos nestes sistemas consiste na utilização de dispositivos passivos, tais como chaves, circuladores, divisores de potência e dispositivos multifuncionais, baseados na mesma.

O princípio de funcionamento destes dispositivos normalmente está associado à existência do *photonic band gap* e à inserção de defeitos, de modo controlado, na estrutura periódica de um cristal fotônico [3]. Estes defeitos podem originar guias de ondas e cavidades ressonantes, que permitem a propagação de ondas eletromagnéticas em um cristal fotônico. Neste caso, o *photonic band gap* associado à estrutura periódica que está ao redor dos defeitos faz com que ondas eletromagnéticas possam se propagar ao longo deles.

Uma das grandes vantagens da tecnologia de cristais fotônicos, quando comparada às outras tradicionalmente empregadas em sistemas de comunicações ópticas, é a possibilidade de construção de novos dispositivos com dimensões reduzidas, favorecendo o aumento na densidade de integração de componentes nestes sistemas. Além disso, permite o projeto de sistemas completamente ópticos, que possuem desempenho muito superior quando comparados aqueles em que há necessidade de conversão de sinais ópticos em elétricos e vice-versa.

Ao longo dos meses de atividades relacionadas a este projeto de doutorado em engenharia elétrica, foram desenvolvidos oito novos dispositivos passivos baseados em cristais fotônicos bidimensionais, para utilização em sistemas de comunicações ópticas com alta densidade de integração de componentes.

As pesquisas realizadas motivaram a publicação de seis artigos científicos em periódicos da área. Estes artigos são listados a seguir, em ordem crescente de complexidade dos dispositivos desenvolvidos:

1. DMITRIEV, Victor; KAWAKATSU, Marcelo; PORTELA, Gianni. Compact optical switch based on 2D photonic crystal and magneto-optical cavity. *Optics Letters*, v. 38, p. 1016-1018, 2013;

2. DMITRIEV, Victor; PORTELA, Gianni; ZIMMER, Daimam. Possible mechanisms of switching in symmetrical two-ports based on 2D photonic crystals with magneto-optical resonators. *Optics Letters*, v. 38, p. 4040-4043, 2013;

3. DMITRIEV, Victor; PORTELA, Gianni; BATISTA, Raphael. Magneto-optical resonator switches in two-dimensional photonic crystals: geometry, symmetry, scattering matrices, and two examples. *Applied Optics*, v. 53, p. 4460-4467, 2014;

4. DMITRIEV, Victor; PORTELA, Gianni; MARTINS, Leno. Three-port circulators with low symmetry based on photonic crystals and magneto-optical resonators. *Photonic Network Communications* (versão eletrônica, 12 de Julho de 2015);

5. DMITRIEV, Victor; PORTELA, Gianni. Optical component: nonreciprocal three-way divider based on magneto-optical resonator. *Applied Optics*, v. 52, p. 6657-6662, 2013;

6. DMITRIEV, Victor; PORTELA, Gianni. Multifunctional 2D photonic crystal optical component based on magneto-optical resonator: nonreciprocal two-way divider-switch, nonreciprocal 120° bending-switch and three-way divider. *Optical Engineering*, v. 53, 115102, 2014.

Os três primeiros artigos desta lista apresentam cinco novas chaves ópticas baseadas em cristais fotônicos bidimensionais compostos por materiais magneto-ópticos. Basicamente, uma chave pode ser usada no controle da propagação de um sinal eletromagnético em um canal de comunicações, permitindo ou bloqueando a passagem do sinal. Portanto, elas possuem os seguintes estados de operação: estado ligado (em inglês, *on*), em que há transmissão do sinal eletromagnético da entrada para a saída da chave, com baixas perdas de inserção; estado desligado (em inglês, *off*), em que a saída da chave é completamente isolada da entrada, não havendo transmissão do sinal de entrada [4]. Neste caso, a transição entre os estados de operação é controlada a partir do ajuste de um campo magnético DC aplicado sobre os dispositivos. A Fig. 1 apresenta uma das cinco chaves desenvolvidas operando nos estados *on* e *off*.

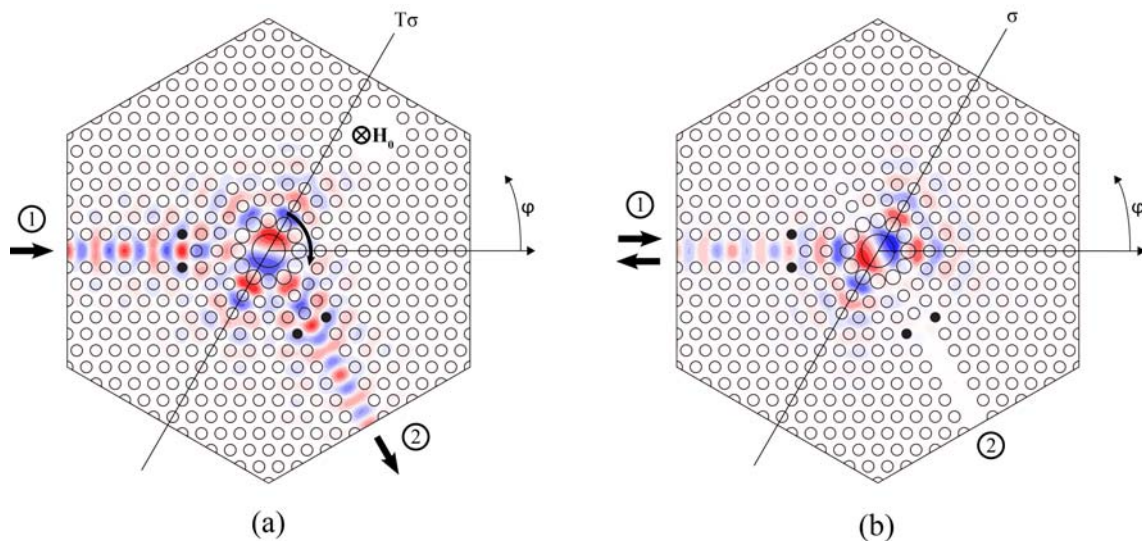Fig. 1: Chave óptica com dobramento de 60° operando nos estados (a) *on* e (b) *off*.

Por outro lado, o quarto artigo apresenta um novo circulador óptico de três portas em formato de garfo. Um circulador é um dispositivo não recíproco que promove a transmissão de sinais eletromagnéticos entre portas consecutivas, em um sentido (horário ou anti-horário) determinado a partir do sinal de um campo magnético DC

aplicado sobre a cavidade ressonante que o compõe [5]. Normalmente é empregado na proteção de fontes de sinais contra reflexões parasitas em sistemas de comunicações.

Já o quinto artigo descreve um divisor de potência não recíproco inédito, baseado em um cristal fotônico magneto-óptico bidimensional. Um divisor de potência convencional possui a função de dividir a potência de um sinal de entrada entre duas ou mais saídas, de modo igual [6]. O divisor desenvolvido é capaz de dividir a potência de um sinal de entrada entre três saídas e, além disso, possui função de isolamento integrada, ou seja, a fonte de sinais conectada à entrada é protegida contra eventuais reflexões parasitas oriundas de cargas não casadas idealmente conectadas às saídas.

Por fim, o sexto artigo trata do projeto de um dispositivo multifuncional inédito, com base em um cristal fotônico magneto-óptico bidimensional, capaz de realizar várias funcionalidades em um sistema de comunicações ópticas. Ele possui as seguintes funções incorporadas: divisão por dois e por três de potência; chaveamento; dobramento de guia de ondas; isolamento. A intensidade do campo magnético DC aplicado sobre o dispositivo e o esquema de conexão de cargas casadas define a função a ser realizada. A Fig. 2 apresenta o dispositivo em questão operando em diferentes modos.

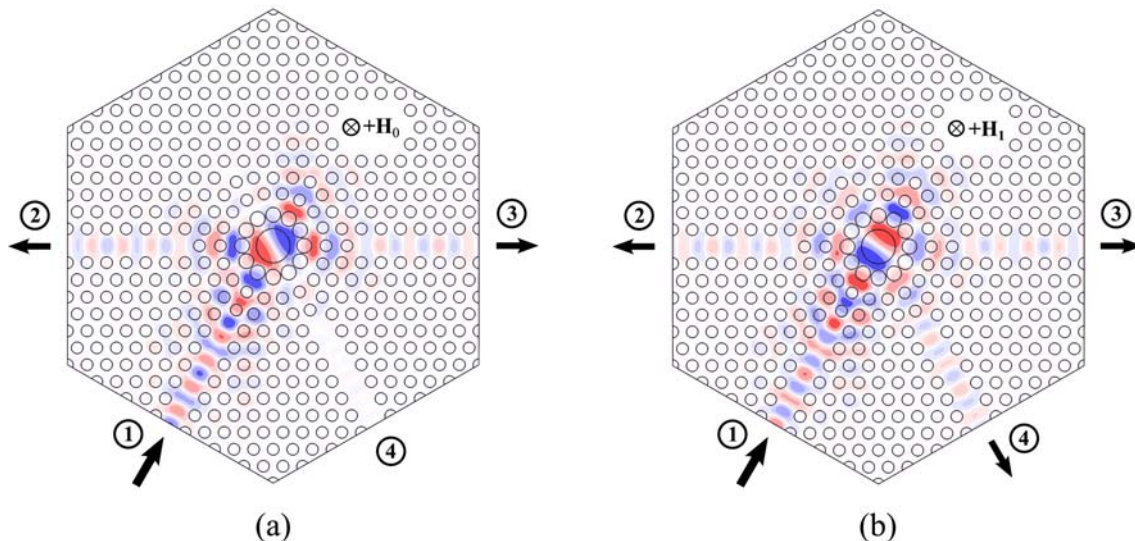Fig. 2: Dispositivo multifuncional operando como (a) divisor por 2 e (b) divisor por três.

Quanto à classificação dos periódicos em que os referidos artigos foram publicados, em termos do sistema QUALIS/CAPES, todos os artigos, com exceção do quarto, foram publicados nos periódicos *Applied Optics*, *Optics Letters* e *Optical Engineering*, que são classificados no estrato A1 deste sistema. O quarto artigo foi

publicado no periódico *Photonic Network Communications*, que por sua vez é classificado no estrato A2 do referido sistema.

Esta tese de doutorado foi baseada na agregação dos seis artigos científicos em questão. Tendo em vista tal modelo, esta tese de doutorado foi dividida em algumas seções, de modo a facilitar o entendimento das pesquisas realizadas.

Na seção "Objetivos", são apresentados o objetivo geral e os objetivos específicos que nortearam as pesquisas desenvolvidas.

Na seção "Metodologia" são descritos os procedimentos adotados durante o desenvolvimento dos dispositivos em questão, de modo geral. Maiores detalhes podem ser conferidos nos artigos científicos anexados.

As seções "Artigo 1: Compact optical switch based on 2D photonic crystal and magneto-optical cavity" a "Artigo 6: Multifunctional two-dimensional photonic crystal optical component based on magneto-optical resonator: nonreciprocal two-way divider-switch, nonreciprocal 120° bending-switch, and three-way divider" contêm cópias de todos os seis artigos científicos publicados em periódicos e são a base desta tese de doutorado, escrita segundo o modelo de agregação de artigos científicos.

Na seção "Considerações Finais" são apresentadas as conclusões decorrentes da realização desta tese de doutorado, bem como uma lista de pesquisas relacionadas ao assunto que estão em curso.

Por fim, a seção "Produção Científica e Tecnológica" lista, além dos seis artigos científicos que foram agregados e originaram esta tese, pedidos de patente de invenção e trabalhos científicos apresentados em eventos nacionais e internacionais da área, que por sua vez possuem relação direta com as pesquisas científicas cujos resultados serão apresentados nas próximas seções.

OBJETIVOS

O principal objetivo das pesquisas que deram origem a este trabalho foi o desenvolvimento de novos dispositivos passivos baseados em cristais fotônicos magneto-ópticos bidimensionais, adequados para utilização em sistemas de comunicações ópticas com alta densidade de integração de componentes.

Entre os objetivos específicos das pesquisas que originaram este trabalho, merecem destaque o (a):

- Construção de novas abordagens baseadas na Teoria de Grupos, de modo a explicar o funcionamento dos dispositivos estudados a partir das simetrias existentes nos mesmos;
- Cálculo de características de desempenho e realização de processos de otimização paramétrica através da utilização de métodos *full wave* no cálculo de campos eletromagnéticos;
- Definição de novas metodologias para o projeto de cavidades ressonantes baseadas em cristais fotônicos bidimensionais;
- Realização de estudos sobre as melhores formas de conexão entre guias de ondas e cavidades ressonantes baseados em cristais fotônicos bidimensionais.

METODOLOGIA

O passo inicial para o desenvolvimento dos dispositivos pretendidos foi a determinação da cavidade ressonante empregada no projeto dos mesmos. Dentre as várias configurações possíveis de cavidades ressonantes, foi adotada aquela apresentada em [7]. Segundo a referência em questão, esta cavidade apresenta um grande desdobramento de frequências para modos dipolo que giram em sentidos opostos, quando comparada a outras cavidades ressonantes baseadas em cristais fotônicos magneto-ópticos. De modo geral, quanto maior este desdobramento, maior a largura de banda de operação e, consequentemente, melhor o desempenho de cada um dos dispositivos que serão apresentados ao longo deste trabalho.

Ela consiste de vários furos inseridos em um material com propriedades magneto-ópticas conhecido como BIG (em inglês, *Bismuth Iron Garnet*). Os furos desta cavidade são dispostos sob a forma de vários anéis concêntricos, conforme pode ser verificado na Fig. 3.
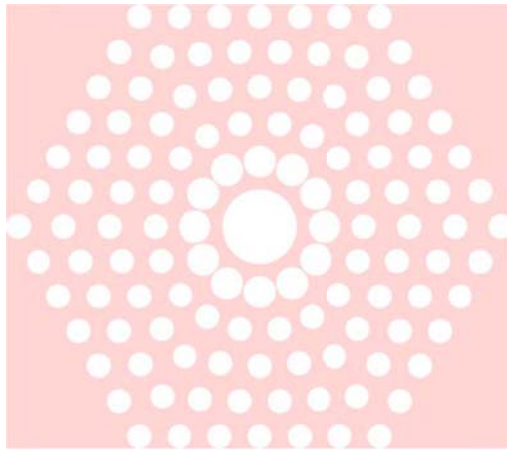
Fig. 3: Cavidade ressonante apresentada em [7].

O material empregado nesta cavidade possui permissividade elétrica e permeabilidade magnética iguais a:

$$[\varepsilon] = \varepsilon_0 \begin{pmatrix} 6,25 & -ig & 0 \\ ig & 6,25 & 0 \\ 0 & 0 & 6,25 \end{pmatrix}; \ \mu = \mu_0$$

onde:

- $[\varepsilon]$ é o tensor permissividade elétrica do material (em Farad por metro);

- ε_0 é a permissividade elétrica do espaço livre (em Farad por metro);

- μ é a permeabilidade magnética do material (em Henry por metro);

- μ_0 é a permeabilidade magnética do espaço livre (em Henry por metro);

- i é a unidade imaginária;

- g é um parâmetro proporcional à intensidade do campo magnético DC aplicado sobre o material.

Nos dispositivos que serão apresentados ao longo deste trabalho, os valores mínimo e máximo do parâmetro g são iguais a 0 (material não magnetizado) e 0,3, respectivamente.

Em [7], esta cavidade foi utilizada no projeto de um circulador de três portas em formato de Y, baseado na conexão de três guias de ondas a esta cavidade, de modo que o arranjo final possui simetria rotacional de 120° (ver Fig. 4). A largura de banda de operação deste circulador é igual a 81 GHz, para operação no comprimento de onda central de 1,3 μm.

Fig. 4: Circulador de três portas apresentado em [7].
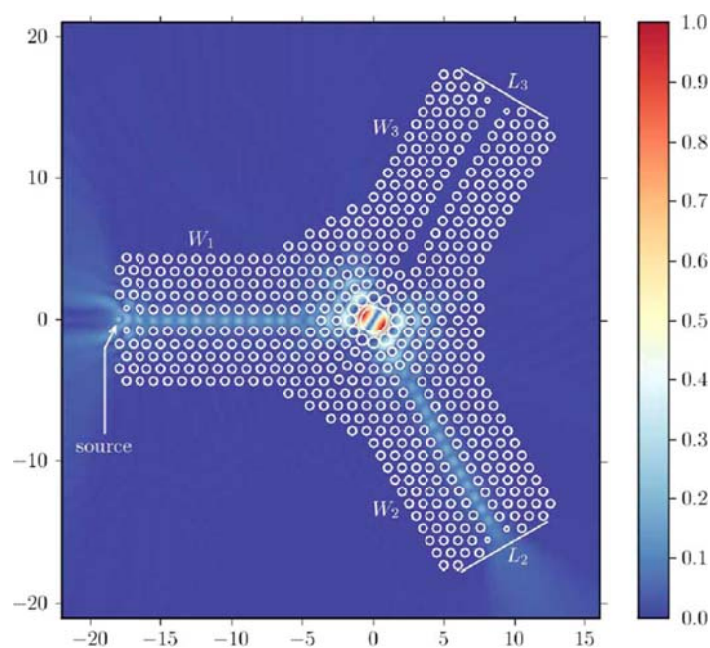
Após a escolha da cavidade ressonante a ser empregada, foram estudados, para cada dispositivo desenvolvido, aspectos relacionados à simetria. Conforme é possível observar nos artigos agregados, os guias de ondas que compõem cada dispositivo podem ser conectados de diferentes formas à cavidade ressonante escolhida. Deste modo, cada arranjo possui grupos de simetria distintos.

Estas questões foram estudadas a partir de uma série de análises teóricas baseadas na Teoria de Grupos [8]. A partir destas análises, foi possível a obtenção de informações importantes sobre os dispositivos estudados, tais como a estrutura da matriz de espalhamento de cada um deles. Estas análises também incluíram a influência da aplicação do campo magnético DC sobre o comportamento dos dispositivos. Com isso, foi possível selecionar os arranjos mais promissores para o projeto dos dispositivos deste trabalho.

Após esta fase, foram realizadas, para cada dispositivo desenvolvido, várias simulações computacionais, com a utilização dos softwares COMSOL Multiphysics [9] e MIT Photonic Bands (MPB) [10]. Estas simulações permitiram a obtenção das características espectrais dos dispositivos estudados, dentre as quais destacamos as perdas de inserção, os níveis de isolação e a largura de banda.

Através de processos de otimização paramétrica realizados com o uso destes softwares, foi possível o projeto dos dispositivos com características de desempenho ótimas, apresentados nos seis artigos científicos anexados a este trabalho.

Uma das principais estratégias utilizadas ao longo do processo de otimização paramétrica consistiu na realização de algumas modificações na estrutura da cavidade ressonante original, apresentada em [7]. Em especial, cada dispositivo desenvolvido possui um furo central com propriedades geométricas distintas, seja nas dimensões, seja no formato (circular ou elíptico). Como se pode observar a partir da Fig. 4, a intensidade do campo eletromagnético no dispositivo é maior no furo central da cavidade, de modo que quaisquer modificações nas propriedades geométricas do mesmo influenciam significativamente as características de desempenho dos dispositivos que nela se baseiam.

A utilização de furos centrais elípticos, ao invés de furos centrais circulares (convencionalmente utilizados), permitiu, principalmente nas chaves ópticas desenvolvidas, a obtenção de melhores características de desempenho.

Um dos principais desafios no projeto de chaves consiste na obtenção, em uma mesma faixa de frequências, de baixos níveis de transmissão no estado *off* e de altos

níveis de transmissão no estado *on*. Esta faixa, que define a banda de operação da chave, pôde ser alargada a partir da utilização de furos centrais elípticos, conforme pode ser verificado nos artigos que serão apresentados. Em alguns casos, este recurso permitiu um aumento superior a 100% na largura de banda de operação dos dispositivos.

Além disso, durante a fase de otimização paramétrica, foi estudada a influência da utilização de furos de casamento na conexão entre cada um dos guias de ondas e a cavidade ressonante dos dispositivos. Estes furos localizam-se na fronteira entre o guia de ondas e a cavidade e possuem raio ou posição perturbados, quando comparados aos demais furos que fazem parte da estrutura periódica do cristal fotônico. Tais elementos de casamento possuem a função de melhorar o casamento de impedâncias em um dispositivo e podem, deste modo, aumentar a performance do mesmo. Conforme pode ser verificado nos artigos que serão apresentados, esta estratégia se mostrou bastante útil no desenvolvimento de novos dispositivos passivos baseados em cristais fotônicos.

A seguir serão apresentados, na íntegra, os seis artigos científicos que foram publicados ao longo dos três anos do curso de doutorado em engenharia elétrica. Neles podem ser encontrados maiores detalhes a respeito do projeto dos dispositivos em questão.

ARTIGO 1

Compact optical switch based on 2D photonic crystal and magneto-optical cavity

Compact optical switch based on 2D photonic crystal and magneto-optical cavity

Victor Dmitriev,* Marcelo N. Kawakatsu, and Gianni Portela

Department of Electrical Engineering, Av. Augusto Correa 01, Belem, Para 66075-900, Brazil
Corresponding author: victor@ufpa.br

A compact optical switch based on a 2D photonic crystal (PhC) and a magneto-optical cavity is suggested and analyzed. The cavity is coupled to two parallel and misaligned PC waveguides and operates with dipole mode. When the cavity is nonmagnetized, the dipole mode excited by a signal in the input waveguide has a node in the output waveguide. Therefore, the input signal is reflected from the cavity. This corresponds to the state *off* of the switch. Normal to the plane of the PhC magnetization by a dc magnetic field produces a rotation of the dipole pattern in the cavity providing equal amplitudes of the electromagnetic fields in the input and the output waveguides. This corresponds to the state *on* with high transmission of the input signal. Numerical calculations show that at the 1.55 μm wavelength the device has the insertion loss −0.42 dB in the *on* state, the isolation −19 dB in the *off* state and the switch *off* and *on* ratio P_{on}/P_{off} about 72. The frequency band at the level of −15 dB of the resonance curve in *off* state is about 160 GHz.   © 2013 Optical Society of America

OCIS codes: 130.4815, 230.5298.

Different types of optical 2D photonic crystal (PhC) switches and modulators, which are based on control of light by light, by electric field, or by heat have been suggested recently [1,2,3]. For light control, magneto-optical (MO) effects in 1D PhCs with a MO material can also be used [4]. Changing the waveguide parameters by a dc magnetic field, one can switch on and off (or modulate) the light.

Three-port circulators of different types [5–7] based on MO resonators can also be used as switches if one changes the sign of the applied dc magnetic field H_0. This causes change in the direction of the circulation from $1 \rightarrow 2 \rightarrow 3 \rightarrow 1$ to $1 \rightarrow 3 \rightarrow 2 \rightarrow 1$ where 1, 2, and 3 denote the circulator ports. To switch the direction of propagation, dc magnetic field in this case must be changed from $+\mathbf{H}_0$ to $-\mathbf{H}_0$.

In this Letter we will show theoretically a possibility to design a new type of switches (which is based on a MO resonator) by changing the dc magnetic field from 0 to $\mathbf{H}_0$. This can reduce significantly the time of switching in comparison with that for the switches based on three-port circulators. Besides, the switch suggested below has reduced dimensions because of the two-port structure instead of the three-port circulator geometry.

The MO cavity of the suggested switch operates with a dipole mode. The cavity is coupled to two parallel and misaligned PhC waveguides. The switching from the state *off* to the state *on* is fulfilled by a dc magnetic field $\mathbf{H}_0$ applied normally to the PhC. The state *off* corresponds to the high reflection of the electromagnetic wave from the resonator.

An idealized scheme showing the principle of the switch functioning is given in Fig. 1. The device consists of a resonator with a magnetic medium which can be magnetized by a dc magnetic field $\mathbf{H}_0$ normal to the PhC plane [Fig. 1(b)]. The input waveguide 1 and the output waveguide 2, which are parallel but misaligned, are connected to the resonator. The resonator on Fig. 1 is bounded by the big circles which define the resonator region. The two small circles in these figures represent schematically the distribution of the ac magnetic field

H_z showing the standing waves (idealized dipole modes) in the resonators for the *off* and *on* states.

Without external magnetic field $\mathbf{H}_0$ the cavity supports two degenerate right- and left-rotating modes with the frequencies ω^- and ω^+ which are equal, i.e., $\omega^- = \omega^+$. Their superposition gives a standing dipole mode with a node in the output waveguide [Fig. 1(a)]. This means that the wave incident in port 1 cannot pass to the port 2, and it will be reflected from the resonator. This corresponds to the switch state *off*.

A dc magnetic field $\mathbf{H}_0$ produces a splitting of the frequencies ω^- and ω^+ of modes rotating in the opposite directions (see Fig. 2). By choosing the parameters of the magnetized MO resonator, the field pattern of the resulting standing wave can be rotated by the angle $\alpha \approx 60°$, forming the required distribution of ac electromagnetic fields with equal amplitudes in the input and output ports [Fig. 1(b)]. This permits propagation of the incident wave from port 1 to port 2, i.e., defines the state *on* of the switch. Notice that the central frequency of the switch is approximately in the middle between the frequencies ω^+ and ω^- (compare Figs. 2 and 4).

The investigated structure has no geometrical symmetry (except the plane $z = 0$ which is irrelevant in our case), therefore, it is described by the scattering matrix of a general form:

$$[S] = \begin{vmatrix} S_{11} & S_{12} \\ S_{21} & S_{22} \end{vmatrix}. \tag{1}$$

Let us consider an ideal switch without losses. In the *off* state, when the resonator is nonmagnetized, the device is
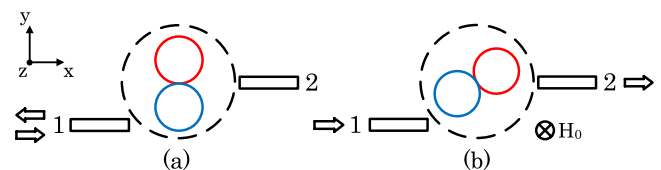

Fig. 1.   (Color online) Optical switch schemes in the (a) *off* and (b) *on* states with dipole mode in MO cavity.
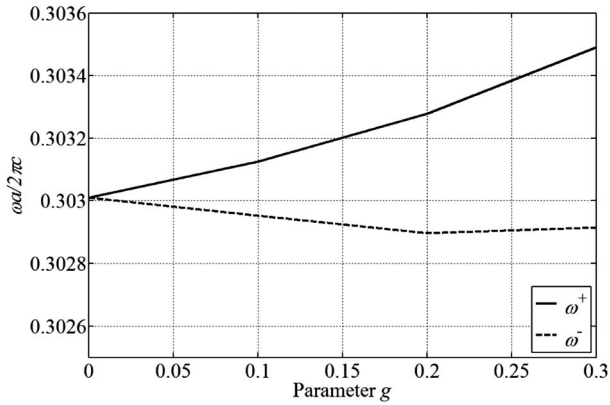
Fig. 2. Frequency splitting between right- and left-rotating modes of resonator versus parameter g.

Fig. 4. Optical switch frequency responses of power transmission in *on* and *off* states for excitation at port 1.

reciprocal, i.e., $S_{12} = S_{21}$. Therefore, the ideal switch without losses in this state should have $S_{11} = S_{22} = 1$ and $S_{12} = S_{21} = 0$. In general, for the magnetized resonator $S_{12} \neq S_{21}$, but from the desired transmission $S_{21} = 1$ in the *on* state and from the unitary condition we obtain $S_{11} = S_{22} = 0$ and $S_{12} = S_{21} = 1$. Thus, the ideal scattering matrices $[S]$ for the two states are:

$$[S]_{\text{on}} = \begin{vmatrix} 0 & 1 \\ 1 & 0 \end{vmatrix}, \qquad [S]_{\text{off}} = \begin{vmatrix} 1 & 0 \\ 0 & 1 \end{vmatrix}. \qquad (2)$$

The absence of geometrical symmetry is reflected in the following: (a) we can not obtain for the real scattering matrix relations following from symmetry (such as $S_{11} = S_{22}$, and $S_{21} = S_{12}$), (b) frequency responses of the switch are not symmetrical with respect to the central frequency, and (c) for a fixed direction of the dc magnetic field, characteristics for the case where the input port of the switch is 1, and for the case where the input port is 2 can be different.

The proposed device was simulated using the software COMSOL [8]. The switch is based on a 2D PhC with the lattice constant a in the plane x–y (Fig. 5). The crystal is a triangular lattice of air holes of radius $0.3a$ in a MO material. The geometry of the resonator is similar to that suggested in [5].

In the *off* state, the material of the resonator is described by the scalar relative permittivity $\varepsilon_r = 6.25$ and
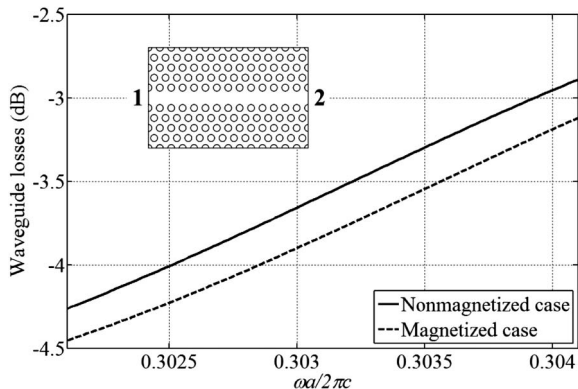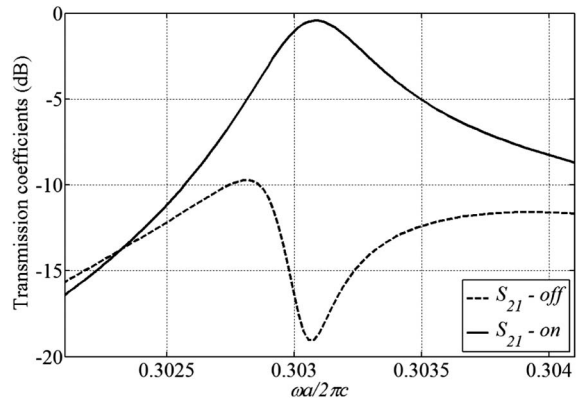
the scalar permeability μ_0. In the *on* state, the MO material of the resonator is characterized by the following permittivity tensor:

$$\varepsilon = \varepsilon_0 \begin{bmatrix} \varepsilon_r & ig & 0 \\ -ig & \varepsilon_r & 0 \\ 0 & 0 & \varepsilon_r \end{bmatrix}, \qquad (3)$$

where $\varepsilon_r = 6.25$, and the permeability μ_0. Notice that parameter g is approximately proportional to $\mathbf{H}_0$. The sign of g is changed with changing the sign of $\mathbf{H}_0$.

Different transparent magnetic materials can be used for our purposes, among them traditional yttrium iron garnet (YIG) and C:YIG garnets [9], and magnetic semiconductors, such as EuO and EuS [10,11]. These materials can provide high values of the parameter g. We have used in our calculations $g = 0.301$ (the Voigt parameter is $g/\varepsilon_r = 0.0482$). Changing the geometry of the device, one can project the switch for lower values of g.

The proposed device was projected to operate for transmission from port 1 to port 2. The rectilinear waveguide losses in the magnetized and nonmagnetized states are shown in Fig. 3. For excitation at port 1, the frequency responses for power transmission of the switch in the *on* and the *off* states are given in Fig. 4. In this figure, the waveguide losses were removed in order to

Fig. 3. Losses in rectilinear PhC waveguide in nonmagnetized and magnetized states.
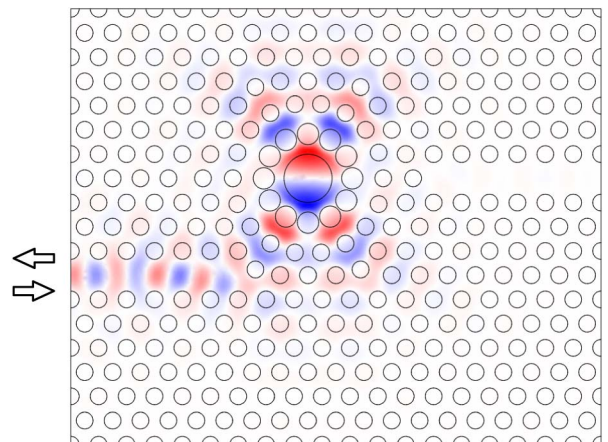

Fig. 5. (Color online) Distribution of component H_z of ac magnetic field in switch excited at port 1 in *off* state.
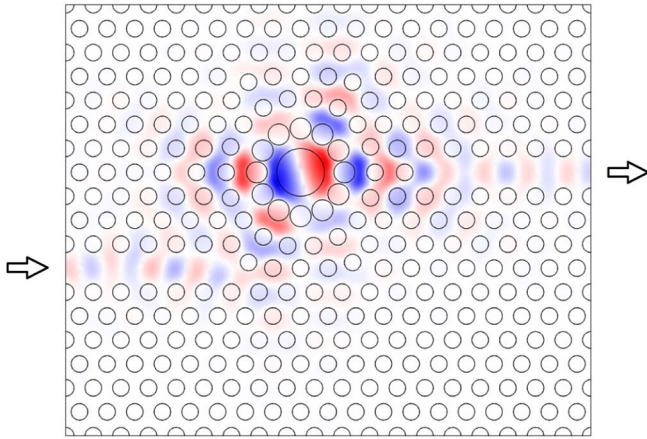
Fig. 6.   (Color online) Distribution of component H_z of ac magnetic field in optical switch excited at port 1 in *on* state.

show only the MO cavity losses, which are $P_{on} = -0.42$ dB and $P_{off} = -19$ dB at the central frequency. This corresponds to the ratio of transmitted power in the *on* and *off* states (P_{on}/P_{off}) equal to 72. The frequency band at the level -15 dB of the resonant curve for the *off* state is about 160 GHz. This band is defined by the resonant nature of the switch. The variation of the losses in the state *on* in this band is $(-0.42 \div -1.76)$ dB.

We also show in Figs. 5 and 6 the ac magnetic field component H_z at the central frequency $\omega a/2\pi c = 0.3031$. As it can be observed, the field amplitude is greatly increased in the MO cavity and the orientations of the standing dipole mode are in accordance with the schemes of Fig. 1.

The required external dc magnetic field $\mathbf{H}_0$ can be evaluated as follows. In order to obtain the maximum frequency band, we need to use the maximum possible magnetization of the material $\mathbf{M}_{max}$ (saturation magnetization) which gives the maximum value of the parameter g in tensor (3). The magnetic field $\mathbf{H}_0$ required for this magnetization is $\mathbf{H}_0 = \mathbf{H}_i + N_z\mathbf{M}_{max}$ where N_z is the demagnetization factor in z-direction and $\mathbf{H}_i$ is the necessary internal dc magnetic field. For a thin magnetic layer, the factor N_z is approximately equal to 1. Thus, the required dc magnetic field $\mathbf{H}_0$ is higher than $\mathbf{H}_i$ and higher than $\mathbf{M}_{max}$ and can reach the value

$(100 \div 200)$ kA/m [7,12]. One can diminish the required field $\mathbf{H}_0$, but at the expense of the frequency band.

Robustness to structural variations (for example, due to fabrication imperfections) of our device is similar to that for the 2D PhC circulators. This issue is discussed in [12].

In conclusion, we have shown in this Letter a theoretical possibility to design a simple and compact optical switch based on 2D PhC and a MO cavity. Its dimensions are bounded by the dimensions of the resonator with the dipole mode, which are typically $10a \times 10a$, where a is the lattice constant (see Figs. 5 and 6). Our 2D simulation results demonstrated that at the wavelength $\lambda = 1.55$ μm, the proposed switch can have the switch *on* and *off* ratio $P_{on}/P_{off} = 72$ with the insertion losses -0.42 dB in the *on* state. The frequency band of the switch at the level of -15 dB of the resonant curve for the *off* state is about 160 GHz. We believe that further optimization of the MO resonator and the waveguide-resonator coupling parameters can provide better characteristics of the switch.

References

1. A. Sharkawy, S. Shi, and D. W. Prather, Opt. Express **10**, 1048 (2002).
2. D. M. Beggs, T. P. White, L. Cairns, L. O'Faolain, and T. F. Krauss, IEEE Photon. Technol. Lett. **21**, 24 (2009).
3. M. Yanik and S. Fan, Appl. Phys. Lett. **83**, 2739 (2003).
4. Z. Wu, M. Levy, V. J. Fratello, and A. M. Merzlikin, Appl. Phys. Lett. **96**, 051125 (2010).
5. W. Smigaj, L. Magdenko, J. Romero-Vivas, S. Guenneau, B. Dagens, B. Gralak, and M. Vanwollghem, Opt. Lett. **35**, 568 (2010).
6. Z. Wang and S. Fan, Opt. Lett. **30**, 1989 (2005).
7. V. Dmitriev, M. Kawakatsu, and F. de Souza, Opt. Lett.**37**, 3192 (2012).
8. www.comsol.com.
9. M. C. Sekhar, M. R. Singh, S. Basu, and S. Pinnepalli, Opt. Express **20**, 9624 (2012).
10. H. Takeda and S. John, Phys. Rev. A **78**, 023804 (2008).
11. J. O. Dimmock, C. E. Hurwitz, and T. B. Reed, Appl. Phys. Lett. **14**, 49 (1969).
12. Z. Wang and S. Fan, Photon. Nanostruct. Fundam. Applic. **4**, 132 (2006).

ARTIGO 2

Possible mechanisms of switching in symmetrical two-ports based on 2D photonic crystals with magneto-optical resonators

Possible mechanisms of switching in symmetrical two-ports based on 2D photonic crystals with magneto-optical resonators

Victor Dmitriev, Gianni Portela,* and Daimam Zimmer

Department of Electrical Engineering, Federal University of Para, Av. Augusto Correa 01, Belem, Para, 66075-090, Brazil
*Corresponding author: gianni_portela@hotmail.com

We analyze possible mechanisms of switching in two-ports based on 2D photonic crystals (PhCs) with a magneto-optical resonator. The input and output waveguides can be side or front coupled with the resonator. The resonator operates with a dipole mode. In the switch with *front coupling* in the nonmagnetic state the standing dipole mode provides equal nonzero wave amplitudes in the input and output waveguides and therefore transmission of the signal from the input to output waveguides. This is the state *on*. The applied magnetic field normal to the plane of the PhC rotates the standing dipole mode by 90° setting the nodes in the input and output waveguides. This corresponds to the state *off*. On the contrary, in the switch with *side coupling* and nonmagnetized resonator, the standing dipole mode excited by a wave in the input waveguide has its node in the output waveguide. Therefore, the signal is reflected from the input port. This corresponds to the state *off* of the switch. Magnetization by a DC magnetic field produces a rotating dipole pattern in the cavity. Due to this rotating, the mode signal passes from the input port to the output one and this is the state *on*.   © 2013 Optical Society of America
OCIS codes: (130.4815) Optical switching devices; (230.5298) Photonic crystals.
http://dx.doi.org/10.1364/OL.38.004040

In 2D photonic crystals (PhCs), switches and modulators that are based on control of light by light, by electric field, by heat, or by DC magnetic field have been suggested recently [1–5]. In particular, changing some parameters of magneto-optical (MO) resonators and waveguides by a DC magnetic field $\mathbf{H}_0$, one can switch *on* and *off* the light. Three- and four-port circulators of different types [6–9] can also be used as switches if one changes the sign of magnetic field $\mathbf{H}_0$. In [5], we suggested a nonsymmetrical switch that is based on a MO resonator with two parallel but misaligned waveguides connected to the resonator. The input waveguide is side coupled to the resonator, but the output waveguide is front coupled.

In this work, we consider symmetrical two-ports (shown schematically in Fig. 1) that consist of a resonator with MO material and two waveguides connected to this resonator. We discuss possible mechanisms of switching by a DC magnetic field $\mathbf{H}_0$ in two different geometries of such switches. In the first one, shown schematically in Figs. 1(a) and 1(b), both the input waveguide 1 and the output waveguide 2 are front coupled to the resonator and aligned. In the second switch both waveguides are side coupled to the resonator. The output waveguide 2, which is parallel to the input waveguide 1, can be oriented in the same direction as the input one or in the opposite direction. In Figs. 1(c) and 1(d) we present the latter case where 180° bending of the output waveguide with respect to the input one can provide more flexibility in design of integrated circuits.

The MO resonator of the two-ports can be magnetized uniformly by a DC magnetic field $\mathbf{H}_0$ in the direction normal to the plane of the two-port x0y (Fig. 1).

First, we consider the unloaded nonmagnetic resonator, shown schematically in Figs. 2(a)–2(c). The eigenvectors $\mathbf{V}_1$ and $\mathbf{V}_2$ with the resonant frequency ω_0 corresponding to two orthogonal dipole eigenmodes of the resonator can be written as follows:

$$\mathbf{V}_1 = \begin{pmatrix} 1 \\ 0 \end{pmatrix}, \qquad \mathbf{V}_2 = \begin{pmatrix} 0 \\ 1 \end{pmatrix}. \tag{1}$$

These two eigenmodes are degenerate [10]. Any combination of them, for example $\mathbf{V}_1 \pm i\mathbf{V}_2$

$$\mathbf{V}^+ = \begin{pmatrix} 1 \\ i \end{pmatrix}, \qquad \mathbf{V}^- = \begin{pmatrix} 1 \\ -i \end{pmatrix}, \tag{2}$$

are also eigenvectors. The last two vectors present rotating in opposite directions eigenmodes with the resonant frequency ω_0 and they are degenerate as well [Fig. 2(c)].

Magnetization of the resonator by a DC magnetic field $\mathbf{H}_0$ removes the degeneracy of $\mathbf{V}^+$ and $\mathbf{V}^-$ [Fig. 2(d)].
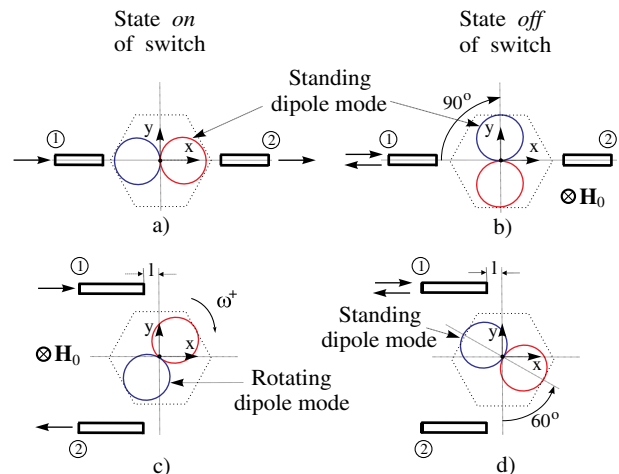

Fig. 1.   Two-port switches: (a) and (b) front–front coupling of waveguides and resonator (case 1), (a) *on* state, (b) *off* state; (c) and (d) side–side coupling (case 2), (c) *on* state, (d) *off* state. Dotted hexagons enclose resonators, circles show H_z component of idealized dipole modes, $\mathbf{H}_0$ is DC magnetic field.
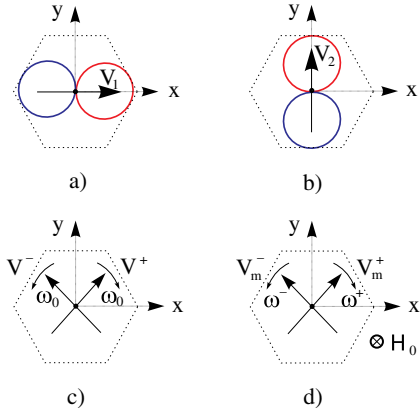
Fig. 2. Eigenvectors for nonmagnetized and magnetized unloaded resonator: (a) dipole $\mathbf{V}_1$ oriented along x, (b) dipole $\mathbf{V}_2$ oriented along y, (c) two degenerate rotating dipoles $\mathbf{V}^+$ and $\mathbf{V}^-$ of nonmagnetic state, and (d) two nondegenerate rotating dipoles $\mathbf{V}_m^+$ and $\mathbf{V}_m^-$ of magnetic state. $\mathbf{H}_0$ is DC magnetic field.

Now, the rotating clockwise and anticlockwise eigenmodes $\mathbf{V}_m^+$ and $\mathbf{V}_m^-$ have different eigenfrequencies ω^+ and ω^- [Figs. 3(a) and 4(a)].

In the nonmagnetic state of the two switches, due to coupling to the waveguides and consequently, lower symmetry, the degeneracy of eigenmodes $\mathbf{V}_1$ and $\mathbf{V}_2$ of the resonator is removed. Qualitatively, one can expect that the stronger the coupling of the resonator with waveguides the higher will be the difference between the eigenfrequencies of $\mathbf{V}_1$ and $\mathbf{V}_2$. In the magnetic state, the

Fig. 3. *Case 1.* (a) Frequency splitting between right- and left-rotating modes of resonator versus tensor parameter g and (b) comparison of frequency characteristics of resonant modes for loaded (right inset) and unloaded (left inset) resonators in nonmagnetized and magnetized PhC.
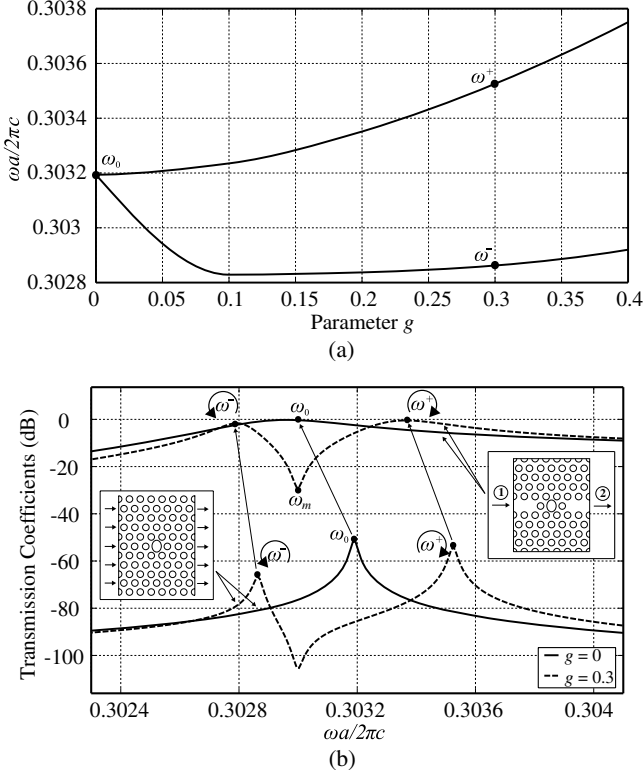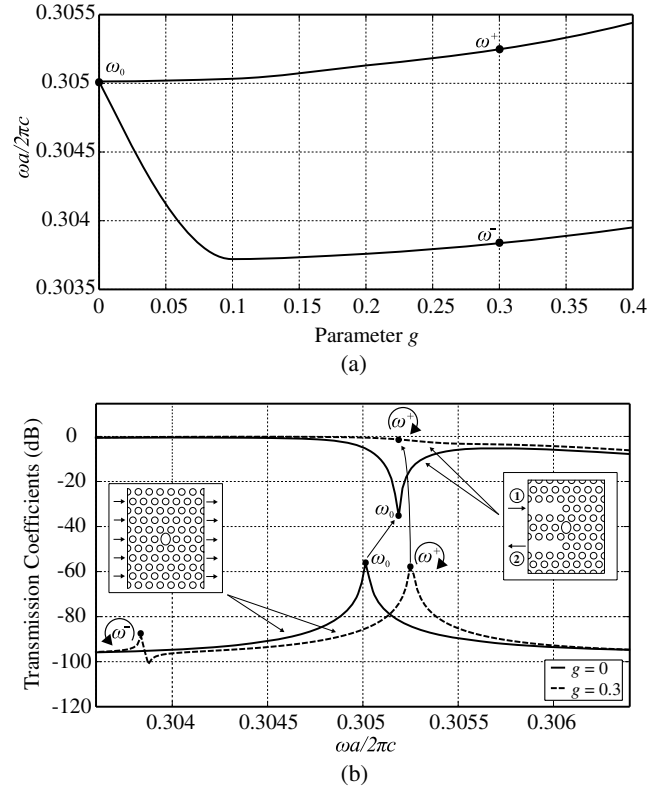

Fig. 4. *Case 2.* (a) Frequency splitting between right- and left-rotating modes of resonator versus tensor parameter g and (b) comparison of frequency characteristics of resonant modes for loaded (right inset) and unloaded (left inset) resonators in nonmagnetized and magnetized PhC.

coupling of the resonator with waveguides also changes the frequencies ω^+ and ω^- of the modes $\mathbf{V}_m^+$ and $\mathbf{V}_m^-$. Besides, the quality factor Q of the loaded resonator will be lower than that of the unloaded one in both nonmagnetic and magnetic states [see Figs. 3(b) and 4(b)].

We shall consider separately the two cases shown in Figs. 1(a) and 1(b) (*case 1*) and Figs. 1(c) and 1(d) (*case 2*).

Case 1. The excited mode in the nonmagnetic resonator is $\mathbf{V}_1$ [see Fig. 2(a)]. From the orientation of dipole $\mathbf{V}_1$, one can see that this mode with the frequency ω_0 will correspond to the state *on* of the switch in Fig. 1(a). In the magnetized resonator, the standing wave with the nodes in the input and output ports will correspond to the state *off* of the switch. Such regime is obtained by the sum of the modes $\mathbf{V}_m^+$ and $\mathbf{V}_m^-$ with the frequency $\omega_m \approx (\omega^+ + \omega^-)/2$ [see Fig. 1(b)]. Thus, with front–front coupling of waveguides with resonator, in the nonmagnetized regime the state is *on* and in the magnetized one the state is *off*. One needs to fulfill the requirements $\omega_0 \approx \omega_m$ and rotation of the standing wave due to DC magnetic field by the angle $90°$ [Fig. 1(b)].

Case 2. In case 2 with side–side coupling, in the nonmagnetized regime with properly chosen length l we can have the state *off* with the standing wave formed by $(\mathbf{V}_2 - \sqrt{3}\mathbf{V}_1)/2$ [Fig. 1(d)], oriented at the angle $60°$ with respect to the axis y. In the magnetized regime, the state *on* is achieved by using one of the rotating modes $\mathbf{V}_m^+$ or $\mathbf{V}_m^-$ [Fig. 1(c)]. For functioning the switch, in this case it is necessary to fulfill the requirement $\omega_0 \approx \omega^+$ (or ω^-).
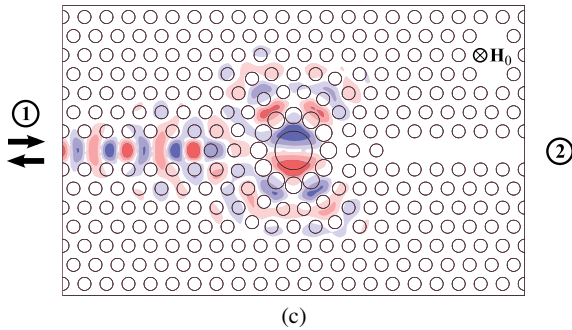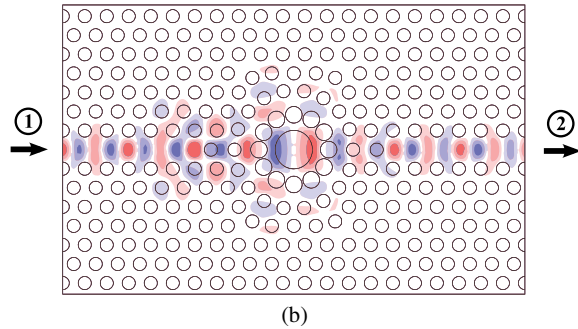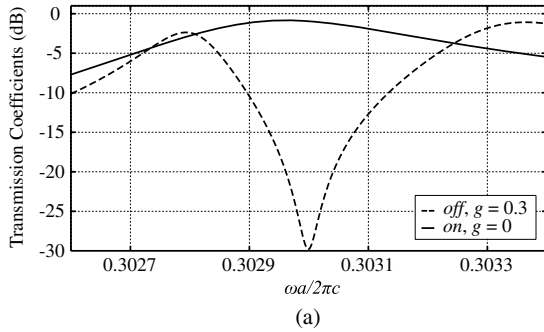
Fig. 5.   Switch of Figs. 1(a) and 1(b). (a) Frequency responses. H_z distribution at central frequency: (b) state *on* and (c) state *off*.

Fig. 6.   Switch of Figs. 1(c) and 1(d). (a) Frequency responses. H_z distribution at central frequency: (b) state *on* (arc arrow shows rotation of dipole mode) and (c) state *off*.

Scrutinizing Fig. 1, one can see a significant difference in the properties of the two switches. In the component of Figs. 1(a) and 1(b), DC magnetic field switches off the channel, but in Figs. 1(c) and 1(d), on the contrary, $\mathbf{H}_0$ switches on the channel.

Notice that in our previous paper [5] devoted to side–front coupled nonsymmetrical switch we erroneously attributed the state *on* (magnetized resonator) of the switch to a standing wave. A more thorough analysis showed that in fact one of the two rotating modes (ω^+ or ω^-) is responsible for this regime. Taking the opportunity, we thank an anonymous reviewer of our paper [5] who pointed out a possibility to use the rotating modes and indicated paper [11].

In our example, the PhC is a triangular lattice of air holes of radius $0.3a$ ($a = 480$ nm is the lattice constant) in a magnetic semiconductor. The splitting of the eigenfrequencies of the resonators by the applied magnetic field is shown in Figs. 3(a) and 4(a).

We have adapted for our purposes the resonator structure suggested in [8]. In order to adjust the resonance frequencies in *on* and *off* states we had to change the geometry of the central hole of the resonator from circular to elliptical. In *case 1*, the central elliptical hole of the resonator has the semi-minor axis equal to

$0.8475a = 406.8$ nm, and semi-major axis equal to $0.8775a = 421.2$ nm. In *case 2*, it has the semi-minor axis $0.85a = 408$ nm and semi-major axis $0.95a = 456$ nm. In both cases, the radius of the 12 air cylinders of the first ring is $0.38a = 182.4$ nm and they form a ring with the radius equal to 760 nm. The 18 air cylinders of the second ring form a ring with the radius equal to 1292.9 nm. The third ring with the radius 1807.2 nm is formed by six air cylinders. The cylinders of the second and the third rings have the radius equal to $0.3a = 144$ nm. The parameter l [Figs. 1(c) and 1(d)] is equal to 1047.6 nm.

The guided electromagnetic wave in PhC waveguide is TE mode. The frequency responses of the resonator and the switches were calculated by the software COMSOL [12].

The MO material is described by the following expressions for the permittivity and the permeability:

$$[\epsilon] = \epsilon_0 \begin{pmatrix} \epsilon_r & -ig & 0 \\ ig & \epsilon_r & 0 \\ 0 & 0 & \epsilon_r \end{pmatrix}; \qquad \mu = \mu_0. \qquad (3)$$

In our calculus, we used the values of the parameters $\epsilon_r = 6.25$ and $g = 0.3$ (information of available parameters of the tensor $[\epsilon]$ one can find, for example, in [13,14]).

In order to exclude the losses in the waveguides (which are at the level of $-2 \div -3$ dB) and to consider only the losses of the switch, we calculated first the losses of the nonmagnetized and magnetized waveguide. In the following we subtracted these losses from those calculated for the switch.

In Fig. 5 we show the calculated frequency responses and the structure of H_z component of the electromagnetic field of the front–front coupling switch (*case 1*). One can see that the frequency characteristic in the state *on* is defined by the resonance of the mode V_1 as it was predicted by our theory [compare with Fig. 1(a)]. In the *off* state, the frequency band is limited by two rotating modes V_m^+ and V_m^- of the resonator. In *case 1*, the bandwidth is about 88 GHz at the level of isolation -15 dB at wavelength 1.55 µm. In *case 2* of side–side coupling of switch, the calculated characteristics are given in Fig. 6. One can see that in this case we also have the predicted by the above theory behavior of the switch. In *case 2*, the bandwidth is about 71 GHz.

Our numerical simulations show that in symmetrical two-ports different mechanisms of switching can be used. The front–front coupled switch without applied DC magnetic field is in *on* state and can work as a passband filter. When the resonator is magnetized, the switch has the characteristic of a stop-band filter. In side–side coupling, vice versa, the switch with the nonmagnetized resonator is in the state *off* and behaves as a stop-band filter. With the magnetized resonator, the switch is in the state *on* and has the characteristic of a passband filter.

References

1. M. Yanik and S. Fan, Appl. Phys. Lett. **83**, 2739 (2003).
2. A. Sharkawy, S. Shi, and D. W. Prather, Opt. Express **10**, 1048 (2002).
3. D. M. Beggs, T. P. White, L. Cairns, L. O. Faolain, and T. F. Krauss, IEEE Photon. Technol. Lett. **21**, 24 (2009).
4. Z. Wu, M. Levy, V. J. Fratello, and A. M. Merzlikin, Appl. Phys. Lett. **96**, 051125 (2010).
5. V. Dmitriev, M. Kawakatsu, and G. Portela, Opt. Lett. **38**, 1016 (2013).
6. V. Dmitriev, M. Kawakatsu, and F. J. M. de Souza, Opt. Lett. **37**, 3192 (2012).
7. Z. Wang and S. Fan, Opt. Lett. **30**, 1989 (2005).
8. W. Smigaj, J. Romero-Vivas, B. Gralak, L. Magdenko, B. Dagens, and M. Vanwolleghem, Opt. Lett. **35**, 568 (2010).
9. Z. Wang and S. Fan, Photon. Nanostr. Fundam. Appl. **4**, 132 (2006).
10. S.-H. Kim and Y.-H. Lee, IEEE J. Quantum Electron. **39**, 1081 (2003).
11. Y. Xu, Y. Li, R. K. Lee, and A. Yariv, Phys. Rev. A **62**, 7389 (2000).
12. www.comsol.com.
13. M. C. Sekhar, M. R. Singh, S. Basu, and S. Pinnepalli, Opt. Express **20**, 9624 (2012).
14. E. L. Nagaev, Sov. Phys.-Usp. **18**, 863 (1975).

ARTIGO 3

Magneto-optical resonator switches in two-dimensional photonic crystals: geometry, symmetry, scattering matrices, and two examples

Magneto-optical resonator switches in two-dimensional photonic crystals: geometry, symmetry, scattering matrices, and two examples

Victor Dmitriev, Gianni Portela,* and Raphael Batista

Department of Electrical Engineering, Federal University of Para, P.O. Box 8619,
Agencia UFPA, CEP 66075-900, Belem, Para, Brazil

*Corresponding author: gianni_portela@hotmail.com

We discuss different geometrical structures of optical switches based on two-dimensional photonic crystals with hexagonal geometry of the unit cell and a magneto-optical resonator. Transition between the states *on* and *off* in these switches is achieved by an external DC magnetic field. The input and output waveguides can be front–front, side–side, or front–side coupled to the resonator and these different types of coupling can lead to different mechanisms of switching. Analysis of symmetry and scattering matrices of the switches is based on magnetic group theory. Two examples of switches with 60° and 120° bends and their characteristics are also presented.   © 2014 Optical Society of America

OCIS codes: (130.4815) Optical switching devices; (230.5298) Photonic crystals.
http://dx.doi.org/10.1364/AO.53.004460

1. Introduction

Different methods can be used to control light in photonic crystals (PhCs). Switches and modulators based on control of light by light, electric field, heat, or DC magnetic field have been suggested recently [1–4]. In particular, changing some parameters of magneto-optic (MO) waveguides and resonators by a magnetic field $\mathbf{H}_0$, one can switch *on* and *off* the light. Three- and four-port circulators of different types [5–7] can also be used as switches if one changes the sign of the applied DC magnetic field.

In our previous papers related to the topic [8,9] we suggested new 2D PhC switches based on an MO resonator and discussed possible mechanisms of switching. These switches are two-port devices and they have some advantages in comparison to the switches based on circulators. In particular, they have reduced

dimensions and approximately two times smaller time of switching because the external magnetic field is changed from 0 to $\mathbf{H}_0$ and not from $-\mathbf{H}_0$ to $\mathbf{H}_0$ as in case of circulators.

One of the problems of PhC integrated circuits is bending of the waveguides. Even with the small 60° bend of waveguides, the scattering losses of the bend can be significant. For example, optimization of the 60° bend allowed Frandsen *et al.* [10] to reduce losses from −8 to −1 dB, but at the expense of a very complex structure of the bend. The switches we developed can simultaneously fulfill the role of 60°, 120°, and even 180° [9] bending elements. Such a diversity of switch geometries can provide a flexibility in design of optical integrated circuits.

In this work we discuss the following general topics: geometry and symmetry of switches and calculation of their scattering matrices using magnetic group theory. We also present two examples of switches with 60° and 120° bends and their calculated characteristics.

2. Possible Geometries of MO Switches in 2D PhCs with a Hexagonal Unit Cell

In the first part of our work we shall consider an MO resonator and two waveguides coupled to the resonator using the symmetry approach. In Figs. 1–3, we denote the resonator schematically by a dotted hexagon without specification of its internal structure. The six-fold rotational symmetry of the hexagon emphasizes the resonator symmetry. Input waveguide 1 and output waveguide 2 can be front-coupled or side-coupled to the resonator.

Due to the hexagonal geometry of the unit cell of 2D PhCs under consideration, one can consider many possible geometrical variants of the two-ports. Front–front coupled resonators are shown in Fig. 1. Side–side coupling is demonstrated in Fig. 2. Examples of mixed front–side coupling are given in Fig. 3.

The schemes of Figs. 1(c) and 2(c) have been investigated in [9], and the possibility to design switch with geometry of Fig. 3(b) has been shown in [8]. Notice that the schemes presented here do not exhaust all the possible variants.

3. Symmetry Analysis of Scattering Matrices

A. Some Restrictions on Symmetry of the Problem

In the following discussion of possible symmetries we shall exclude from consideration some types of symmetry. First we shall not discuss the consequences of the periodicity of the crystals, which are mathematically expressed in Bloch's theorem and geometrically presented by the Brillouin zone. For nonmagnetic PhCs this can be found, for example, in [11] and for magnetic ones in [12]. Instead, we shall concentrate on the point group symmetry of the crystals.

The second reduction of the problem complexity is 2D approximation. Though generally any real device or component based on PhCs is three-dimensional (3D), in this paper, we shall consider 2D PhCs described by 2D discrete symmetries, i.e., the symmetries of plane figures in the plane $x0y$ (see Fig. 1). The reason for this reduction of dimensionality of the problem is as follows. Two possible elements of symmetry in a 3D variant corresponding to the third coordinate z are the horizontal plane of symmetry $z = 0$ and the horizontal axis, for example, the x and y axis.

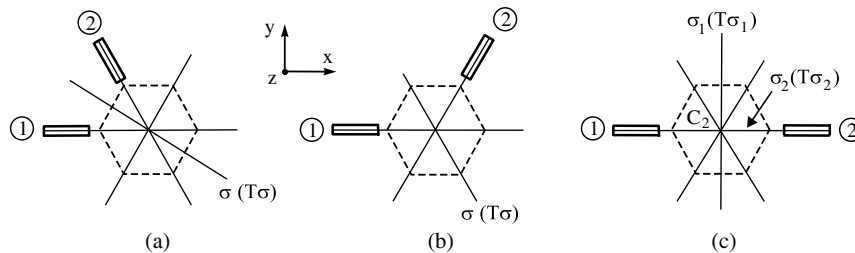Fig. 1. Examples of front–front coupling of waveguides and resonator and symmetry elements of switches in magnetized and nonmagnetized states: (a) 120° bend, (b) 60° bend, and (c) without bending.
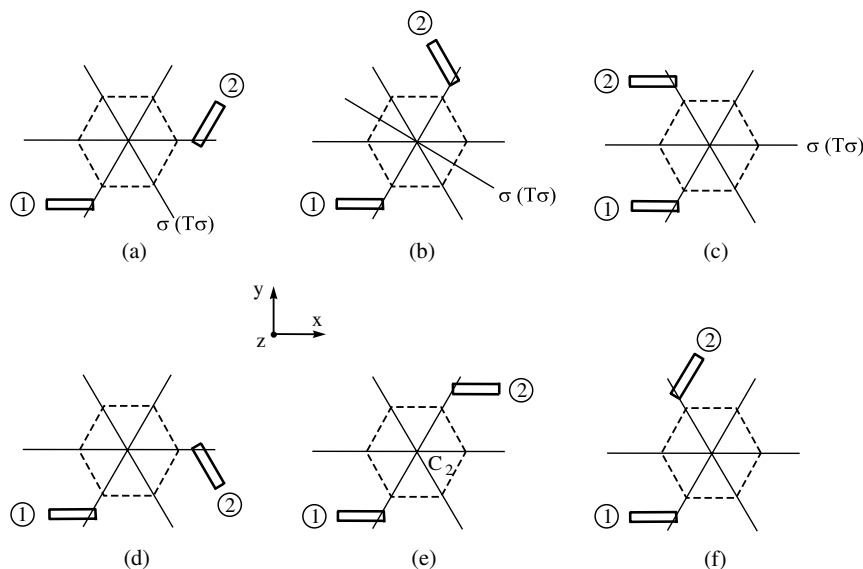

Fig. 2. Examples of side–side coupling of waveguides and resonator and symmetry elements of switches in magnetized and nonmagnetized states: (a), (d), (f) 60° bend, (b) 120° bend, (c) 180° bend, and (e) without bending.
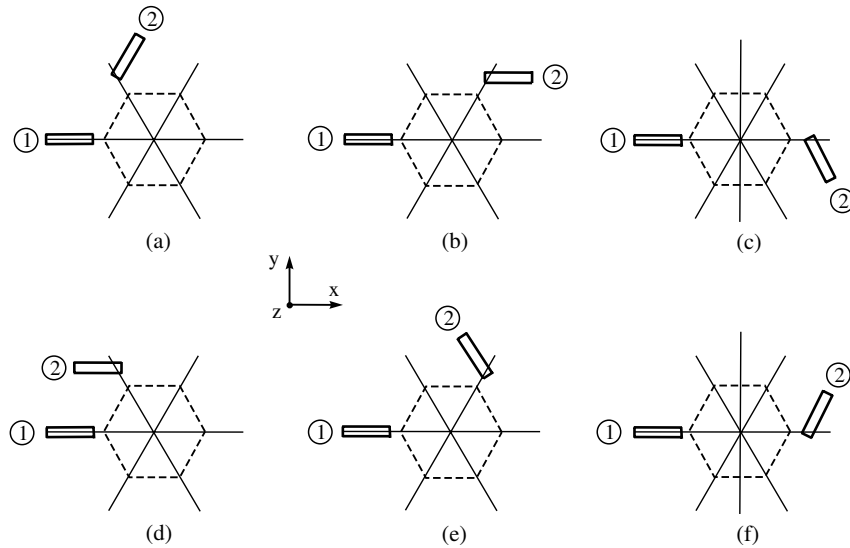
Fig. 3. Examples of combined front–side coupling of waveguides and resonator: (a), (c), (f) 60° bend, (e) 120° bend, (d) 180° bend, and (b) without bending.

The usual approximation in the analysis of the PhC theory is uniform distribution of the electromagnetic field along the axis z. Thus, instead of the two possible solutions with respect to the third coordinate, namely, the even and odd modes, we can consider only one of them.

The third restriction to the problem is the specific direction of the external DC magnetic field (or magnetization). We choose the direction of uniform magnetization by a DC magnetic field $\mathbf{H}_0$, which is perpendicular to the plane $x0y$ of a PhC, i.e., along the axis z. This orientation is typical, for example, for 2D PhC based three-port circulators [5–7]. Such orientation allows one to consider higher symmetries in comparison to the cases of other possible orientations of $\mathbf{H}_0$. This is because it preserves the two-fold rotational symmetry around the axis z if it exists in the nonmagnetic PhC. All other orientations of the DC magnetic field destroy this rotational symmetry. Besides, $\mathbf{H}_0 \| z$ preserves the horizontal plane of symmetry $z = 0$ of the nonmagnetic crystal, which is responsible for separation of the eigenmodes as TE and TM [13]. Any other orientation of $\mathbf{H}_0$ deletes this plane symmetry and consequently mixes these eigenmodes.

In the following we shall use the Schoenflies notations of magnetic groups [14], where G, $\mathbf{G}$, and $G(H)$ are groups of the first (nonmagnetic), second, and third category, respectively.

Symmetry of a two-port depends on symmetry of the PhC, scheme of ports connection, on inner symmetry of the resonator and symmetry of the applied DC magnetic field. In turn, symmetry of the PhC is defined by the symmetry of its materials, geometrical symmetry of its elements, symmetry of unit cells, and the time reversal symmetry (if any).

The resonator can have different formats [5,15–17]. Though its symmetry can be included in the analysis in the same way as other constituents,

for simplicity we will not discuss details of the geometry of the resonator. We assume only that the symmetry of the resonator is not lower than the symmetry of the other constituents of the problem, i.e., the symmetry of the resonator does not influence the resulting symmetry of the problem.

B. Symmetry of Resonator and Degeneracy of Eigenmodes in Nonmagnetic and Magnetic Regimes

First we consider the unloaded resonator in a nonmagnetic regime shown schematically in Fig. 4 with the symmetry C_{6v} (symmetry of a hexagon). The standing eigenmodes of our interest are the dipole ones $\mathbf{V}_i$ ($i = 1, 2, \ldots, 6$). A general form of these modes can be written as follows:

$$\mathbf{V}_i = \begin{pmatrix} a \\ b \end{pmatrix}. \tag{1}$$

These modes are highly degenerate. Two of these modes are shown schematically in Fig. 4, namely, with ($a = 0, b = 1$) in Fig. 4(a) and ($a = 1/2, b = \sqrt{3}/2$) in Fig. 4(b). The arrows in the figures indicate orientation of the dipoles. The other eigenmodes can be obtained by rotation of these two modes by 60° and 120° around the axis z. All of these modes have the same resonant frequency ω_0 [18].
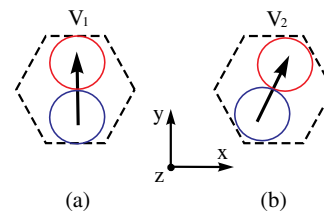

Fig. 4. Examples of standing eigenmodes in nonmagnetized resonator with symmetry C_{6v}.
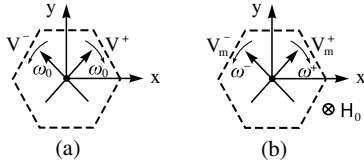
Fig. 5. Rotating eigenvectors for (a) nonmagnetized and (b) magnetized resonator.

The standing modes can be combined in order to produce two rotating degenerate eigenmodes $\mathbf{V}^+$ and $\mathbf{V}^-$:

$$\mathbf{V}^+ = \begin{pmatrix} 1 \\ i \end{pmatrix}, \qquad \mathbf{V}^- = \begin{pmatrix} 1 \\ -i \end{pmatrix}. \tag{2}$$

These modes also have the resonant frequency ω_0 and rotate in opposite directions [Fig. 5(a)]. The description in terms of rotating modes is useful in the magnetic regime of switches.

The MO resonator can be magnetized uniformly by a DC magnetic field $\mathbf{H}_0$ in the direction z, normal to the plane $x0y$. Magnetization of the resonator leads to the magnetic group $C_{6v}(C_6)$. The degeneracy of the modes $\mathbf{V}_i$ is preserved because the group $C_{6v}(C_6)$ contains the six-fold rotational symmetry. However, the magnetization removes the degeneracy of $\mathbf{V}^+$ and $\mathbf{V}^-$. Now, the rotating clockwise and anticlockwise eigenmodes $\mathbf{V}_m^+$ and $\mathbf{V}_m^-$ have different frequencies ω^+ and ω^- [see Fig. 5(b)].

C. Possible Symmetries of Two-Ports

The input and output waveguides connected to the resonator reduce symmetry of the structure. In nonmagnetic states, due to coupling to the waveguides and consequently, lower symmetry (the groups C_{2v}, C_2, and C_s), the degeneracy of eigenmodes $\mathbf{V}_i$ of the unloaded resonator is removed. From the group theoretical point of view, this is because the groups C_{2v}, C_2, and C_s have no 2D irreducible representations and, hence, no degenerate modes. The resonant frequencies of $\mathbf{V}_i$ will be denoted as ω_i. Qualitatively, one can expect that the stronger the coupling of the resonator with waveguides the higher the difference between the frequencies ω_i will be.

In the magnetic regime, the coupling of the resonator with waveguides also changes the frequencies ω^+ and ω^- of the modes $\mathbf{V}_m^+$ and $\mathbf{V}_m^-$. Besides, the quality factor Q of the loaded resonator will be lower than that of the unloaded one in both nonmagnetic and magnetic regimes.

We start our analysis of the possible groups of symmetry with the geometry of Fig. 1(c), which corresponds to the highest symmetry. The nonmagnetic two-port has the symmetry C_{2v} with the following elements: e (identity), the plane of symmetry σ_1 (the plane $x = 0$), the plane of symmetry σ_2 (the plane $y = 0$), the two-fold rotation around the z axis C_2, and the time reversal T. In the magnetic regime of Fig. 1(c), the group is $C_{2v}(C_2)$ with the elements e, $T\sigma_1$ (the antiplane $x = 0$), $T\sigma_2$ (the antiplane

$y = 0$), and C_2. The time reversal T in pure form is absent in this magnetic group. The elements and anti-elements of symmetry are shown in Figs. 1 and 2. For the magnetic regime, they are given in parentheses.

Now, let us consider the two-ports with lower symmetry. Three subgroups of C_{2v} can be considered. For the two-ports in Figs. 1(a), 1(b), 2(a)–2(c) in the nonmagnetic regime, the symmetry is C_s with the elements e, the plane of symmetry σ, and the time reversal T. With an applied DC magnetic field $\mathbf{H}_0$, the magnetic group is $C_s(C_1)$ having the elements e and the antiplane $T\sigma$.

Another possible symmetry is the group C_2 [Fig. 2(e)]. In the nonmagnetic regime, the group has the elements e, the axis of symmetry C_2, and the time reversal T. In the magnetic regime, the group is $\mathbf{C}_2$ where the axis of symmetry is preserved but the time reversal T is absent.

Still another possibility can exist in the two-port of Fig. 1(c), where the only element present is $\sigma_2(T\sigma_2)$. The two other elements, namely $\sigma_1(T\sigma_1)$ and $C_2(C_2)$, are absent. Thus, the group of symmetry of this case is the same as for Figs. 1(a), 1(b) and 2(a)–2(c) but with different orientation of the plane (antiplane) of symmetry.

Notice that all the two-ports of Fig. 3 with front–side coupling are nonsymmetrical.

D. Calculation of Scattering Matrices

The amplitudes of TE (with components H_z, E_x, and E_y) incident and reflected waves in two-ports can be represented by 2D vectors of the magnetic field $\mathbf{H}^i = (H_{z1}^i, H_{z2}^i)^t$ and $\mathbf{H}^r = (H_{z1}^r, H_{z2}^r)^t$, respectively, where t denotes transposition. They are defined by Bloch waves $H_{zn}^i \exp j(\omega t - \mathbf{k}_n^i \cdot \mathbf{r})$ and $H_{zn}^r \exp j(\omega t - \mathbf{k}_n^r \cdot \mathbf{r})$, respectively, where j is the imaginary unit, H_{zn}^i and H_{zn}^r are complex amplitudes of the eigenmodes in the waveguides of the two-port ($n = 1, 2$), and $\mathbf{k}_n$ is the corresponding wave vector. The incident and the reflected waves are related by the 2×2 scattering matrix [S] as follows: $\mathbf{H}^r = [S]\mathbf{H}^i$.

In order to define the structure of the scattering matrix [S] following from symmetry for the unitary elements σ and C_2, we use the commutation relation $[R][S] = [S][R]$. For the anti-unitary one $T\sigma$ however, the following relation is valid: $[R][S] = [S]^t[R]$, where t denotes transposition. The 2×2 matrix representations of the elements σ_1, σ_2, and C_2 are $[R]_{\sigma_1}$, $[R]_{\sigma_2}$, and $[R]_{C_2}$, respectively:

$$[R]_{\sigma_1} = \begin{pmatrix} 1 & 0 \\ 0 & 1 \end{pmatrix}, \qquad [R]_{\sigma_2} = [R]_{C_2} = \begin{pmatrix} 0 & 1 \\ 1 & 0 \end{pmatrix}. \tag{3}$$

The calculated scattering matrices for the groups C_{2v} and $C_{2v}(C_2)$ [Fig. 1(c)] are

$$[S]_{C_{2v}} = \begin{pmatrix} S_{11} & S_{12} \\ S_{12} & S_{11} \end{pmatrix}, \quad [S]_{C_{2v}(C_2)} = \begin{pmatrix} S_{11} & S_{12} \\ S_{12} & S_{11} \end{pmatrix}, \tag{4}$$

and for the groups C_s and $C_s(C_1)$ [Figs. 1(a), 1(b) and 2(a)–2(c)]

$$[S]_{C_s} = \begin{pmatrix} S_{11} & S_{12} \\ S_{12} & S_{11} \end{pmatrix}, \qquad [S]_{C_s(C_1)} = \begin{pmatrix} S_{11} & S_{12} \\ S_{21} & S_{11} \end{pmatrix}.$$
(5)

For the groups C_2 and $\mathbf{C}_2$, the calculated matrices are

$$[S]_{C_2} = \begin{pmatrix} S_{11} & S_{12} \\ S_{12} & S_{11} \end{pmatrix}, \qquad [S]_{\mathbf{C}_2} = \begin{pmatrix} S_{11} & S_{12} \\ S_{21} & S_{11} \end{pmatrix}.$$
(6)

Finally, for the groups C_s and $C_s(C_1)$ [Fig. 1(c), the group elements $\sigma_2(T\sigma_2)$]

$$[S]_{C_s} = \begin{pmatrix} S_{11} & S_{12} \\ S_{12} & S_{22} \end{pmatrix}, \qquad [S]_{C_s(C_1)} = \begin{pmatrix} S_{11} & S_{12} \\ S_{12} & S_{22} \end{pmatrix}.$$
(7)

Notice that the elements of matrices (4)–(7), obtained by symmetry constraints, are frequency independent.

Due to symmetry, the number of independent complex parameters of the matrices is reduced from four to three or even two. The matrices in the first column of (4)–(7), corresponding to nonmagnetic regime, are symmetrical ($S_{21} = S_{12}$), i.e., the corresponding two-ports are reciprocal. The matrices of the second column of (5) and (6) are nonsymmetrical, i.e., the corresponding two-ports are nonreciprocal. However, the matrices of (4) and (7) are symmetrical, i.e., in spite of magnetic regime, these two-ports are reciprocal. The reflection coefficients from port 1 and port 2 are equal ($S_{22} = S_{11}$) for the matrices (4)–(6), but they are different for the matrices (7). Thus, the presence of the antiplane of symmetry $T\sigma_2$ in this two-port leads only to equality of the transmission coefficients $S_{21} = S_{12}$.

4. Photonic Crystal and MO Resonator

The switches discussed below are based on a 2D PhC with the lattice constant a in the plane $x0y$. The crystal is a triangular lattice of air holes of radius $0.3a$ in an MO material. In the nonmagnetized regime, the material of the resonator is described by the scalar relative permittivity $\epsilon_r = 6.25$ and the scalar permeability μ_0. In the magnetized regime, the MO material of the resonator is characterized by the permeability μ_0 and the following permittivity tensor

$$[\epsilon] = \epsilon_0 \begin{pmatrix} \epsilon_r & -ig & 0 \\ ig & \epsilon_r & 0 \\ 0 & 0 & \epsilon_r \end{pmatrix},$$
(8)

where $\epsilon_r = 6.25, g = 0$ for nonmagnetic regime. Some examples of materials with magnetic properties that can be used in our switches are given in [19–22].

Using the free software MPB (MIT Photonic-Bands) [23], we have calculated the band diagram
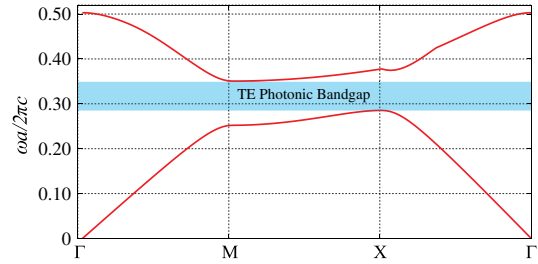
Fig. 6.   First and second TE frequency bands for nonmagnetized PhC.

of the PhC (Fig. 6). The TE photonic bandgap corresponds to the normalized frequencies $\omega a/2\pi c = 0.285$–0.35.

For our purposes we adapted the resonator structure suggested in [5] shown in Figs. 11 and 14. The main parameter for adjusting the resonator frequency is the radius of the central hole r_0. Using the commercial software COMSOL [24], we have calculated the change in frequency of the localized dipole mode in the nonmagnetized nonloaded resonator with respect to r_0 (Fig. 7). One can see that this parameter can be effectively used in the project of switch synthesis. In the magnetized nonloaded resonator, the splitting of the rotating modes $\mathbf{V}^+$ and $\mathbf{V}^-$ (see Section 3.B) with respect to the tensor parameter g is shown in Fig. 8.

5. Examples of Switches with 60° and 120° Bending

Two new compact optical switches based on a 2D PhC and a magneto-optical cavity are suggested and analyzed below. The resonator is front coupled to two PhC waveguides and operates with a dipole

Fig. 7.   Resonant frequency of dipole mode versus radius r_0 of resonator central hole.

Fig. 8.   Frequency splitting of dipole modes excited in an MO resonator, $r_0 = 0.8625a$.

mode. In case 1 the waveguides form a 60° bend, and in case 2 they form a 120° bend. When the cavity is nonmagnetized, the dipole mode excited by a signal in the input waveguide has a node in the output waveguide. Therefore, the input signal is refle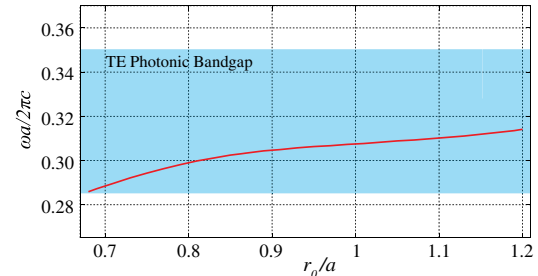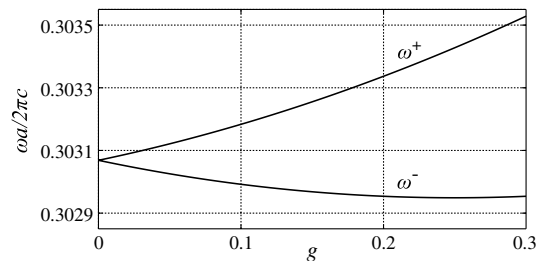cted from the cavity (state *off*). The application of a DC magnetic field $\mathbf{H}_0$ produces splitting of the frequencies ω^- and ω^+ of modes rotating in opposite directions. By adjusting the parameters of the magnetized MO resonator, one can choose one of these rotating modes (ω^- or ω^+). These modes are related to the propagation of the incident wave from input to output (state *on*).

The central frequency of the switches must be adjusted for the two states, magnetized and nonmagnetized. The properties of the PhC resonator in these two states are different (in particular, in the nonmagnetized state we have a standing wave but in the magnetized state a rotating wave). Therefore, even when the resonator is well projected for the magnetized state, in the nonmagnetized state it is not, and vice versa. We have used as the main parameters to adjust the two resonant frequencies the diameter of the central hole of the resonator, the ellipticity of this hole, and the orientation of the main axis of the ellipse.

Besides, we have modified the radius of four air holes located on the frontier between the two waveguides and the MO resonator (black circles in Figs. 11 and 14). By decreasing their radius to $0.25a$ (instead of $0.3a$) and by adjusting the parameter g, we have optimized our devices from the point of view of bandwidth.

Notice also that the rectilinear waveguides losses in both states of both switches were calculated. We then remove 2/3 of these losses corresponding to input and output waveguides from the calculated frequency responses of the devices.

A. Case 1: 60° Bend

In this case $g = 0.3$ and the Voigt parameter is $g/\epsilon_r = 0.048$. In Fig. 9 we show the frequency

Fig. 10. Frequency response of switch, 60° bend.

response of the switch for $g = 0$ (state *off*) for different parameters of the elliptical central hole (the semi-major axis, semi-minor axis, and the tilt angle). The maximum of the bandwidth corresponds to the following parameters: the semi-major axis of the central hole is $0.8629a$, the semi-minor axis is $0.8621a$, and the tilt angle 150°. The frequency responses for power transmission in this case are given in Fig. 10. As can be seen, at the central frequency

Fig. 9. Substitution of the circular central hole by an elliptical one, 60° bend.

No.	Semi-major axis	Semi-minor axis	Tilt angle φ	$g = 0$
1	$0.8646a$	$0.8604a$	150°	—
2	$0.8635a$	$0.8615a$	150°	—
3	$0.8629a$	$0.8621a$	150°	—
4	$0.8625a$	$0.8625a$		—
5	$0.8646a$	$0.8604a$	60°	—

Fig. 11. H_z distribution at central frequency of switch, 60° bend: (a) state *on* and (b) state *off*.
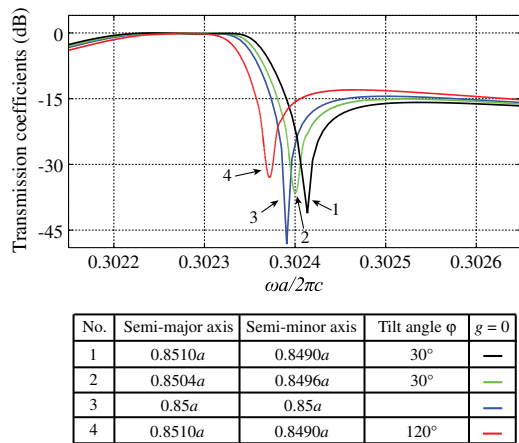
Fig. 12. Substitution of the circular central hole by an elliptical one, 120° bend.

No.	Semi-major axis	Semi-minor axis	Tilt angle φ	g = 0
1	0.8510a	0.8490a	30°	—
2	0.8504a	0.8496a	30°	—
3	0.85a	0.85a		—
4	0.8510a	0.8490a	120°	—

$\omega a/2\pi c = 0.30308$, the transmission coefficients are $P_{on} = -0.91$ dB and $P_{off} = -54$ dB.

The frequency band, defined at the levels -15 dB of the resonant curve for the *off* state and -2 dB of the resonant curve for the *on* state, is about 186 GHz.

In Fig. 11 we show the AC magnetic field component H_z at the central frequency for both cases [state *on*, Fig. 11(a) and state *off*, Fig. 11(b)].

B. Case 2: 120° Bend

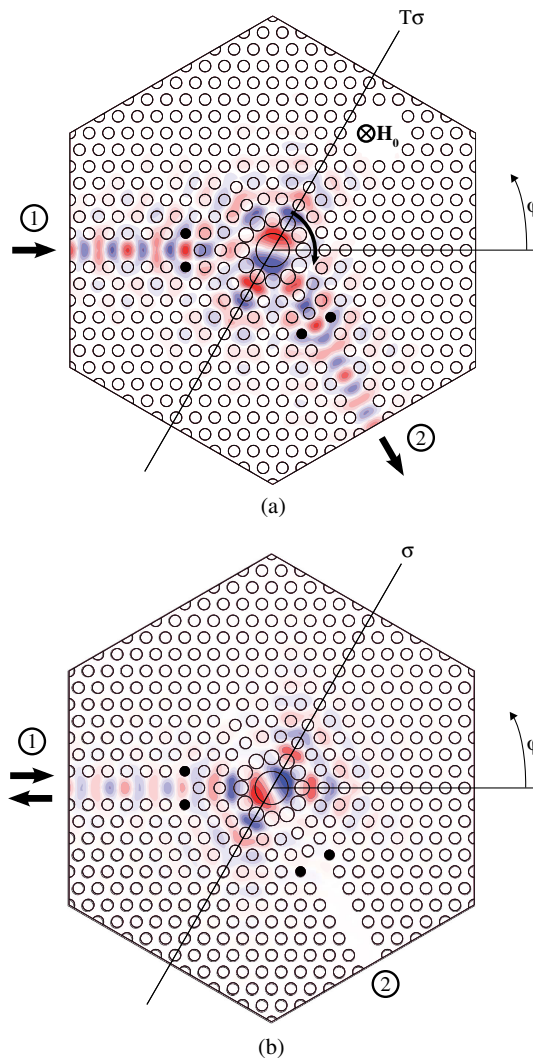The frequency response of the switch for $g = 0$ (state *off*) for different parameters of the elliptical central hole is given in Fig. 12.

The optimized parameters for this switch are $g = 0.26$, the Voigt parameter is $g/\epsilon_r = 0.0416$, the semi-major axis of the central hole is $0.8504a$, the semi-minor axis is $0.8496a$, and the tilt angle 30°. The frequency characteristics are shown in Fig. 13. At the central frequency $\omega a/2\pi c = 0.30235$, the transmission coefficients are $P_{on} = -1.55$ dB and $P_{off} = -53$ dB.

In this case the frequency band defined at the same levels as in the previous case is about 146 GHz. In Fig. 14 we show the field distribution inside the device ($\overline{H}_z$ component) at the central frequency in the state *on*, Fig. 14(a), and in the state *off*, Fig. 14(b).
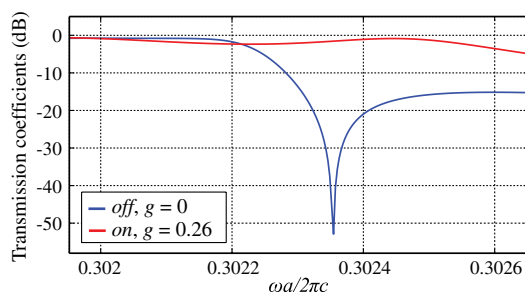
Fig. 13. Frequency response of switch, 120° bend.

(a)

(b)
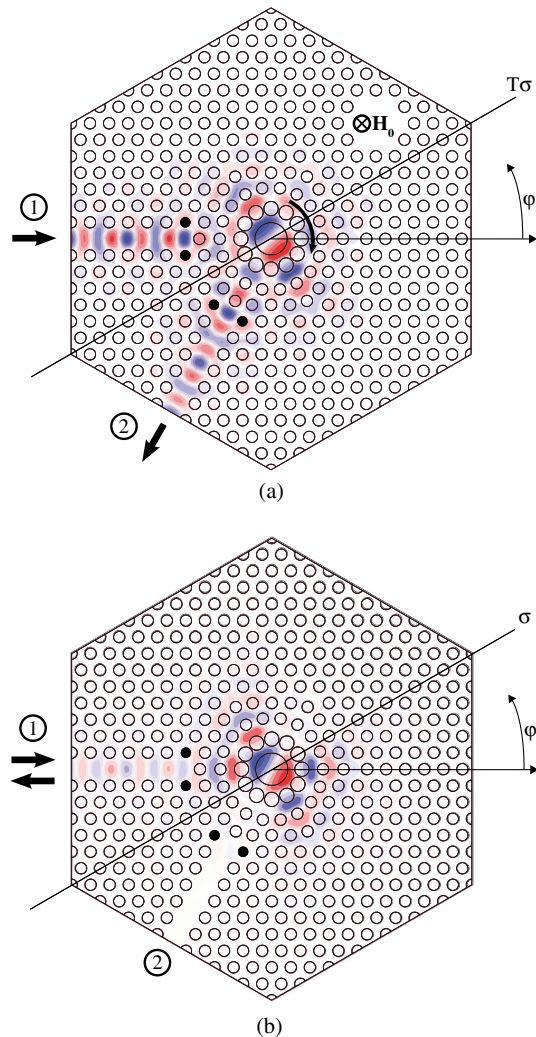
Fig. 14. H_z distribution at central frequency of switch, 120° bend. (a) state *on* and (b) state *off*.

6. Conclusion

In this paper we have discussed different geometries and symmetries of MO switches based on MO resonators in PhCs. Using magnetic group theory we have calculated the structure of the scattering matrices of the switches. We have suggested and analyzed two new switches with different angles of bending. This variety of switches with different types of coupling between the waveguides and the MO resonator and different angles of bending can provide more flexibility in design of new optical systems. We have also presented the characteristics of two switches with 60° and 120° bends and discussed the process of their optimization.

References

1. M. Yanik and S. Fan, "High-contrast all-optical bistable switching in photonic crystal microcavities," Appl. Phys. Lett. **83**, 2739–2741 (2003).

2. A. Sharkawy, S. Shi, and D. W. Prather, "Electro-optical switching using coupled photonic crystal waveguides," Opt. Express **10**, 1048–1059 (2002).

3. D. M. Beggs, T. P. White, L. Cairns, L. O'Faolain, and T. F. Krauss, "Ultrashort photonic crystal optical switch actuated by a microheater," IEEE Photon. Technol. Lett. **21**, 24–26 (2009).

4. Z. Wu, M. Levy, V. J. Fratello, and A. M. Merzlikin, "Gyrotropic photonic crystal waveguide switches," Appl. Phys. Lett. **96**, 051125 (2010).

5. W. Smigaj, J. Romero-Vivas, B. Gralak, L. Magdenko, B. Dagens, and M. Vanwolleghem, "Magneto-optical circulator designed for operation in a uniform external magnetic field," Opt. Lett. **35**, 568–570 (2010).

6. V. Dmitriev, M. Kawakatsu, and F. J. M. de Souza, "Compact three-port optical 2D photonic crystal-based circulator of W-format," Opt. Lett. **37**, 3192–3194 (2012).

7. Z. Wang and S. Fan, "Optical circulators in two-dimensional magneto-optical photonic crystal," Opt. Lett. **30**, 1989–1991 (2005).

8. V. Dmitriev, M. Kawakatsu, and G. Portela, "Compact optical switch based on 2D photonic crystal and magneto-optical cavity," Opt. Lett. **38**, 1016–1018 (2013).

9. V. Dmitriev, G. Portela, and D. Zimmer, "Possible mechanisms of switching in symmetrical two-ports based on 2D photonic crystals with magneto-optical resonators," Opt. Lett. **38**, 4040–4043 (2013).

10. L. H. Frandsen, A. Harpoth, P. I. Borel, and M. Kristensen, "Broadband photonic crystal waveguide 60° bend obtained utilizing topology optimization," Opt. Express **12**, 5916–5921 (2004).

11. J. D. Joannopoulos, S. G. Johnson, J. N. Winn, and R. D. Meade, *Photonic Crystals: Molding the Flow of Light* (Princeton, 2008).

12. V. Dmitriev, "Symmetry properties of 2D magnetic photonic crystals with square lattice," Eur. Phys. J. Appl. Phys. **32**, 159–165 (2005).

13. V. Dmitriev, "Permeability tensor versus permittivity one in theory of nonreciprocal optical components," Photon. Nanostr. Fundam. Appl. **11**, 203–209 (2013).

14. A. A. Barybin and V. A. Dmitriev, *Modern Electrodynamics and Coupled-Mode Theory: Application to Guided-Wave Optics* (Rinton, 2002).

15. Q. Wang, Z. Ouyang, K. Tao, M. Lin, and S. Ruan, "T-shaped optical circulator based on coupled magneto-optical rods and a side-coupled cavity in a square-lattice photonic crystal," Phys. Lett. A **376**, 646–649 (2012).

16. Z. Wang and S. Fan, "Magneto-optical defects in two-dimensional photonic crystals," Appl. Phys. B **81**, 369–375 (2005).

17. F. Fan, S.-J. Chang, C. Niu, Y. Hou, and X.-H. Wang, "Magnetically tunable silicon-ferrite photonic crystals for terahertz circulator," Opt. Commun. **285**, 3763–3769 (2012).

18. S.-H. Kim and Y.-H. Lee, "Symmetry relations of two-dimensional photonic crystal cavity modes," IEEE J. Quantum Electron. **39**, 1081–1085 (2003).

19. M. C. Sekhar, M. R. Singh, S. Basu, and S. Pinnepalli, "Giant Faraday rotation in $Bi_xCe_{3-x}Fe_5O_{12}$ epitaxial garnet films," Opt. Express **20**, 9624–9639 (2012).

20. E. L. Nagaev, "Ferromagnetic and antiferromagnetic semiconductors," Sov. Phys. Usp. **18**, 863–892 (1975).

21. S. Methfessel and D. C. Mattis, "Magnetic semiconductors," in *Handbuch der Physik*, S. Fliigge and H. P. J. Wijn, eds. (Springer, 1968).

22. A. K. Zvezdin and V. A. Kotov, *Modern Magneto-Optics and Magneto-Optical Materials* (IOP, 1997).

23. http://ab-initio.mit.edu.

24. www.comsol.com.

ARTIGO 4

Three-port circulators with low symmetry based on

photonic crystals and magneto-optical resonators

CrossMark

Three-port circulators with low symmetry based on photonic crystals and magneto-optical resonators

Victor Dmitriev[1] · Gianni Portela[1] · Leno Martins[1]

Abstract Three-port circulators based on magneto-optical resonators in 2D photonic crystals with low symmetry are investigated. We consider different geometries of the circulators in photonic crystals with triangular and square unit cells. All of the three-ports possess only one specific element of symmetry named antiplane of symmetry. The theoretical part of our paper concerns scattering matrix analysis for different regimes of circulation. In particular, we define the scattering matrices of ideal circulator and a special type of conditions which allow one to transform the non-reciprocal three-port in ideal circulator. One case of non-ideal circulators is considered as well. We also discuss some peculiarities of a special regime of the circulators when they are used as isolators. Finally, one example of the circulator simulations with calculated frequency responses in photonic crystals based on triangular unit cells is presented.

Keywords Integrated optics devices · Photonic crystals · Circulators · Isolators

1 Introduction

Non-reciprocal components such as isolators and circulators based on magneto-optical (MO) effects are used in optical communication systems to reduce undesirable harmful reflections which provoke instabilities and degradation of performance in optical circuits.

✉ Gianni Portela
  gianni_portela@hotmail.com

[1] Faculty of Electrical Engineering, Department of Electrical Engineering, Federal University of Para, Av. Augusto Correa, 01, Belém, Para 66075-900, Brazil

Circulators fulfill non-reciprocal transmission of electromagnetic signals in communications systems. The non-reciprocity can be obtained by applying a DC magnetic field to magneto-optical resonator. In a three-port circulator, two regimes of propagation exist (input port → output port): clockwise regime ($1 \rightarrow 2, 2 \rightarrow 3, 3 \rightarrow 1$) and counterclockwise regime ($1 \rightarrow 3, 3 \rightarrow 2, 2 \rightarrow 1$). The difference between both regimes is the direction of the applied DC magnetic field, and they are schematically represented in Fig. 1.

Different types of circulators in photonic crystals (PhCs) technology are described in the literature. Among them are traditional three-port Y-circulators in PhCs with triangular lattice in optical region [1,2] and in THz [3], W-circulator [4], and also T-circulator in PhCs with square lattice [5]. All of them are based on resonance of the standing dipole mode of the MO resonator. Another possible mechanism of circulation is described in [6] for the four-port circulator which works with a rotating quadrupole mode of the resonator. A multifunctional device based on circulators is described in [7].

In the circuit theory of the conventional three-port circulators of Y-type with threefold rotational symmetry, the symmetry and the unitary conditions give the following result: A matched and lossless non-reciprocal three-port is a perfect circulator [8]. Therefore, in the theory and experiments one needs to consider only one port and only to match it. This leads, in particular, to a possible representation of the circulator as a one-port and to a great simplification of analysis and synthesis of this component [8]. However, in photonic crystals, the threefold rotational symmetry and, consequently, an implementation of Y-circulators are possible only in triangular lattice and cannot be realized in square lattice. It can be shown that the highest possible symmetry for a three-port circulator in the square lattice is $C_s (C_1)$ (in Schoenflies notations) which corresponds to the so-called T-circulator.
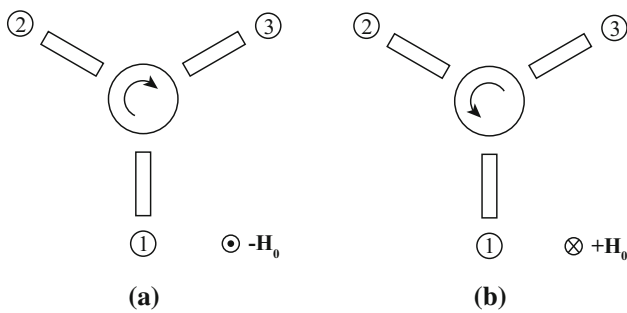
Fig. 1 Three-port circulator operating in **a** clockwise regime and **b** counterclockwise regime

In this work, we suggest and analyze new geometries of three-port circulators with symmetry $C_s(C_1)$. These electromagnetic components possess only one special element of symmetry which exists in magnetic groups [9]. More exactly, it is antiplane of symmetry. We discuss these components fulfilled on the basis of 2D photonic crystals with both square and triangle lattice and a resonator with MO material. The circulators can have different geometry; however, all of them possess the same symmetry and, consequently, they are described by the scattering matrix with the same structure. The number of the independent elements of this matrix is higher than that in case of Y-circulators.

A common mechanism of functioning of optical Y-circulators described in the literature is based on a standing wave which is a sum of clockwise (with frequency ω^+) and anticlockwise (with frequency ω^-) rotating dipole modes. The central frequency of the circulator in this case is $\omega_0 \approx (\omega^+ + \omega^-)/2$. Due to antisymmetry of the permittivity or permeability tensor, the standing wave in the resonator can be rotated by 30° and therefore oriented with a node in the isolated port. This provides a mechanism of circulation in geometries with threefold rotational symmetry. We will show that the mechanism of circulation in the discussed circulators is similar, but because of low symmetry, it has some peculiarities.

In the theoretical part of our paper, the scattering matrix of the three-ports with antiplane of symmetry is analyzed, and on this basis, some general properties of the three-ports are defined. One example of calculated characteristics of such circulators is presented as well.

2 Possible magnetic symmetries of 2D electromagnetic three-ports

The possible elements of symmetry for non-magnetic 2D three-ports are the rotations around z axis by $2\pi/3$ clockwise and anticlockwise (the elements C_3^{-1} and C_3, respectively) and three planes of symmetry σ_i ($i = 1, 2, 3$). These elements
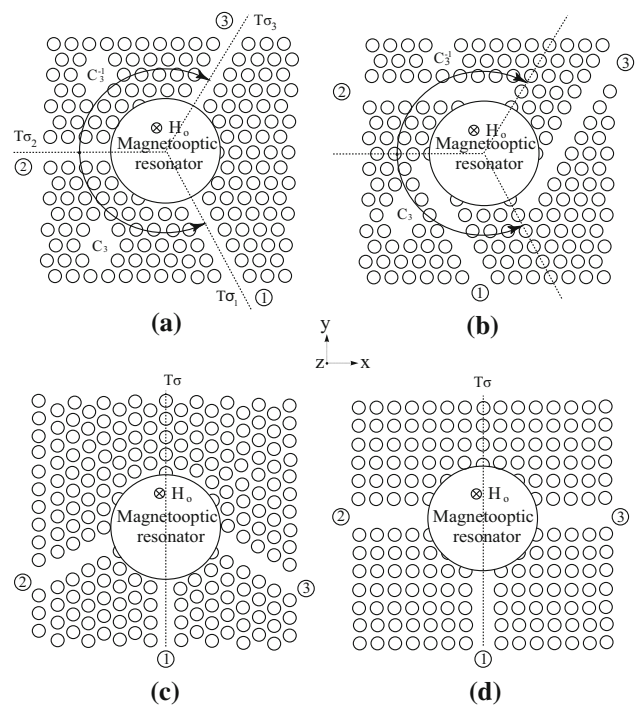
Fig. 2 Three-ports with their elements of symmetry: **a** circulator with symmetry $C_{3v}(C_3)$ with front coupling [2], **b** circulator with symmetry C_3 with side coupling [1], **c** W-circulator with symmetry $C_s(C_1)$ with front coupling [4], **d** T-circulator with symmetry $C_s(C_1)$ with front coupling [5]. $T\sigma$ is antiplane of symmetry, $\mathbf{H}_0$ is the applied DC magnetic field

together with the unit element e and the time reversal T form the group of the first category C_{3v}.

For magnetic components with DC magnetic field $\mathbf{H}_0$ oriented along the axis z, the possible symmetries are limited by two magnetic groups of the third category $C_{3v}(C_3)$ and $C_s(C_1)$ and one group of the second category $\mathbf{C}_3$. The group $C_{3v}(C_3)$ consists of the following elements: the unit element e, anticlockwise rotation around axis z by $2\pi/3$ C_3, clockwise rotation z by $2\pi/3$ C_3^{-1}, and three antiplanes of symmetry $T\sigma_i$, ($i = 1, 2, 3$) as shown in Fig. 2a. The group $\mathbf{C}_3$ contains three elements: e, C_3, and C_3^{-1}, and the time reversal does not enter in the group even in combination with other elements (see Fig. 2b). Finally, the group $C_s(C_1)$ has e and only one antiplane of symmetry $T\sigma$, Fig. 2c, d.

The scattering matrix of the three-ports described by groups $C_{3v}(C_3)$ and $\mathbf{C}_3$ is identical, and they are known from the theory of microwave circulators [8]:

$$[\mathbf{S}] = \begin{pmatrix} S_{11} & S_{12} & S_{13} \\ S_{13} & S_{11} & S_{12} \\ S_{12} & S_{13} & S_{11} \end{pmatrix}, \tag{1}$$

with three independent complex parameters. This matrix can be obtained using only the rotational symmetry element C_3. The elements $T\sigma_i$ ($i = 1, 2, 3$) of the group $C_{3v}(C_3)$ do not
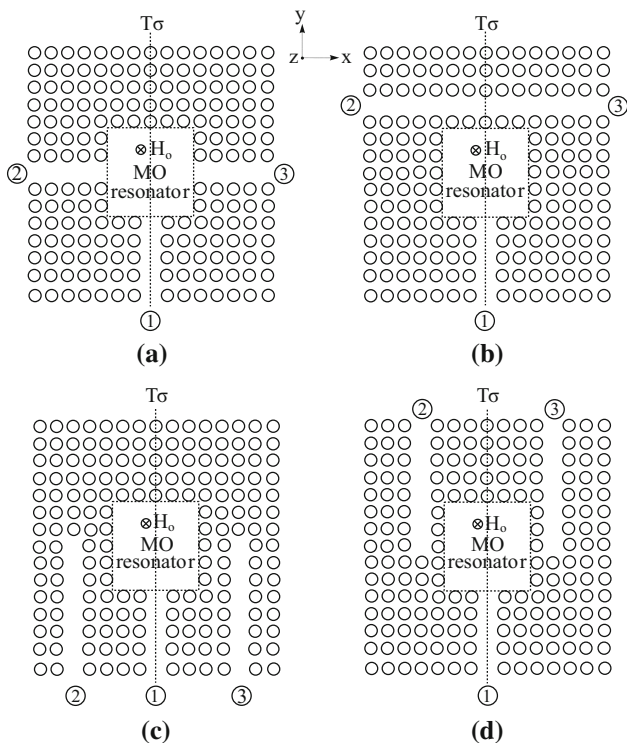
Fig. 3 Three-ports magnetized by DC magnetic field $\mathbf{H}_0$ MO resonator in square lattice: **a** T-type front–front–front coupling with 90° bending of ports 2 and 3 with respect to port 1, **b** T-type front–side–side coupling with 90° bending of ports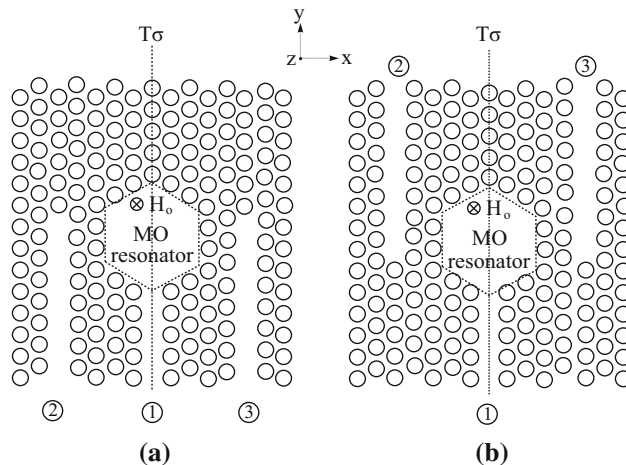 2 and 3, **c** octopus-like front–side–side coupling with 180° bending of ports 2 and 3, **d** fork-like front–side–side coupling without bending of ports 2 and 3. $T\sigma$ is antiplane of symmetry

give any new information. Alternatively, in case of the group $C_{3v}(C_3)$, one can use for the scattering matrices calculus any two of the antielements $T\sigma_i$.

Three-port circulators based on PhCs with the above symmetries are described in the literature: Y-circulators with the symmetry $C_{3v}(C_3)$ in [2], with the symmetry $\mathbf{C}_3$ in [1], W-circulator with the symmetry $C_s(C_1)$ in [4], and T-circulator, also with the symmetry $C_s(C_1)$, in [5]. Thus, in spite of different symmetry of unit cells and different geometry of waveguide connections to resonators, the W- and T-circulators have the same magnetic symmetry.

3 Problem description

We consider a junction consisting of a resonator with MO material and three waveguides coupled to the resonator. In Figs. 3 and 4, we denote schematically the resonators by a dotted square and a dotted hexagon, respectively, without specification of their internal structure. The three waveguides can be front-coupled or side-coupled to the resonator. In these figures, four different types of resonator–waveguide coupling for the structures with square lattice and two variants for triangle lattice are shown.

Fig. 4 Three-ports magnetized by DC magnetic field $\mathbf{H}_0$ MO resonator in triangle lattice: **a** octopus-like front–side–side coupling with 180° bending of ports 2 and 3, **b** fork-like front–side–side coupling without bending of ports. $T\sigma$ is antiplane of symmetry

The special symmetry of the three-ports under consideration leads to some peculiarities of their properties. Our objectives are to study characteristics of these structures starting from a general scattering matrix obtained in our previous publication [4] and to show feasibility of the circulators by one simulation example.

4 Scattering matrix analysis of non-reciprocal three-port with antiplane of symmetry

The scattering matrix [**S**] relates the incident **a** and the reflected waves **b** as follows: $\mathbf{b} = [S]\mathbf{a}$. The exact structure of this matrix for the three-port with antiplane of symmetry obtained in [4] by using the theory of magnetic groups is as follows:

$$[\mathbf{S}] = \begin{pmatrix} S_{11} & S_{12} & S_{13} \\ S_{13} & S_{22} & S_{23} \\ S_{12} & S_{32} & S_{22} \end{pmatrix}, \tag{2}$$

where the equalities $S_{21} = S_{13}$, $S_{31} = S_{12}$, $S_{33} = S_{22}$ are due to symmetry constraints. Thus, the matrix [**S**] has six independent complex parameters [compare with (1)].

Supposing small losses related to the MO material in the resonator and in the photonic crystal waveguides, some general properties of the three-port can be defined applying the unitary constraint on the scattering matrix $[\mathbf{S}]([\mathbf{S}]^*)^t = ([\mathbf{S}]^*)^t[\mathbf{S}] = [\mathbf{I}]$, where [**I**] is the 3×3 unit matrix [10]. For amplitudes of the matrix elements, one obtains:

(a) $|S_{11}|^2 + |S_{12}|^2 + |S_{13}|^2 = 1,$
(b) $|S_{13}|^2 + |S_{22}|^2 + |S_{23}|^2 = 1,$ (3)
(c) $|S_{12}|^2 + |S_{32}|^2 + |S_{22}|^2 = 1,$

and for phases

(a) $S_{11}S_{13}^* + S_{12}S_{22}^* + S_{13}S_{23}^* = 0,$
(b) $S_{11}S_{12}^* + S_{12}S_{32}^* + S_{13}S_{22}^* = 0,$ (4)
(c) $S_{13}S_{12}^* + S_{22}S_{32}^* + S_{23}S_{22}^* = 0,$

where $*$ means complex conjugation. Below, we shall use Eqs. (3) and (4) for analysis of the three-ports. On this stage, we do not specify details of the devices; therefore, the following analysis can be used for different types of waveguiding and resonator structures and for different resonator modes.

4.1 Ideal circulator

4.1.1 Conditions for perfect circulator in terms of ideal matching of all ports

In general theory of circulators, there is a theorem which states that any non-reciprocal three-port without losses ideally matched from all three ports is a perfect circulator [11]. In case of Y-circulator with threefold rotational symmetry $S_{11} = S_{22} = S_{33}$, one needs to match only one of its ports. This property is used in the problems of analysis and synthesis of circulators [12].

From the point of view of symmetry, our case is an intermediate one between the case of full rotational symmetry and the absence of symmetry because we need two conditions, namely $S_{11} = 0$ and $S_{22} = 0$. Analyzing Eqs. (3) and (4), one can easily come to the following two ideal scattering matrices:

$$[\mathbf{S}]_{id1} = \begin{pmatrix} 0 & 0 & e^{j\phi_{13}} \\ e^{j\phi_{13}} & 0 & 0 \\ 0 & e^{j\phi_{32}} & 0 \end{pmatrix} = e^{j\phi_{13}} \begin{pmatrix} 0 & 0 & 1 \\ 1 & 0 & 0 \\ 0 & e^{j(\phi_{32}-\phi_{13})} & 0 \end{pmatrix}$$
(5)

for the direction of circulation $(1 \to 2 \to 3 \to 1)$, and

$$[\mathbf{S}]_{id2} = \begin{pmatrix} 0 & e^{j\phi_{12}} & 0 \\ 0 & 0 & e^{j\phi_{23}} \\ e^{j\phi_{12}} & 0 & 0 \end{pmatrix} = e^{j\phi_{12}} \begin{pmatrix} 0 & 1 & 0 \\ 0 & 0 & e^{j(\phi_{23}-\phi_{12})} \\ 1 & 0 & 0 \end{pmatrix}$$
(6)

for the direction of circulation $(1 \to 3 \to 2 \to 1)$. In Eqs. (5) and (6), ϕ_{ij} are phases of the corresponding matrix elements. Notice that the equalities of phases $\phi_{21} = \phi_{13}$ and $\phi_{31} = \phi_{12}$ in the above equations follow from magnetic symmetry.

In the circulators with threefold rotational symmetry, all the unit matrix elements have the same phase, but it is not the case in our devices. Omitting common phase shifts $\exp(j\phi_{13})$ and $\exp(j\phi_{12})$, one can see that each of matrices (5) and (6) is defined by one phase angle, namely $(\phi_{32} - \phi_{13})$ and $(\phi_{12} - \phi_{13})$, respectively.

Obtaining Eqs. (5) and (6), we did not make any assumption about the sign of DC magnetic field $\mathbf{H}_0$. Therefore, these matrices are valid both for $+\mathbf{H}_0$ and $-\mathbf{H}_0$. Let us consider a case when matrix (5) corresponds to the magnetization with $+\mathbf{H}_0$ and matrix (6) to $-\mathbf{H}_0$. By changing the sign of $\mathbf{H}_0$, matrix (5) is transposed; therefore, one comes to equality $[S]_{id1}^t = [S]_{id2}$ with an additional restriction on the phases $(\phi_{32} - \phi_{13}) = (\phi_{23} - \phi_{12})$. Notice that transposition of the scattering matrix changes the direction of circulation.

4.1.2 Conditions for perfect circulator in terms of ideal matching and perfect isolation or full transmission

Below, we shall discuss some other conditions to transform a non-reciprocal lossless three-port with an antiplane of symmetry in an ideal circulator.

We start with the case of the ideally matched first port, i.e., $|S_{11}| = 0$ and ideal isolation of this port from port 2, i.e., $|S_{21}| = 0$. Using unitary condition (3a), one obtains $|S_{12}| = 1$. Then, using Eqs. (3b) and (3c), one comes to $|S_{32}| = |S_{22}| = 0$ and $|S_{23}| = 1$. In this way, we come to matrix (6). Analogously, starting with $|S_{11}| = 0$ and $|S_{31}| = 0$, one deduces $|S_{23}| = |S_{22}| = 0$ and $|S_{32}| = 1$ and obtains matrix (5).

The same logic can be used for the cases of ideal matching of ports 2 or 3, i.e., $|S_{22}| = |S_{33}| = 0$. However, a peculiarity can appear in the analysis of these cases. Let us demonstrate this by an example. If we use additionally to $|S_{22}| = 0$ the condition of ideal isolation of port 2 from port 1, i.e., $|S_{21}| = 0$, from Eq. (3b), we obtain $|S_{23}| = 1$. Then, from Eq. (4b), we have $S_{11}S_{13}^* = 0$ with two solutions. The first one gives $|S_{11}| = 0$ and $|S_{13}| = 1$, and this is the case of ideal circulator with matrix (5). The second possibility is $|S_{11}| = 1$ and $|S_{13}| = 0$, and this is not the case of a circulator. Instead, we have the scattering matrix for the modulus of its elements of the following form:

$$[\mathbf{S}] = \begin{pmatrix} 1 & 0 & 0 \\ 0 & 0 & 1 \\ 0 & 1 & 0 \end{pmatrix}.$$
(7)

Thus, this matrix describes a reciprocal three-port with port 1 completely isolated from port 2 and port 3.

Thus, we have shown that a non-reciprocal lossless three-port with antiplane of symmetry is transformed in ideal circulator if it is matched from port 1 and, additionally, if it has ideal transmission to or ideal isolation from any other of the two ports. For ideal matching of ports 2 and 3, one of the two possible solutions does not correspond to a circulator.

4.2 Imperfect circulator

Here, we give an example of scattering matrix analysis of imperfect circulators. Let us consider the case of matching

only ports 2 and 3, i.e., $S_{22} = S_{33} = 0$ but $S_{11} \neq 0$. Then, Eqs. (3) and (4) are written as follows:

(a) $|S_{11}|^2 + |S_{12}|^2 + |S_{13}|^2 = 1$,
(b) $|S_{13}|^2 + |S_{23}|^2 = 1$,   (8)
(c) $|S_{12}|^2 + |S_{32}|^2 = 1$.

and

(a) $S_{11}S_{13}^* + S_{13}S_{23}^* = 0$,
(b) $S_{11}S_{12}^* + S_{12}S_{32}^* = 0$,   (9)
(c) $S_{13}S_{12}^* = 0$.

Considering anticlockwise circulation ($1 \rightarrow 3 \rightarrow 2 \rightarrow 1$), from (9c), we have $S_{13} = 0$, and from (8b) $|S_{23}| = 1$. Choosing suitably reference planes, one can put $S_{11} = \alpha$ as a real number, and from (8a) and (8c), we derive $|S_{12}| = \sqrt{1 - \alpha^2}$ and $S_{32} = -\alpha$, respectively. The scattering matrix becomes

$$[S] = \begin{pmatrix} \alpha & \sqrt{1-\alpha^2} & 0 \\ 0 & 0 & 1 \\ \sqrt{1-\alpha^2} & -\alpha & 0 \end{pmatrix}. \qquad (10)$$

Thus, the element $S_{23} = 1$, i.e., there is ideal transmission from port 3 to port 2. Also, isolation of port 1 from port 3 and of port 2 from port 1 is ideal. However, isolation S_{32} and the insertion losses S_{12} and S_{31} are related to the level of port 1 matching $S_{11} = \alpha$. Analogously, one can analyze some other cases of an imperfect circulator, for example, non-ideal isolation ($|S_{ij}| \neq 0, i \neq j$) or non-ideal transmission ($|S_{ij}| \neq 1, i \neq j$).
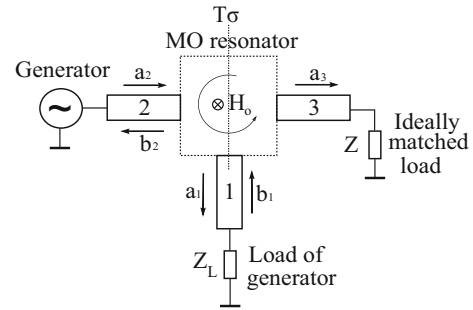
4.3 Circulator as isolator

As another example of the scattering matrix approach, we shall consider one important case of applications of the circulator, namely its use as an isolator. We shall investigate three connection schemes of ports.

A generator can be connected to port 2; i.e., it serves as the input port of the circulator. A mismatched load Z_L with the reflection coefficient Γ_L is linked to port 1, and an ideally matched load Z with the reflection coefficient $\Gamma_Z = 0$ to port 3 (see Fig. 5). The reflected waves from Z_L are absorbed in Z.

Due to the absence of reflections from Z, i.e., $\Gamma_Z = b_3/a_3 = 0$, one can reduce the scattering matrix (1) to the following 2×2 one:

$$[S] = \begin{pmatrix} S_{11} & S_{12} \\ S_{21} & S_{22} \end{pmatrix}, \qquad (11)$$

where $S_{21} = S_{13}$ by symmetry. The reflection coefficient $\Gamma_2 = b_2/a_2$ (see Fig. 5) in port 2 for this two-port in terms of the scattering matrix elements and the reflection coefficient of the load $\Gamma_L = b_1/a_1$ can be calculated as follows [12]:

Fig. 5 Non-reciprocal three-port with anticlockwise circulation as isolator. *1*, *2*, and *3* are waveguides. $T\sigma$ is antiplane of symmetry

$$\Gamma_2 = S_{22} + \frac{S_{12}S_{21}\Gamma_L}{1 - S_{11}\Gamma_L}. \qquad (12)$$

The parameters S_{11} and S_{22} of well-projected circulators are small, i.e., $|S_{11}| \approx |S_{22}| \approx 0$, and the transmission coefficients for the direction of circulation ($1 \rightarrow 3 \rightarrow 2 \rightarrow 1$) are $|S_{12}| \approx 1$ and $|S_{21}| \approx 0$. Therefore, the product of two small numbers $S_{11}\Gamma_L$ can be neglected and one can approximate (12) as follows:

$$\Gamma_2 \approx S_{22} + S_{12}S_{21}\Gamma_L. \qquad (13)$$

Omitting for simplicity the phases of Γ and $[S]$ elements, one can see that in comparison with $|\Gamma_L|$, the reflection coefficient $|\Gamma_2|$ is reduced approximately by the factor $1/|S_{12}S_{21}|$. Thus, the reduction in the reflection coefficient Γ_2 due to the circulator is directly related to the level of isolation $|S_{21}|$ of input port 2 from output port 1. This should be taken into consideration in cases where the load Z_L presents a large mismatch and the generator is very sensible to reflections which are defined by Γ_2. Now, if we consider an imperfect circulator described by matrix (10), from (12) we obtain $\Gamma_2 = \alpha$.

Analogously, for the generator in port 1, one can obtain

$$\Gamma_1 = S_{11} + \frac{S_{13}S_{31}\Gamma_L}{1 - S_{33}\Gamma_L} \approx S_{11} + S_{13}S_{31}\Gamma_L, \qquad (14)$$

For an imperfect circulator described by matrix (10), we obtain $\Gamma_1 = \alpha$.

For the generator in port 3, we have

$$\Gamma_3 = S_{33} + \frac{S_{23}S_{32}\Gamma_L}{1 - S_{22}\Gamma_L} \approx S_{33} + S_{23}S_{32}\Gamma_L. \qquad (15)$$

Considering again the imperfect circulator described by matrix (10), we obtain $\Gamma_3 = -\alpha\Gamma_L$; i.e., in contrast to the cases of generator in port 1 and 2, the coefficient Γ_3 depends both on α and Γ_L.

Another aspect of the case "circulator as isolator" is related to bandwidth of the device. If in a project of the circulator with generator in port 2 one succeeded to achieve a sufficient frequency band for the parameters S_{21} and S_{12} (channel $1 \leftrightarrow 2$),

with a good matching of port 2, i.e., for a low value of S_{22} in the desired band, the frequency band of our component will be defined mostly by the parameters S_{21} and S_{12} [see (14)]. If the circulator has a lower bandwidth for channel 2 ↔ 3, (see an example in Sect. 5 below), this will not affect the bandwidth of the isolator because S_{23} and S_{32} do not enter in (13).

The same is true for the case of generator in port 1, because due to symmetry the scattering matrix elements S_{13} and S_{31} (channel 1 ↔ 3) will have the same frequency characteristics as S_{21} and S_{12}, respectively, and S_{23} and S_{32} do not enter in (14). Besides, from symmetry we have $S_{12}S_{21} = S_{13}S_{31}$; therefore, the choice between the schemes "generator in port 1" and "generator in port 2" will depend on the frequency dependence of the parameters S_{11} and S_{22} [compare (13) and (14)].

However, if the channel 2 ↔ 3 has a lower bandwidth in comparison with that of 1 ↔ 2, and if one put generator in port 3 [see (15)], the frequency band of the isolator will be reduced. Resuming, the choice of the scheme of generator connection in the isolator regime depends on the frequency characteristics of the circulator.

5 Numerical simulations

Below, we shall give one example of numerical analysis of the circulators with low symmetry. The calculations are related to the fork-like circulator shown in Fig. 4b. The presented simulation results were obtained by using the software products COMSOL [13] and MPB [14]. As can be seen in Fig. 4b, this device is based on a 2D PhC with triangular lattice of air holes etched on a MO material. The lattice constant is a, and the radius of the air holes is $0.3a$.

The magnetic permeability of the MO material is $\mu = \mu_0$, and its electric permittivity tensor is defined as follows:

$$[\epsilon] = \epsilon_0 \begin{pmatrix} \epsilon_r & -ig & 0 \\ ig & \epsilon_r & 0 \\ 0 & 0 & \epsilon_r \end{pmatrix}, \qquad (16)$$

where $\epsilon_r = 6.25$ and $g = 0.3$ (this parameter for existing MO materials can be found, for example, in [15–18]). The off-diagonal element g of the tensor $[\epsilon]$ is proportional to the applied DC magnetic field $\mathbf{H}_0$.

5.1 Optical fork-like circulator in PhC with triangle lattice

The physical and geometrical parameters of the circulator are given in Appendix. The idea of the resonator structure is borrowed from [2]. Some modifications were made in our resonator in order to adapt it to the new geometry of the
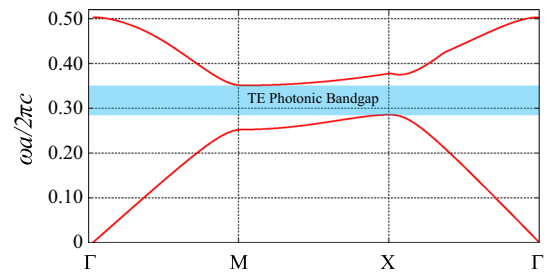

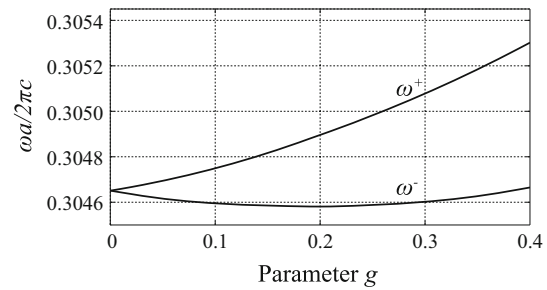**Fig. 6** Band diagram of photonic crystal (Color figure online)

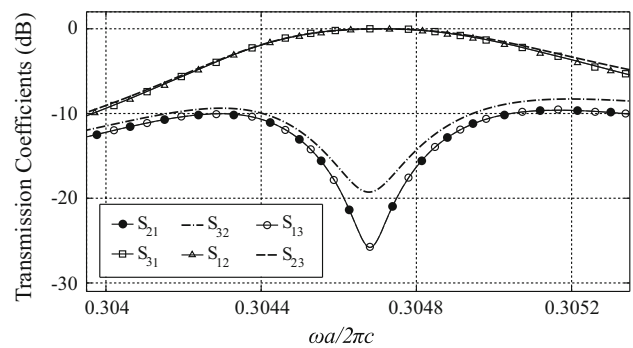**Fig. 7** Frequency splitting of rotating modes ω^+ and ω^-

Fig. 8 Frequency response of fork-like circulator

circulator. The waveguides support TE modes with H_z, E_x, and E_y components of electromagnetic field.

The calculated band structure of the PhC is shown in Fig. 6, and the frequency splitting of the rotating modes ω^+ and ω^- is shown in Fig. 7. The frequency responses for different port excitations are presented in Fig. 8, and the electromagnetic field structure for the central frequency $\omega a/2\pi c = 0.30467$ is given in Fig. 9 (the direction of circulation is $1 \rightarrow 3 \rightarrow 2 \rightarrow 1$). The parameters of the circulator are as follows: The central frequency is $\omega a/2\pi c = 0.30467$, the insertion losses are less than -0.45 dB, and isolation is higher than -15 dB in the frequency band 173 GHz (at $\lambda = 1.55\,\mu$m) for ports 1 and 3 and 133 GHz for port 2.

By scrutinizing Fig. 9, one can see that the field distribution of the dipole mode at the central frequency is approximately the same in the input and output waveguides, while its node is orientated in the direction of the isolated waveguide. This special orientation of the dipole mode is fundamental to
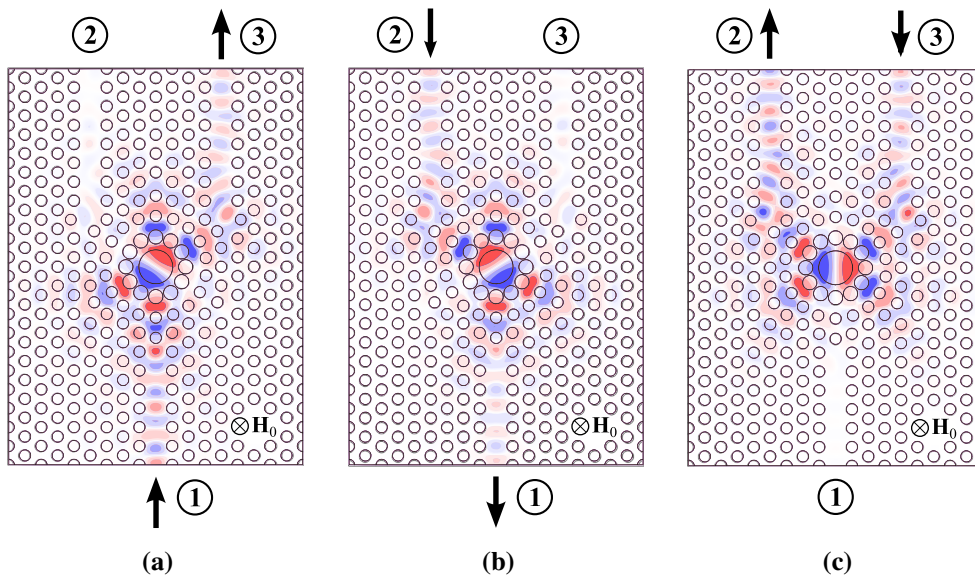
Fig. 9 H_z distribution at central frequency for excitation at **a** port 1, **b** port 2, and **c** port 3 (Color figure online)
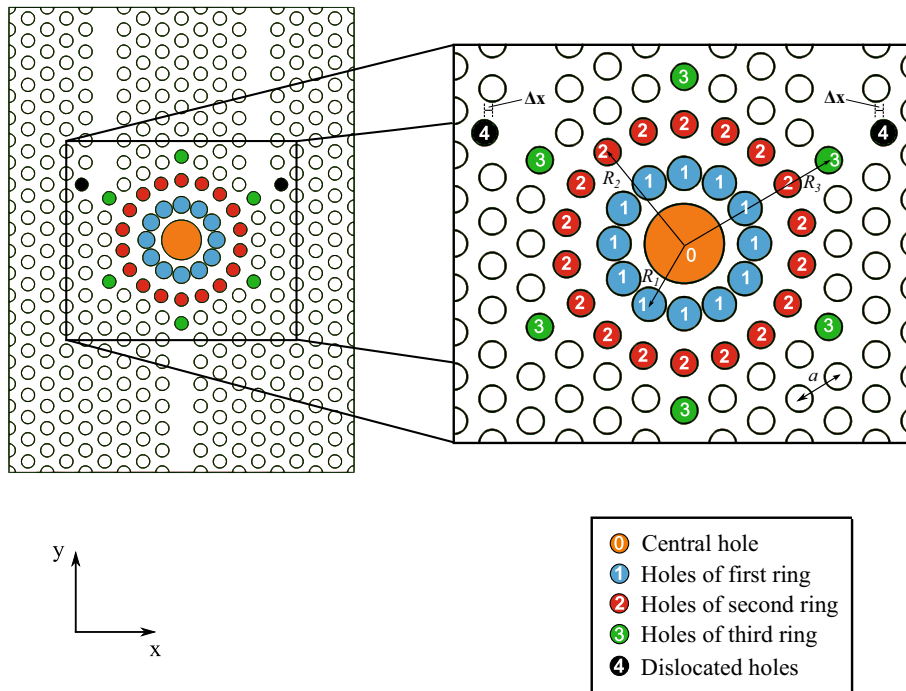
Fig. 10 Geometry of circulator (Color figure online)

the operation of the proposed circulator, and it can be adjusted by tuning the geometrical parameters of the resonator and the intensity of the applied DC magnetic field $\mathbf{H}_0$.

6 Conclusions

We have investigated in this work circulators with low symmetry. Several new geometries of such circulators were suggested. We have discussed some peculiarities of the circulators using their scattering matrix. The fulfilled matrix analysis is quite general because it is based only on symmetry and unitary constraints. Therefore, this analysis can be applied to circulators with antiplane of symmetry which are based on other technologies.

The frequency characteristics of the circulators for excitation of different ports can be different because of the low symmetry. This property should be taken into consideration
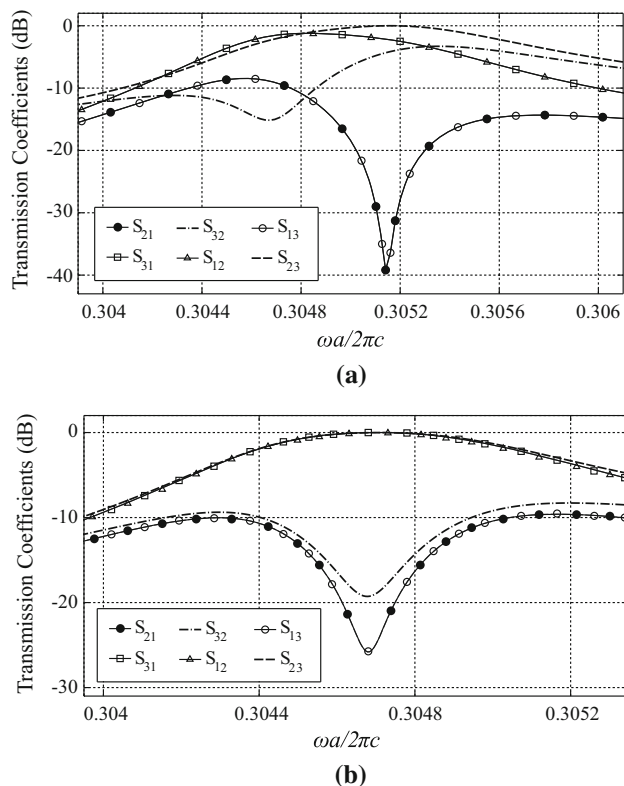
Fig. 11 Frequency response of device in **a** non-optimized case and **b** optimized case

in the projects of photonic circuits. Some consequences of the differences in frequency responses have been discussed.

We have given also one example of numerical simulations of the circulators, namely fork-like circulator with TE mode in crystal with triangular lattice. The presented variety of circulator geometries can provide a flexibility in design of optical integrated circuits and a reduction in their dimensions.

Appendix: Details of optical fork-type circulator

A detailed geometry of the proposed optical fork-like circulator is given in Fig. 10. The periodic structure of the employed PhC is represented by the circular white holes (unnumbered ones) in Fig. 10. Each of them has radius equal to $0.3a$, where a is the lattice constant. For $\lambda = 1.55\,\mu$m, $a = 480$ nm.

The resonant cavity corresponds to the central part of the device (circular holes No. 0, 1, 2, and 3). The radius of the orange central hole (No. 0) is $0.9a$. The radius of 12 blue holes (No. 1) is $0.38a$, and they form the ring with radius $R_1 = 1.58a$. On the other hand, the radius of 18 red holes (No. 2) is $0.3a$ and they form the ring with radius $R_2 = 2.69a$.

Finally, the radius of six green holes (No. 3) is $0.3a$ and they form the ring with radius $R_3 = 3.76a$.

One needs to project geometry of the resonator that provides at the central frequency of the circulator the maximum values of isolation and the minimum values of insertion losses for all the ports. In Fig. 11a, one can see that the direct connections of port 2 and port 3 to the resonator without any modification give a large dislocation of the peak of S_{32} in comparison with S_{13} and S_{21}. In order to solve this problem, we have modified two black holes (No. 4). In the non-optimized circulator, the radius of them is $0.3a$ and $\Delta x = 0$. Choosing the radius of these holes equal to $0.288a$ and $\Delta x = 0.173a$, we come to the frequency responses of the circulator shown in Fig. 11b.

References

[1] Wang, Z., Fan, S.: Optical circulators in two-dimensional magneto-optical photonic crystals. Opt. Lett. **30**, 1989–1991 (2005)

[2] Smigaj, W., Romero-Vivas, J., Gralak, B., Magdenko, L., Dagens, B., Vanwolleghem, M.: Magneto-optical circulator designed for operation in a uniform external magnetic field. Opt. Lett. **35**, 568–570 (2010)

[3] Fan, F., Chang, S.J., Niu, C., Hou, Y., Wang, X.H.: Magnetically tunable silicon-ferrite photonic crystals for terahertz circulator. Opt. Commun. **285**, 3763–3769 (2012)

[4] Dmitriev, V., Kawakatsu, M., Souza, F.: Compact three-port optical 2D photonic crystal-based circulator of W-format. Opt. Lett. **37**, 3192–3194 (2012)

[5] Wang, Q., Ouyang, Z., Tau, K., Lin, M., Ruan, S.: T-shaped optical circulator based on coupled magneto-optical rods and a side-coupled cavity in a square-lattice photonic crystal. Phys. Lett. A **376**, 646–649 (2012)

[6] Wang, Z., Fan, S.: Suppressing the effect of disorders using time-reversal symmetry breaking in magneto-optical photonic crystals: An illustration with a four-port circulator. Photonics Nanostructures Fundam. Appl. **4**, 132–140 (2006)

[7] Dmitriev, V., Portela, G.: Multifunctional two-dimensional photonic crystal optical component based on magneto-optical resonator: nonreciprocal two-way divider-switch, nonreciprocal 120 deg bending-switch, and three-way divider. Opt. Eng. **53**, 115102 (2014)

[8] Helszajn, J.: Nonreciprocal Microwave Junctions and Circulators. Wiley, New York (1975)

[9] Barybin, A., Dmitriev, V.: Modern Electrodynamics and Coupled-Mode Theory: Application to Guided-Wave Optics. Rinton, New Jersey (2002)

[10] Helszajn, J.: The Stripline Circulators: Theory and Practice. Wiley-IEEE Press, New Jersey (2008)

[11] Lax, B., Button, K.: Microwave Ferrites and Ferrimagnetics. McGraw-Hill, New York (1962)

[12] Sadiku, M.: Elements of Electromagnetics. Oxford University Press, New York (2014)

[13] www.comsol.com

[14] http://ab-initio.mit.edu/mpb/

[15] Sekhar, M.C., Singh, M.R., Basu, S., Pinnepalli, S.: Giant faraday rotation in $Bi_xCe_{3-x}Fe_5O_{12}$ epitaxial garnet films. Opt. Express **20**, 9624–9639 (2012)

[16] Nagaev, E.L.: Ferromagnetic and antiferromagnetic semiconductors. Sov. Phys. Uspekhi **18**, 863–892 (1975)
[17] Methfessel, S., Mattis, D.C.: Magnetic Semiconductors (in Handbuch der Physik). Springer, Berlin (1968)
[18] Zvezdin, A.K., Khotov, V.A.: Modern Magneto-Optics and Magneto-Optical Materials. IOP, Bristol (1997)

Victor Dmitriev received the M.Eng. and PhD degrees in electrical engineering from the Bauman Moscow State University, Moscow, Russia, in 1971 and 1977, respectively. His research interest includes group theoretical methods in electromagnetic theory, propagation of electromagnetic waves in complex media, metamaterials, antennas and nanoantennas, photonic crystals, nanoelectronics, and nanophotonics. He published more than 200 conference papers, 100 journal papers, two books, and six book chapters.

Gianni Portela is a PhD student at the Federal University of Para. He received his BS in mathematics in 2006 from the Para State University and his BS and MS degrees in electrical engineering from the Federal University of Para in 2007 and 2008, respectively. He is an author of 5 journal papers and 8 patent grant requests related to passive devices based on photonic crystals. His current research interests include photonic crystals-based devices, like switches, dividers, and circulators.

Leno Martins is an MSc student at the Federal University of Para. He received his BS in computer engineering from the Federal University of Para in 2013. His research interests are related to the development of photonic crystals-based circulators.

ARTIGO 5

Optical component: nonreciprocal three-way divider based on magneto-optical resonator

Optical component: nonreciprocal three-way divider based on magneto-optical resonator

Victor Dmitriev* and Gianni Portela

Department of Electrical Engineering, Federal University of Para, P.O. Box 8619, Agencia UFPA,
CEP 66075-900, Belem, Para, Brazil

*Corresponding author: victor@ufpa.br

We suggest and analyze a new compact nonreciprocal optical component based on a magneto-optical (MO) resonator. This component fulfills simultaneously two functions, namely, equal division of the input signal between three output ports and isolation of the input port from output ones. Using group theory, we analyze the scattering matrix of this symmetrical component. Our numerical results for one of the possible schemes of the divider based on 2D photonic crystal with MO material demonstrate that, at the central frequency, the division of the signal between the three output ports is about −6.4 dB. The variation of the division levels in the output ports in this band is (−6.4 ± 0.4) dB. For two of the output ports, the calculated bandwidth for the level −20 dB of the isolation is around 219 GHz at the wavelength 1.55 μm. For the third output port, the isolation at the central frequency is about −6 dB.   © 2013 Optical Society of America

OCIS codes: (130.3120) Integrated optics devices; (230.5298) Photonic crystals.
http://dx.doi.org/10.1364/AO.52.006657

1. Introduction

In microwave technology, two-port isolators and three-port circulators are widely used as nonreciprocal components. In the last 5–8 years, it was shown that such components can also be implemented in optical photonic bandgap structures [1–5]. Many other photonic crystal (PhC) reciprocal components have been investigated as well, among them power dividers [6].

In [7], we suggested a new nonreciprocal optical component which fulfills simultaneously two functions: division of an optical signal between two output channels and isolation of the input port from the two output ones. An advantage of this component is a significant reduction of scheme dimensions in comparison with the combination of two separated components (namely, a reciprocal divider and an isolator or a circulator), which fulfill the same functions.

Another optical component based on magneto-optical (MO) resonator, namely, a three-way switchable power divider, was investigated in [8]. It is a four-port device. The deficiencies of this component are small bandwidth and low isolation of the input port from the output ones.

In this paper, we suggest a new nonreciprocal three-way divider with improved characteristics in comparison with that discussed in [8]. We suggest the use of a six-port symmetrical component with MO resonator. It works with uniform magnetization, and has a good bandwidth and high isolation of the input port from output ones. The last property is important to protect the generator in the input port from harmful reflections from nonideally matched elements in the output ports.

2. Geometry, Symmetry, and Scattering Matrix

In this section, we present symmetry analysis of the suggested component which fulfills simultaneously two functions: equal division of the input signal between three output channels and isolation of the

input port from three output ones. This is a nonreciprocal three-way divider. We shall consider a multiport with a resonator with MO material magnetized uniformly by a dc magnetic field $\mathbf{H}_0$ in the direction normal to the plane of multiport $x0y$ (see the coordinate system in Fig. 1). The multiport under consideration is shown schematically in Fig. 1(a).

The number of ports of the suggested divider is six: one input port, three output ports where the input signal is divided, and two additional ports terminated with ideally matched loads. In these two loads, the signals, due to undesirable reflections in the output ports, are absorbed so that the input port is isolated from the output channels.

In Fig. 1(b), we sketched the six-port for the case of a nonmagnetized material, i.e., for the case of $\mathbf{H}_0 = 0$. The big dotted circle in this figure confines a resonator, and two smaller circles show idealized field distributions of the dipole standing wave inside the resonator. Six equal waveguides numbered by 1, 2,..., 6 are connected to the resonator. The input port is denoted by arrow. One can see that in this case we have nonequal division of the input signal between all the other ports 2, 3, 4, 5, and 6. In the following, we will show that, in the magnetized state of the resonator, it is possible to achieve equal −5 dB division [more exactly, $10\log_{10}(P_{\mathrm{out}}/P_{\mathrm{in}}) = 10\log_{10}(1/3) = -4.77$ dB] between three output ports.

The following analysis of the six-port will be fulfilled in terms of its scattering matrix. The amplitudes of the incident and reflected waves in the multiport can be represented by six-dimensional vectors of the electric field $\mathbf{E}^i = (E_{z1}^i, E_{z2}^i, ..., E_{z6}^i)^t$ and $\mathbf{E}^r = (E_{z1}^r, E_{z2}^r, ..., E_{z6}^r)^t$, respectively, where t denotes transposition. They are defined by $E_{zn}^i \exp j(\omega t - \mathbf{k}_n^i \cdot \mathbf{r})$ and $E_{zn}^r \exp j(\omega t - \mathbf{k}_n^r \cdot \mathbf{r})$, respectively, where j is the imaginary unit, E_{zn}^i and E_{zn}^r are complex amplitudes of the eigenmodes in the n port, and $\mathbf{k}_n$ is the corresponding wave vector. Analogously, the description can be made in terms of magnetic field components H_{zn}^i and H_{zn}^r. The incident and the reflected waves in the six-port are related by 6×6 scattering matrix $[S]$ as follows: $\mathbf{E}^r = [S]\mathbf{E}^i$ or $\mathbf{H}^r = [S]\mathbf{H}^i$.

We start our analysis using symmetry approach. We shall consider a device with the highest possible symmetry, i.e., with the six-fold rotational one. In PhCs, this symmetry is possible in structures with hexagonal unit cell. Thus, the nonmagnetic symmetry of the six-port is C_{6v} (in Schoenflies notations [9]) with the following elements: C_6-anticlockwise rotation by $\pi/3$, C_6^{-1}-clockwise rotation rotation by $\pi/3$, C_3-anticlockwise rotation by $2\pi/3$, C_3^{-1}-clockwise rotation by $2\pi/3$, and C_2-rotation by π. The group contains also twelve vertical planes of symmetry $\sigma_i (i = 1, 2, ..., 12)$.

In the magnetic state, the group is $C_{6v}(C_6)$ which contains the same rotational elements as C_{6v}. However, the planes are transformed into antielements of symmetry [9] which are six vertical antiplanes of symmetry $T\sigma_i' (i = 1, 2, ..., 6)$ which pass through the center and two opposite ports, and six vertical antiplanes of symmetry $T\sigma_i'' (i = 1, 2, ..., 6)$, which pass through the center and between the ports. The elements C_6, $T\sigma_i'$ and $T\sigma_i''$ are shown in Fig. 1(a).

It can be shown [9] that for symmetry analysis of the scattering matrix $[S]$ of the six-port component, we can use only one symmetry element, namely C_6. In order to calculate the structure of the 6×6 scattering matrix which is dictated by symmetry $C_{6v}(C_6)$, we need the 6×6 matrix representation $[R]_{C_6}$ of the element C_6. The matrix $[R]_{C_6}$ is

$$[R]_{C_6} = \begin{pmatrix} 0 & 0 & 0 & 0 & 0 & 1 \\ 1 & 0 & 0 & 0 & 0 & 0 \\ 0 & 1 & 0 & 0 & 0 & 0 \\ 0 & 0 & 1 & 0 & 0 & 0 \\ 0 & 0 & 0 & 1 & 0 & 0 \\ 0 & 0 & 0 & 0 & 1 & 0 \end{pmatrix}. \tag{1}$$

This matrix is written as follows. After anticlockwise rotation by $\pi/3$, the port 1 occupies the position of port 6 [see Fig. 1(a)]. Therefore, in position (1,6) of the matrix $[R]_{C_6}$ we put the number 1, and in the other positions of line 1 and of column 6 we put 0 s. Analogously, we have the number 1 in position (2,1), in position (3,2), etc.

The commutation relation $[R]_{C_6}[S] = [S][R]_{C_6}$ for the rotation by $\pi/3$ allows us to calculate the $[S]$ matrix structure [9]. Thus, due to C_6 symmetry, we have the following relations between the matrix elements: $S_{21} = S_{16}$, $S_{22} = S_{11}$, $S_{31} = S_{12}$, etc. Notice that, due
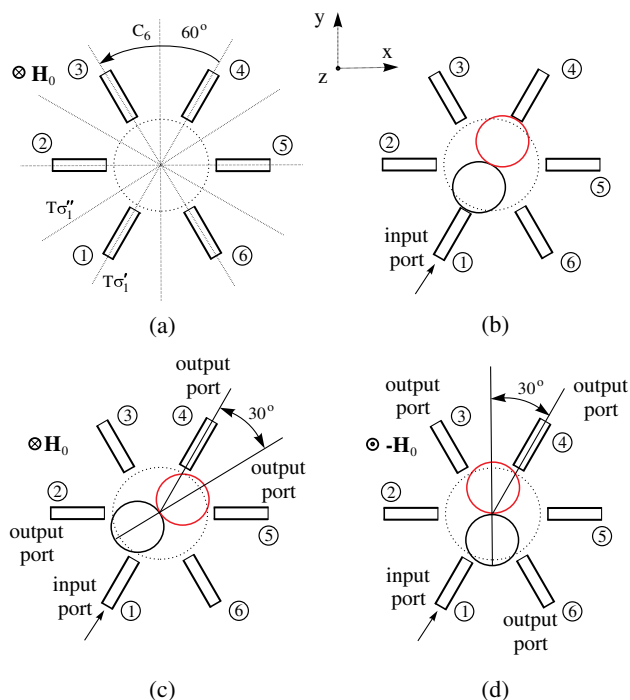

Fig. 1. Six-port with dipole mode resonator: (a) symmetry elements of magnetic group $C_{6v}(C_6)$, (b) dipole mode without magnetization, (c) dipole mode rotated by dc field $\mathbf{H}_0$ by 30° clockwise, and (d) dipole mode rotated by dc field $-\mathbf{H}_0$ by 30° anticlockwise.

to the symmetry nature, these relations are frequency independent. Notice also that the antiunitary elements $T\sigma_i'$ and $T\sigma_i''$ do not give any new information about the matrix $[S]$.

As a result, the calculated scattering matrix of the six-port is as follows:

$$[S] = \begin{pmatrix} S_{11} & S_{12} & S_{13} & S_{14} & S_{15} & S_{16} \\ S_{16} & S_{11} & S_{12} & S_{13} & S_{14} & S_{15} \\ S_{15} & S_{16} & S_{11} & S_{12} & S_{13} & S_{14} \\ S_{14} & S_{15} & S_{16} & S_{11} & S_{12} & S_{13} \\ S_{13} & S_{14} & S_{15} & S_{16} & S_{11} & S_{12} \\ S_{12} & S_{13} & S_{14} & S_{15} & S_{16} & S_{11} \end{pmatrix}. \quad (2)$$

Thus, the number of independent complex parameters S_{ij}, $i,j = 1,2,\ldots,6$ of the scattering matrix has been reduced from 36 to 6.

For reciprocal case without magnetization, the matrix has the property $[S] = [S]^t$, so that there are two additional restrictions on its matrix elements: $S_{16} = S_{12}$ and $S_{15} = S_{13}$ [see Fig. 1(b)] and the number of independent matrix elements is reduced to four. But in the following, we shall not consider this case.

Below, we will describe the divider using the scattering matrix in terms of power $P_{ij} = |S_{ij}|^2$, i.e., for simplicity, we exclude from consideration phases of the elements S_{ij}. We put the following desired restrictions on the elements of the scattering matrix $[P]$: $P_{21} = P_{41} = P_{51} = 1/3$ (Fig. 2). We shall also consider the ideally matched device with $P_{ii} = 0$, $i = 1,\ldots,6$. All these requirements allow us to write the desired matrix $[P]$ as follows:

$$[P] = \begin{pmatrix} 0 & 0 & 1/3 & 1/3 & 0 & 1/3 \\ 1/3 & 0 & 0 & 1/3 & 1/3 & 0 \\ 0 & 1/3 & 0 & 0 & 1/3 & 1/3 \\ 1/3 & 0 & 1/3 & 0 & 0 & 1/3 \\ 1/3 & 1/3 & 0 & 1/3 & 0 & 0 \\ 0 & 1/3 & 1/3 & 0 & 1/3 & 0 \end{pmatrix}. \quad (3)$$

This matrix satisfies partially the requirement of being unitary (which is $[S]([S]^*)^t = ([S]^*)^t[S] = [I]$ [10] where $[I]$ is the 6×6 unit matrix) since the sum of the elements in every column and in every line in Eq. (3) is equal to 1.
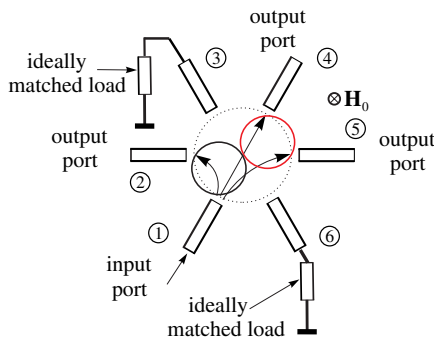

Fig. 2. Details of divider in Fig. 1(c) with two matched loads. Arrows inside the resonator show division of incident wave.

Matrix (3) is nonsymmetrical with respect to the main diagonal and, consequently, the corresponding six-port is nonreciprocal. Notice also a peculiarity of this matrix: input port 1 is completely decoupled from ports 2 and 5, because $P_{12} = 0$ and $P_{15} = 0$, and partially decoupled from port 4 ($P_{14} = 1/3$).

Providing in matrix (2) the conditions $|S_{11}| = 0$ (matching), $|S_{21}| = 1/\sqrt{3}$ (division of signal), $|S_{31}| = 0$ (decoupling port 1 from port 3), $|S_{41}| = 1/\sqrt{3}$ (division of signal), $|S_{51}| = 1/\sqrt{3}$ (division of signal), and $|S_{61}| = 0$ (decoupling port 1 from port 6), we come from matrix (2) to the desired matrix (3). Below, we will show that all these conditions can be fulfilled using magnetized MO resonator with dipole mode.

3. Operating Principle of Divider

We assume that in nonmagnetic state, the resonator of the divider supports two degenerate localized modes rotating in opposite directions. Their superposition gives a standing dipole mode shown in Fig. 1(b). At ports 2, 3, 4, 5, and 6, the electromagnetic field of this mode excites electromagnetic waves in the corresponding waveguides. The division of the input signal is not equal and the divider is reciprocal.

Applying dc magnetic field $\mathbf{H}_0$, one can achieve rotation of the standing pattern around the z axis clockwise by 30°. As a result, the nodes of the pattern are now at ports 3 and 6 as it is shown in Fig. 1(c). Notice that this rotation is because of MO properties of the resonator and it can be provided by adjusting the resonator parameters and dc magnetic field. Therefore, due to the nodes, the waveguides in ports 3 and 6 will not be excited. Scrutinizing Fig. 1(c), one can also see that the field intensities of the standing wave in ports 2, 4, and 5 are equal. It means that the division of the input power between these ports will be in the desired proportion $(1/3):(1/3):(1/3)$.

For the opposite direction of the dc magnetic field [i.e., for $-\mathbf{H}_0$, Fig. 1(d)], the rotation of the field pattern around the z axis will be in the opposite direction (anticlockwise) by 30°. The isolated ports in this case are 2 and 5 and the division of electromagnetic power will be between ports 3, 4, and 6. In the following, we shall discuss only the case of Fig. 1(c), which is shown in more detail in Fig. 2. In this figure, one can see two ideally matched loads connected to ports 3 and 6. The three arrows inside the resonator show the desired division of the incident wave.

In order to demonstrate isolation properties of the divider, we should consider excitations of output ports 2, 4, and 5, which represent the signals reflected from nonideally matched elements in these ports. In fact, due to six-fold rotational symmetry, we need to investigate the characteristics of the divider for excitation only from one port; for example, from port 1. The excitations from other ports can be obtained from those of port 1 by cyclic permutation of the ports (i.e., port renumbering). We show these cases in Figs. 3(a)–3(c), which are obtained by simple clockwise rotation of the dipole pattern of Fig. 2 by 30°, 180°, and 210°, respectively.
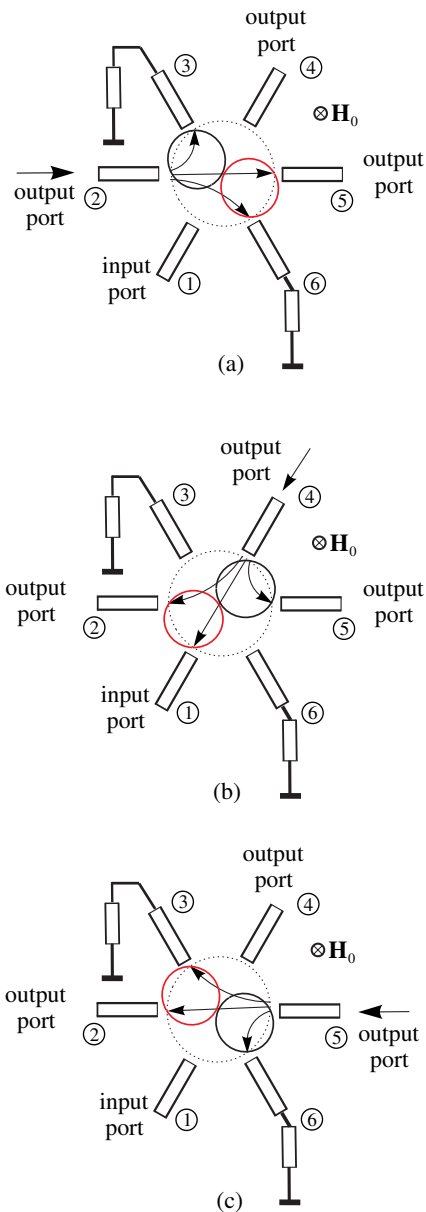
Fig. 3. Divider of Fig. 2. (a) Excitation of port 2, (b) excitation of port 4, and (c) excitation of port 5.

In all three cases of Fig. 3, two ports where the nodes of the standing wave are situated are decoupled from the port of excitation. The power which can come back, for example, to input port 1 from output ports 2, 4, and 5 is very small (only one-third of the power reflected from port 4), i.e., most of the parasitic power reflected from the output ports will be absorbed in the matched loads connected to ports 3 and 6. Thus, we have a significant reduction of influence of possible parasitic reflections from not ideally matched scheme elements, and this is the main idea of our work.

4. Example of Theory Application: 2D Photonic Crystal-Based Divider

Until now, we did not specify frequency range, type of waveguides, and type of resonator. The above scattering matrix analysis is valid both in the microwave and the optical regions. It can be applied to components with different types of resonators and waveguides, for example, with traditional optical dielectric waveguides.

Below, we shall demonstrate one of the possible realizations of the nonreciprocal three-way divider which is based on a uniformly magnetized MO resonator in a 2D PhC. In our example, the PhC is a triangular lattice of air holes of radius $0.3a$ (a is the lattice constant) in a magnetic semiconductor (see Fig. 8). The guided electromagnetic wave in PhC waveguide is TE mode with the components H_z, E_x, and E_y. We have adapted for our purposes the resonator structure suggested in [5]. The frequency responses of the divider were calculated by the software COMSOL [11].

A. Resonator Properties

The MO material is described by the following expressions for the permittivity and the permeability:

$$[\epsilon] = \epsilon_0 \begin{pmatrix} \epsilon_r & -ig & 0 \\ ig & \epsilon_r & 0 \\ 0 & 0 & \epsilon_r \end{pmatrix}; \qquad \mu = \mu_0. \qquad (4)$$

There exist various transparent materials with magnetic properties which can be used in our three-way divider (see, for example, [12–15]). In the literature, one can encounter different values of the parameter g of tensor in Eq. (4) used for analysis of optical nonreciprocal devices. For example, for calculations of a circulator, the authors of [5] used $g = 0.1$. In the analysis of nonreciprocal two-way divider [7], this parameter was $g = 0.3$. For an optical isolator in [2], the value $g = 0.41$ was chosen by the authors. In our theoretical calculations, we used $g = 0.3$. The Voigt parameter in the case of $\epsilon_r = 6.25$ is $g/\epsilon_r = 0.048$.

The applied magnetic field $\mathbf{H}_0$ splits the frequencies ω^+ and ω^- of two degenerate (in nonmagnetic state) dipole modes of the resonator. The calculated frequency splitting for our resonator is shown in Fig. 4. For the unloaded resonator with $g = 0.3$ (see the lower inset in Fig. 5), the two peaks of the transmission coefficient correspond to the rotating modes with the frequencies ω^+ and ω^- (compare Figs. 4 and 5). Six waveguides connected to the resonator (shown in the upper inset of Fig. 5) change significantly the frequencies of these two modes and the quality factor of the resonator. The correspondence of the modes in the unloaded and loaded resonators is shown in Fig. 5 by the dotted arrows.

The frequency band of the divider is proportional to the splitting of ω^+ and ω^-. Thus, the more the value of the parameter g the higher frequency band of the divider can be obtained. The parameter g in its turn is proportional to magnetization $\mathbf{M}$ of the magnetic material.
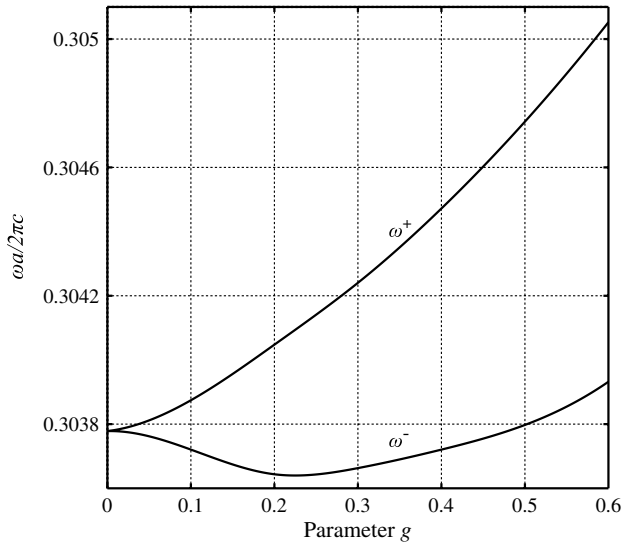
Fig. 4. Frequency splitting between right- and left-rotating modes of resonator versus tensor parameter g.

B. Divider Characteristics

The geometry of the divider in our calculation scheme is shown in Fig. 8. The entire PhC is made of MO material. In order to exclude the losses in the waveguides connected to the resonator [which are at the level of $(-2.6 \div -3)$ dB, see Fig. 6] and to consider only the losses of the resonator, we first calculated the losses of the magnetized waveguide connecting port 2 and port 5 on straight line (this waveguide is shown schematically in the inset of Fig. 6). We can evaluate the losses of the waveguides as follows. The length of the resonator in Fig. 8 is approximately 1/3 of the total length of the switch. Therefore, in the following, we subtract from the calculated losses of the switch 2/3 of the losses of Fig. 6.

Fig. 6. Losses in rectilinear PhC waveguide in magnetized state.

We excited the divider at input port 1 and calculated the transmission powers at the others ports. In Fig. 7, the frequency responses for the transmitted waves in ports 2, 3, 4, 5, and 6 are shown. One can see that the division of input power between ports 2, 4, and 5 at the central frequency $\omega a/2\pi c = 0.3035$ is around -6.4 dB, and ports 3 and 6, where the ideally matched loads are connected, are isolated from the
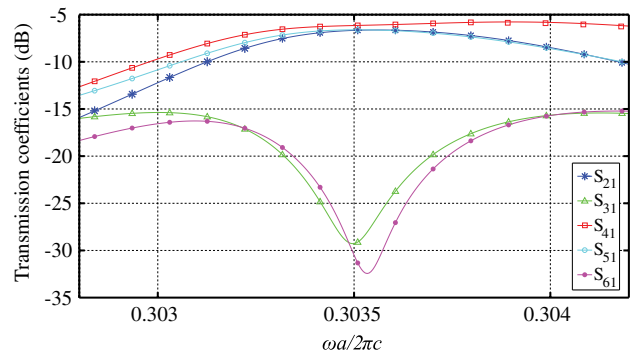
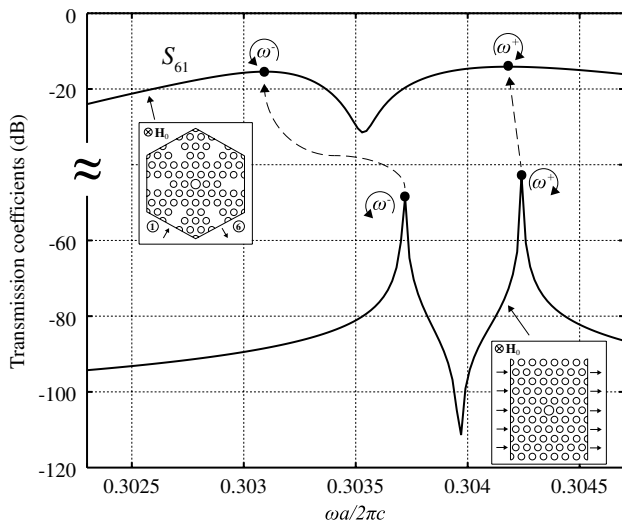Fig. 7. Frequency responses of divider for excitation at port 1.

Fig. 5. Comparison of frequency characteristics of resonance modes ω^+ and ω^- for loaded (upper inset) and unloaded (lower inset) resonators in magnetized PhC with $g = 0.3$.
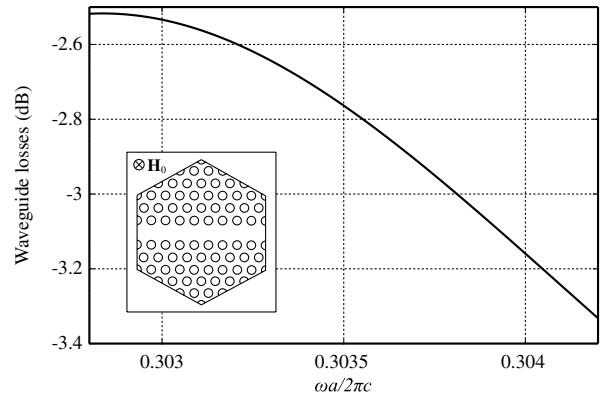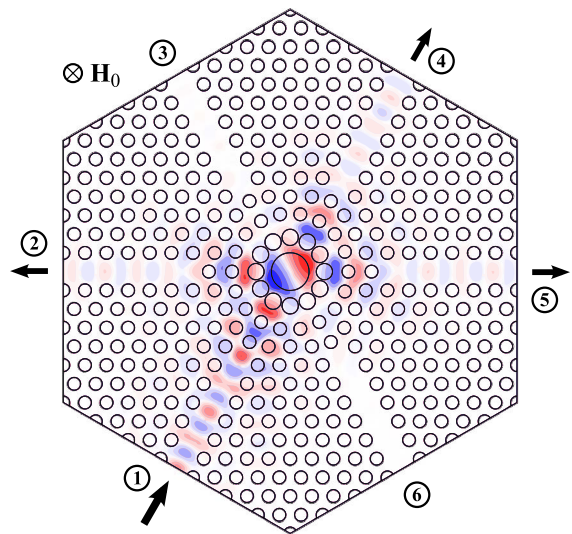

Fig. 8. H_z component of electromagnetic field in divider for excitation at port 1 at central frequency $\omega a/2\pi c = 0.3035$.

input port by approximately −29 dB. This means that there are practically no power losses of the incident wave in these ports. Also, scrutinizing Fig. 7, one can see that the isolation of port 1 from ports 2 and 5 is about −29 dB, but isolation of port 1 from port 4 is −6 dB as it was predicted by the theory in Section 3. At 1.55 μm, the frequency band of the divider defined at the level −20 dB is 219 GHz. In this band, the variation of the division between the output ports is (-6.4 ± 0.4) dB.

In Fig. 8, we show distribution of H_z electromagnetic wave component in the divider at the central frequency $\omega a / 2\pi c = 0.3035$ of its band. One can see that the field distribution corresponds to the predicted one in Fig. 1(c) with the nodes in ports 3 and 6.

Robustness to geometrical tolerances, material parameter deviation, and fabrication imperfections of our device are similar to that for the 2D PhC circulators. This issue is discussed in detail in [1].

5. Conclusion

We have suggested and investigated in this paper a new optical power divider which possesses also a special property of isolation of input port from three output ones. By matrix analysis, we have shown theoretically a feasibility of these components using a MO resonator with dipole mode. This prediction was confirmed by numerical simulations of the divider based on PhC with a uniformly magnetized MO resonator. An advantage of the suggested device is small dimensions which are defined by dimensions of the resonator. The area occupied by the resonator is typically bounded by the dimensions $10a \times 10a$, where a is the lattice constant.

Another possible application of our divider is switching the division in one case between ports 2, 4, 5, and in the other case between the ports 3, 4, 6 [compare Figs. 1(c) and 1(d)] which can be achieved by changing dc magnetic field from the value $\mathbf{H}_0$ to the value $-\mathbf{H}_0$.

References

1. Z. Wang and S. Fan, "Suppressing the effect of disorders using time-reversal symmetry breaking in magneto-optical photonic crystals: an illustration with a four-port circulator," Photon. Nanostr. Fundam. Appl. **4**, 132–140 (2006).
2. H. Takeda and S. John, "Compact optical one-way waveguide isolators for photonic-band-gap microchips," Phys. Rev. A **78**, 023804 (2008).
3. V. Dmitriev, M. Kawakatsu, and F. J. M. de Souza, "Compact three-port optical 2D photonic crystal-based circulator of W-format," Opt. Lett. **37**, 3192–3194 (2012).
4. Z. Wang and S. Fan, "Optical circulators in two-dimensional magneto-optical photonic crystal," Opt. Lett. **30**, 1989–1991 (2005).
5. W. Smigaj, J. Romero-Vivas, B. Gralak, L. Magdenko, B. Dagens, and M. Vanwolleghem, "Magneto–optical circulator designed for operation in a uniform external magnetic field," Opt. Lett. **35**, 568–570 (2010).
6. S. Boscolo, M. Midrio, and T. F. Kraus, "Y junctions in photonic crystals channel waveguides: high transmission and impedance matching," Opt. Lett. **27**, 1001–1003 (2002).
7. V. Dmitriev and M. Kawakatsu, "Nonreciprocal optical divider based on 2D photonic crystal and magneto-optical cavity," Appl. Opt. **51**, 5917–5920 (2012).
8. A. Esmaieli and R. Ghayour, "Magneto-optical photonic crystal 1×3 switchable power divider," Photon. Nanostr. Fundam. Appl. **10**, 131–139 (2012).
9. A. A. Barybin and V. A. Dmitriev, *Modern Electrodynamics and Coupled-Mode Theory: Application to Guided-Wave Optics* (Rinton, 2002).
10. J. L. Altman, *Microwave Circuits* (van Nostrand, 1964).
11. www.comsol.com.
12. M. C. Sekhar, M. R. Singh, S. Basu, and S. Pinnepalli, "Giant Faraday rotation in $Bi_xCe_{3-x}Fe_5O_{12}$ epitaxial garnet films," Opt. Express **20**, 9624–9639 (2012).
13. E. L. Nagaev, "Ferromagnetic and antiferromagnetic semiconductors," Sov. Phys. Usp. **18**, 863–892 (1975).
14. S. Methfessel and D. C. Mattis, "Magnetic semiconductors," in *Handbuch der Physik*, S. Fliigge and H. P. J. Wijn, eds. (Springer-Verlag, 1968).
15. A. K. Zvezdin and V. A. Kotov, *Modern Magneto-Optics and Magneto-Optical Materials* (IOP, 1997).

ARTIGO 6

Multifunctional two-dimensional photonic crystal optical component based on magneto-optical resonator: nonreciprocal two-way divider-switch, nonreciprocal 120° bending-switch, and three-way divider

Multifunctional two-dimensional photonic crystal optical component based on magneto-optical resonator: nonreciprocal two-way divider-switch, nonreciprocal 120 deg bending-switch, and three-way divider

Victor Dmitriev
Gianni Portela

Multifunctional two-dimensional photonic crystal optical component based on magneto-optical resonator: nonreciprocal two-way divider-switch, nonreciprocal 120 deg bending-switch, and three-way divider

Victor Dmitriev and Gianni Portela*
Federal University of Para, Faculty of Electrical Engineering, Department of Electrical Engineering, Av. Augusto Correa, 01, Belem, Para 66075-900, Brazil

Abstract. We suggest and analyze a compact nonreciprocal optical four-port based on a magneto-optical resonator in two-dimensional photonic crystal, which can fulfill many functions. This component can be used in three regimes: first, with magnetization by a direct current (DC) magnetic field $+\mathbf{H}_0$, second, with magnetization by the DC magnetic field $-\mathbf{H}_0$, and finally, with magnetization by the DC magnetic field $+\mathbf{H}_1$. In the first regime, the four-port ensures equal division of the input signal between two output ones simultaneously providing protection of the generator in the input port from harmful reflected signals in the output ports; this can also be used as a switch by reversing $+\mathbf{H}_0$ to $-\mathbf{H}_0$. In the second regime, the same four-port fulfills 120-deg bending and it provides protection of the generator in the input port from reflected signals; it can also be used as a switch by reversing $-\mathbf{H}_0$ to $+\mathbf{H}_0$. In the third regime, with DC magnetic field $+\mathbf{H}_1$, the device can be used as a three-way divider with equal division to the output ports. We analyze the scattering matrix of this component and discuss the physical mechanisms of its functioning. In addition, computational simulations were performed and their results confirm our theoretical predictions. © 2014 Society of Photo-Optical Instrumentation Engineers (SPIE) [DOI: 10.1117/1.OE.53.11.115102]

Keywords: photonic crystals; dividers; switches; circulators; isolators; multifunctional devices.

Paper 141110 received Jul. 11, 2014; revised manuscript received Oct. 7, 2014; accepted for publication Oct. 9, 2014; published online Nov. 11, 2014.

1 Introduction

In future nanoscale optoelectronic devices, photonic crystals (PhCs) are one of the promising technologies.[1] During the last two decades, many active and passive components of this technology have been developed. Among the passive components are switches,[2] dividers,[3,4] bending elements,[5] and also different nonreciprocal devices, such as isolators[6] and circulators.[7–9]

In general, nonreciprocal devices can be used for protecting active elements (lasers and diodes) from the harmful effects of reflected waves caused by nonideally matched elements of the optical circuit. Isolators and circulators eliminate these waves, providing stable functioning of the active elements. The mechanism of isolation of the input port from the output one in these devices is different. The reflected waves in circulators are directed to an additional port and absorbed in a special matched load outside of the component. In isolators, there is no additional port and the absorption is realized inside the component.

In this paper, we shall consider a multifunctional element which can fulfill different functions such as switching of the signal, division of the signal, bending of the waveguides, and isolation. The isolation properties are of the circulator type, i.e., parasitic waves are absorbed in a specially projected absorber placed in one or two of the waveguides of the multiport.

The multifunctional element discussed below is a four-port that can be viewed as a modification of the traditional Y-circulator[8,9] [see Fig. 1(a)]. If one connects port 2 in the point rotated by a 180-deg rotation, then one comes to W-circulator[7] [see Fig. 1(b)]. Connecting the fourth port in the position symmetrically to the output port, we obtain a nonreciprocal divider[3] [see Fig. 1(c)].

In this paper, we present the matrix analysis of the four-port and discuss the physical mechanisms of its functioning based on a dipole mode resonator with a magneto-optical (MO) material. We show that, depending on the sign and the value of external direct current (DC) magnetic field, this component can fulfill many functions. Some numerical results for this component realized in two-dimensional (2-D) PhC with MO resonator will be given as well.

2 Nonreciprocal Divider

In our previous paper,[3] we suggested a 2-D PhC two-way nonreciprocal divider based on an MO resonator. For convenience, in this section, we shall briefly describe the main results of the paper, which will serve as a starting point for the following discussion.

The PhC is formed by the lattice with triangular cells. Four waveguides are connected to the resonator in a special way. These four-ports can be implemented in two different geometries. They are shown schematically in Figs. 2 and 3. In this paper, we restrict our theoretical analysis and

*Address all correspondence to: Gianni Portela, E-mail: gianni_portela@hotmail.com
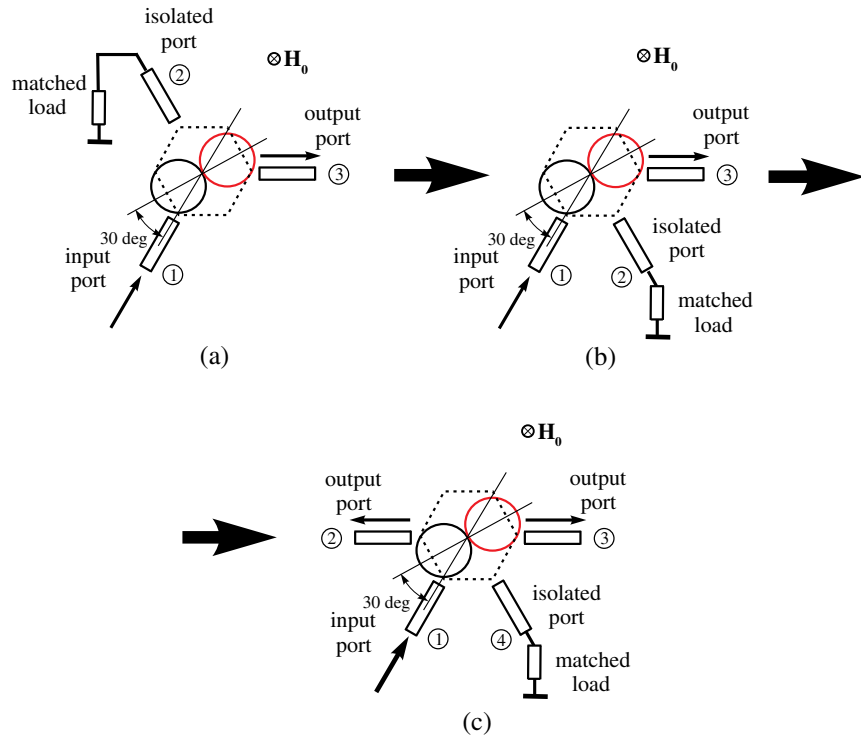
Fig. 1 Evolution of (a) Y-circulator into (b) W-circulator and into (c) two-way nonreciprocal divider.

numerical simulations to the case of Fig. 2 with excitation at port 1.

Without magnetization, the four-ports are reciprocal and they possess a plane of symmetry σ. They can be used as three-way dividers [Figs. 2(b) and 3(b)]. With magnetization [Figs. 2(c), 2(d), 3(c), and 3(d)], both of them possess one

element of physical symmetry, namely a plane of geometrical symmetry σ combined with the time reversal operator T. We call this combined element Tσ the antiplane of symmetry.[10]

The exact structure of the scattering matrix [S] of the divider obtained in Ref. 3 by using the theory of magnetic group of symmetry is

Fig. 2 Four-port with dipole mode resonator, case 1: (a) port nomenclature and orientation of ports with respect to plane of symmetry σ, (b) dipole mode without magnetization, (c) dipole mode rotated by direct current (DC) magnetic field +H_0 by 30 deg clockwise, and (d) dipole mode rotated by DC magnetic field −H_0 by 30 deg counterclockwise.
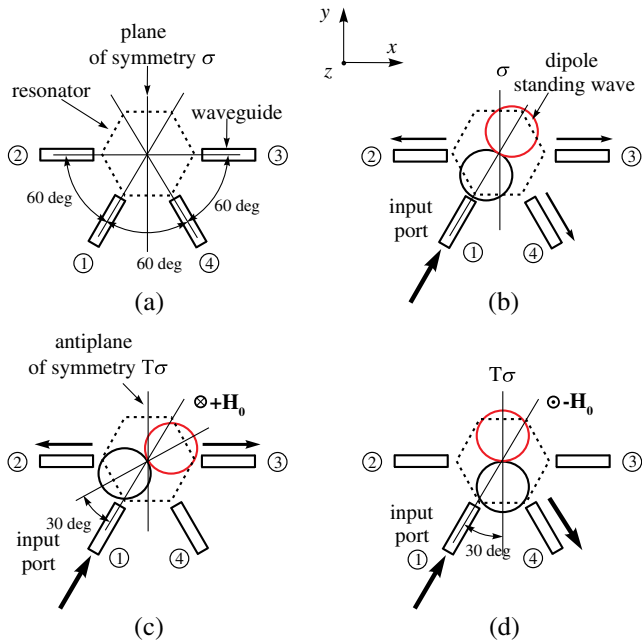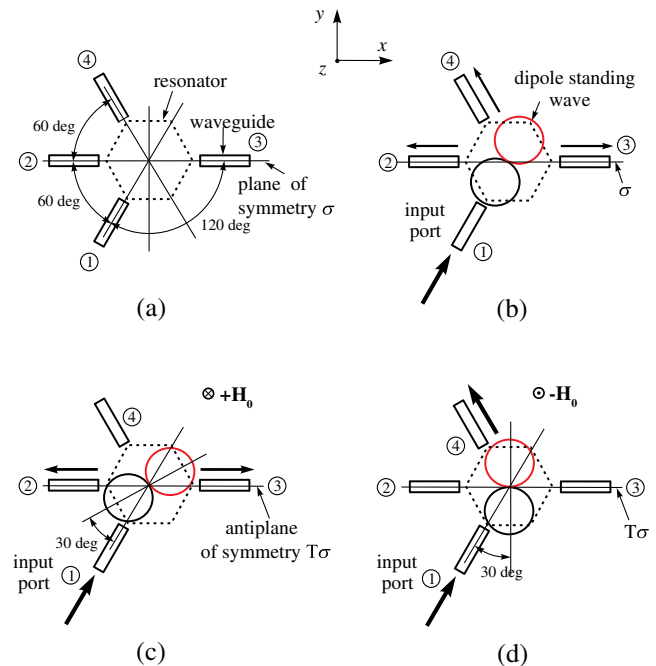

Fig. 3 Four-port with dipole mode resonator, case 2: (a) port nomenclature and orientation of ports with respect to plane of symmetry σ, (b) dipole mode without magnetization, (c) dipole mode rotated by DC magnetic field +H_0 by 30 deg clockwise, and (d) dipole mode rotated by DC magnetic field −H_0 by 30 deg counterclockwise.

$$[S] = \begin{pmatrix} S_{11} & S_{12} & S_{13} & S_{14} \\ S_{21} & S_{22} & S_{23} & S_{13} \\ S_{31} & S_{32} & S_{22} & S_{12} \\ S_{41} & S_{31} & S_{21} & S_{11} \end{pmatrix}. \tag{1}$$

The ideal matrix $[S]_{\text{ideal}}$ of the divider[3] is as follows:

$$[S]_{\text{ideal}} = \begin{pmatrix} 0 & 0 & 0 & e^{j\phi_{14}} \\ \frac{1}{\sqrt{2}}e^{j\phi_{21}} & 0 & \frac{1}{\sqrt{2}}e^{j\phi_{23}} & 0 \\ \frac{1}{\sqrt{2}}e^{j\phi_{31}} & \frac{1}{\sqrt{2}}e^{j\phi_{32}} & 0 & 0 \\ 0 & \frac{1}{\sqrt{2}}e^{j\phi_{31}} & \frac{1}{\sqrt{2}}e^{j\phi_{21}} & 0 \end{pmatrix}. \tag{2}$$

We have shown in Ref. 3 that the suggested structures can fulfill two functions: (1) equal division of the input signal between two output waveguides; and (2) isolation of the input waveguide from the output ones. Below, we shall present a further analysis of the scattering matrix discussed in Ref. 3 and demonstrate new functional possibilities of this component using some mathematical and physical arguments and also numerical simulations.

3 Scattering Matrix Analysis

In this section, we shall rectify the matrix description of the nonreciprocal divider presented in Ref. 3 including analysis of phases of matrix elements.

Supposing small losses in the four-port, we apply the unitary constraint on the matrix of Eq. (2). The matrix $[S]_{\text{ideal}}$ partially satisfies the requirement of being unitary (which is $[S]([S]^*)^t = ([S]^*)^t[S] = [I]$,[11] where $[I]$ is the 4×4 unit matrix), since the sum of the squares of the moduli of the elements in every column and in every line of it is equal to 1. However, this matrix does not satisfy the unitary conditions for phases ϕ_{ij} of the matrix elements. For example, one of the equations obtained from the second and the third lines of matrix presented in Eq. (2) is $(1/2) \exp[j(\phi_{21} - \phi_{31})] = 0$, which has no solution.

In order to come to a realistic case, we go back to exact matrix [Eq. (1)] and relax some restrictions on matrix $[S]_{\text{ideal}}$, putting nonideal matching in ports 2 and 3 (the elements S_{22} and S_{33}) and introducing nonzero elements S_{23} and S_{32}

$$[S] = \begin{pmatrix} 0 & 0 & 0 & e^{j\phi_{14}} \\ \frac{1}{\sqrt{2}}e^{j\phi_{21}} & |S_{22}|e^{j\phi_{22}} & |S_{23}|e^{j\phi_{23}} & 0 \\ \frac{1}{\sqrt{2}}e^{j\phi_{31}} & |S_{32}|e^{j\phi_{32}} & |S_{22}|e^{j\phi_{22}} & 0 \\ 0 & \frac{1}{\sqrt{2}}e^{j\phi_{31}} & \frac{1}{\sqrt{2}}e^{j\phi_{21}} & 0 \end{pmatrix}. \tag{3}$$

From the unitary constraints for the moduli of the elements, one can obtain $|S_{22}| = |S_{32}| = |S_{23}| = 1/2$ and this gives a certain symmetry which is related to the used dipole mode of the resonator. Thus, one can write the scattering matrix as follows:

$$[S] = \begin{pmatrix} 0 & 0 & 0 & e^{j\phi_{14}} \\ \frac{1}{\sqrt{2}}e^{j\phi_{21}} & \frac{1}{2}e^{j\phi_{22}} & \frac{1}{2}e^{j\phi_{23}} & 0 \\ \frac{1}{\sqrt{2}}e^{j\phi_{31}} & \frac{1}{2}e^{j\phi_{32}} & \frac{1}{2}e^{j\phi_{22}} & 0 \\ 0 & \frac{1}{\sqrt{2}}e^{j\phi_{31}} & \frac{1}{\sqrt{2}}e^{j\phi_{21}} & 0 \end{pmatrix}. \tag{4}$$

This matrix is described by six real parameters, namely by the phases ϕ_{14}, ϕ_{21}, ϕ_{22}, ϕ_{23}, ϕ_{31} and ϕ_{32}. Notice that the phases ϕ_{ij} depend on the geometry of the resonator, on the parameters of the waveguides, and on coupling between the resonator and the waveguides.

Now we shall verify whether it is possible to satisfy the unitary constraints on the phases of the elements of the scattering matrix presented in Eq. (4). By using the unitary condition $[S]([S]^*)^t = ([S]^*)^t[S] = [I]$ for Eq. (4), one can see that there is no restriction on the parameter ϕ_{14}. We also obtain three complex equations for the other phases

$$2e^{j(\phi_{21}-\phi_{31})} + e^{j(\phi_{22}-\phi_{32})} + e^{j(\phi_{23}-\phi_{22})} = 0, \tag{5}$$

$$e^{j(\phi_{22}-\phi_{31})} + e^{j(\phi_{23}-\phi_{21})} = 0, \tag{6}$$

$$e^{j(\phi_{32}-\phi_{31})} + e^{j(\phi_{22}-\phi_{21})} = 0. \tag{7}$$

From Eqs. (5) and (6) one can obtain, respectively,

$$\phi_{23} - \phi_{22} = \phi_{21} - \phi_{31} + \pi(2n+1), \tag{8}$$

and

$$\phi_{22} - \phi_{32} = \phi_{21} - \phi_{31} + \pi(2m+1), \tag{9}$$

where $n = 0, \pm 1, \pm 2, \ldots$ and $m = 0, \pm 1, \pm 2, \ldots$.

Substituting the last two equations in Eq. (5), we come to the identity. Due to the freedom of choosing the positions of reference planes, one of the phases, for example ϕ_{22}, can be chosen as equal to 0. Thus, the unitary constraints are reduced to Eqs. (6) and (7) with four independent real parameters. The system formed by Eqs. (6) and (7) has many solutions. One of the possible solutions of this system corresponding to our geometry [Figs. 2(c) and 3(c)] and the chosen dipole mode of the resonator is given by

$$\phi_{23} = \phi_{32} = \pi, \qquad \phi_{31} = \phi_{21} + \pi. \tag{10}$$

These relations between the phases can be seen clearly in Figs. 2(c) and 3(c), where the phase shift between the waves in output ports 2 and 3 is π. In addition, the signal in output port 3 is out of phase with respect to the input signal in port 1, but the signal in output port 2 is in phase with respect to the input signal as it is predicted by Eq. (10). Below, we shall demonstrate these relations also by numerical simulations [see, e.g., Fig. 10(b)].

4 Regime 1, Nonreciprocal Divider-Switch: Mechanisms of Isolation and Switching

This regime is presented in Fig. 4. The on state is shown in Figs. 4(a)–4(c), while the off state is shown in Fig. 4(d). In the following, both states will be described.

4.1 On State

With the DC magnetic field $+\mathbf{H}_0$ [Fig. 4(a)], the input signal is divided between the output ports 2 and 3 and the reflected waves do not enter in port 1 [Figs. 4(b) and 4(c)]. This can be shown by using Eq. (4) and calculating $\mathbf{V}_{\text{out}} = [S]\mathbf{V}_{\text{in}}$, where $\mathbf{V}_{\text{in}}$ and $\mathbf{V}_{\text{out}}$ are incident and reflected waves, respectively. With $\mathbf{V}_{\text{in}} = (1,0,0,0)$, one comes to $\mathbf{V}_{\text{out}} = (0, 1/\sqrt{2}e^{j\phi_{21}},$
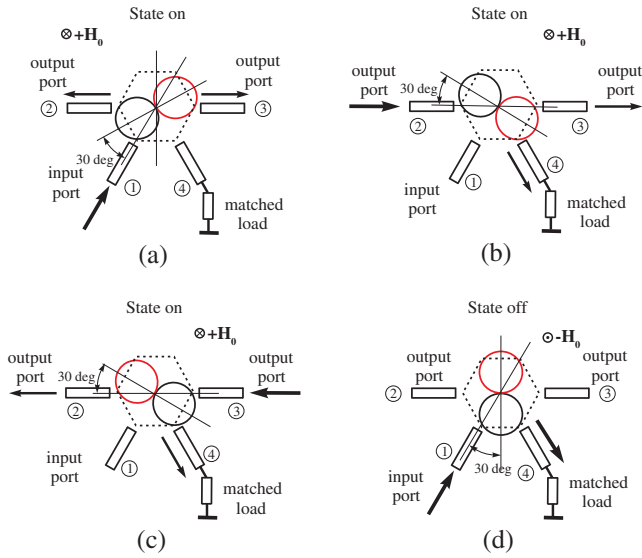
Fig. 4 Four-port with dipole mode resonator in the first regime: (a) dipole mode rotated by DC magnetic field $+\mathbf{H}_0$ by 30 deg clockwise, state on. (b and c) The reflected waves from unmatched elements connected to ports 2 and 3 are absorbed in a matched load connected to port 4. (d) Dipole mode rotated by DC magnetic field $-\mathbf{H}_0$ by 30 deg counterclockwise, state off.

$1/\sqrt{2}e^{j\phi_{31}}, 0)$. From the point of view of switching, this is the on state.

4.2 Off State

The off state, corresponding to the absence of the signal in the output ports 2 and 3, can be achieved by changing the external DC magnetic field from $+\mathbf{H}_0$ to $-\mathbf{H}_0$, i.e., by reversing the magnetization of the MO material [Fig. 4(d)]. Mathematically, the switching is described as follows. It

is well known that in multiports with magnetic media, change in the sign of the external magnetic field leads to transposition of the scattering matrix of this multiport,[10] i.e., $[S] \rightarrow [S]^t$. But for the transposed matrix, the signal in port 1 goes to port 4, where the matched load is connected. This can be seen from $\mathbf{V}_{\text{out}} = [S]^t\mathbf{V}_{\text{in}}$. With $\mathbf{V}_{\text{in}} = (1,0,0,0)$, one comes in this case to $\mathbf{V}_{\text{out}} = (0,0,0, e^{j\phi_{14}})$. Thus, the input signal does not enter in ports 2 and 3.

From the point of view of physical processes, the switching can be explained in the following way. The state on with the DC magnetic field $+\mathbf{H}_0$ is shown schematically in Fig. 4(a). With respect to the nonmagnetized resonator of Fig. 2(b), the dipole pattern is rotated by 30 deg clockwise. The node of the standing wave is at port 4 (where the matched load is connected), and the input power is divided between output ports 2 and 3. For the reversed DC magnetic field $-\mathbf{H}_0$, the dipole is rotated with respect to the nonmagnetized resonator of Fig. 2(b) by 30 deg counterclockwise such that the nodes of the standing wave are in ports 2 and 3. The input signal goes to port 4 and this corresponds to the state off.

5 Regime 2, Nonreciprocal 120 Deg Bending-Switch: Mechanisms of Isolation and Switching

This regime of the suggested component is demonstrated in Fig. 5. State on is shown in Figs. 5(a) and 5(b) and the state off is shown in Fig. 5(c).

5.1 On State

The on state of this component is defined by the DC magnetic field $-\mathbf{H}_0$ [Fig. 5(a)]. The input signal goes to output port 4, which is bent by 120 deg with respect to input port 1. The parasitic waves originated from a not matched elements in output port 4 go to ports 2 and 3 and are absorbed in two matched loads [see Fig. 5(b)].
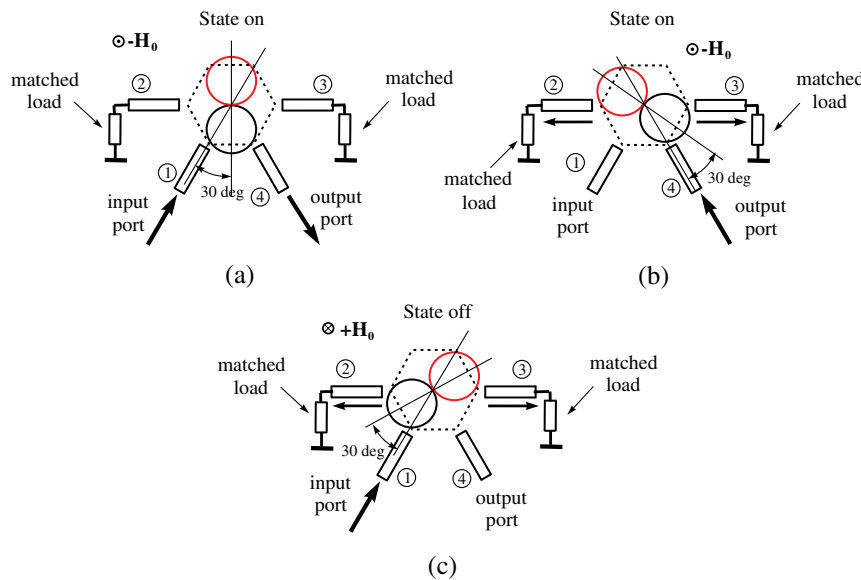
Fig. 5 Four-port with dipole mode resonator in the second regime: (a) dipole mode rotated by DC magnetic field $-\mathbf{H}_0$ by 30 deg counterclockwise, state on. (b) The reflected waves from unmatched elements connected to port 4 are absorbed in ports 2 and 3. (c) Dipole mode rotated by DC magnetic field $+\mathbf{H}_0$ by 30 deg clockwise, state off.

5.2 Off State

In the off state, with the reversed DC magnetic field $+\mathbf{H}_0$ [Fig. 5(c)], the input signal in port 1 goes to ports 2 and 3 and is absorbed in two matched loads. Therefore, output port 4 is not excited. The mathematical formulation and physical interpretation of this regime are analogous to those described in Sec. 4.

6 Regime 3, Three-Way Divider

In this regime, the multifunctional component divides the input power between three output waveguides. In an ideal case, the resonator should be nonmagnetized, as follows from Fig. 2(b). However, our numerical simulations show that the division between three output ports 2, 3, and 4 in this case is not equal. By applying a small DC magnetic field $+\mathbf{H}_1$, the orientation of the dipole mode inside the resonator can be slightly corrected and the division levels between the three output ports can be equalized. In the optimized case, the field intensities of the dipole mode in ports 2, 3, and 4 are almost equal, and each of the three ports receives about one third of the input power. This regime is presented in Fig. 6.

7 Numerical Simulations
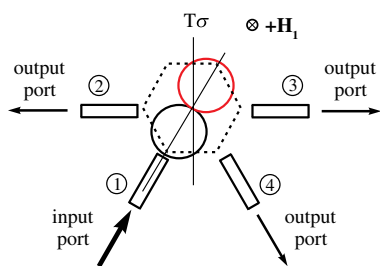
7.1 Resonator and Waveguides

In our numerical simulations, the PhC is a triangular lattice of air holes of radius $0.3a$ (a is the lattice constant) in a magnetic semiconductor. The guided electromagnetic wave in the PhC waveguide is the TE mode with the components H_z, E_x, and E_y. The frequency responses of the multifunctional divider were calculated by using the software COMSOL Multiphysics.[12]
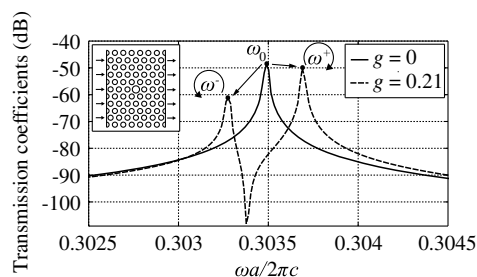
The permittivity tensor of the MO material is

$$[\epsilon] = \epsilon_0 \begin{pmatrix} \epsilon_r & -ig & 0 \\ ig & \epsilon_r & 0 \\ 0 & 0 & \epsilon_r \end{pmatrix}, \qquad (11)$$

and the permeability is $\mu = \mu_0$. The parameters of the tensor $[\epsilon]$ used in the simulations are $\epsilon_r = 6.25$, $g = 0.21$ (regime 1), $g = -0.21$ (regime 2), and $g = 0.07$ (regime 3). Notice that the nondiagonal element g of the tensor is proportional to the applied DC magnetic field.

We have adapted for our purposes the MO resonator proposed in Ref. 8. A more detailed description of the resonator is given in the Appendix. First, we investigated the unloaded resonator, i.e., without waveguides connected to it. Exciting

Fig. 7 Frequency characteristics of resonant dipole modes for unloaded resonator (left inset) in nonmagnetized and magnetized PhCs.

the resonator with waves whose frequency ω_0 is located in a determined range, one can provide a standing dipole mode inside the resonator in the nonmagnetic state as shown in Fig. 7. With the applied DC magnetic field, there is a splitting of the frequency ω_0 of the two degenerate (in nonmagnetic state) modes into two nondegenerate ones ω^+ and ω^-, which are associated with clockwise and counterclockwise rotating dipole modes. The higher the value of the DC magnetic field (of the parameter g), the higher the splitting of ω^+ and ω^-, as can be seen in Fig. 8.

The bandgap of the PhC which lies in the frequency interval $\omega a / 2\pi c = (0.285/0.35)$ is shown in Fig. 9. We also show in this figure the dispersion characteristics for the even mode of the waveguide.

7.2 Regime 1, Divider-Switch

7.2.1 On State

In this regime, $g = 0.21$ and the Voigt parameter is $g/\epsilon_r = 0.034$. The transmission coefficients are shown in Fig. 10(a).

As can be seen, at the central frequency $\omega a / 2\pi c = 0.30318$, the division levels between ports 2 and 3 are about -3.88 dB and port 4, where a matched load is connected, is isolated from the input port (port 1) by
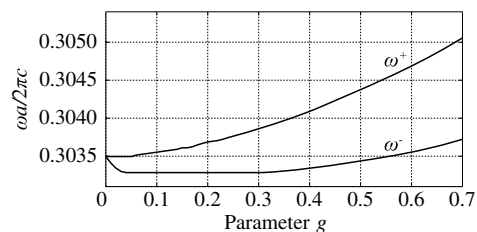
Fig. 8 Frequency splitting between clockwise and counterclockwise dipole modes of resonator versus tensor parameter g.

Fig. 6 Four-port with dipole mode resonator in third regime. Input power is equally divided between three output ports.
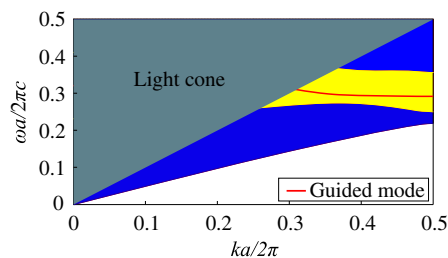
Fig. 9 Band gap and guided modes in PhC waveguide.

(a)

(b)
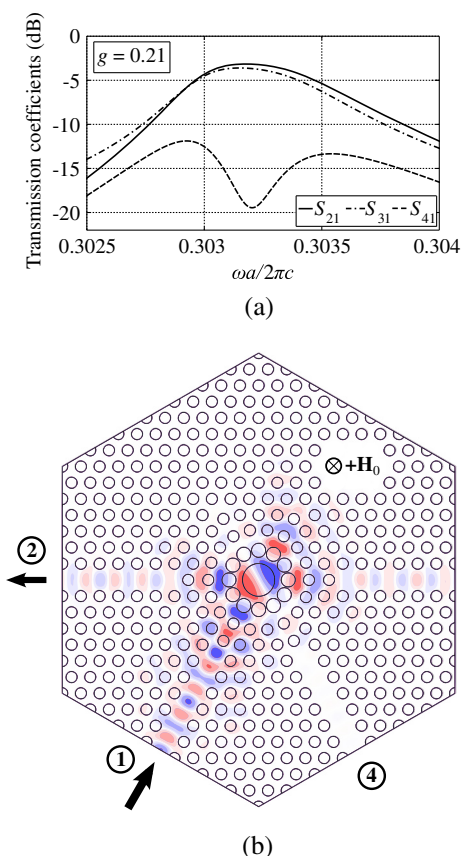
Fig. 10 Multifunctional component operating in regime 1 (on state) for excitation at port 1. (a) Frequency response. (b) H_z distribution at central frequency.

approximately -19 dB. The frequency band, defined at the level -15 dB, is about 178 GHz. In this band, the variation of the division levels in the output ports is (-3.88 ± 0.73) dB. In Fig. 10(b), the AC magnetic field component H_z at the central frequency $\omega a/2\pi c = 0.30318$ is shown. The phase relations between the waves in the output ports and in the input port are in agreement with our theoretical results of Sec. 3 [see Eq. (10)].

In order to confirm that a signal source connected to port 1 is protected from harmful reflections, we have considered excitation of the device through ports 2 and 3. These situations are related to parasitic reflections caused by unmatched elements in the circuits connected in these ports. In Figs. 11(a) and 12(a), the transmission coefficients related to the two situations are shown. In Figs. 11(b) and 12(b), it can be seen that most of these reflections do not return to port 1.

7.2.2 Off State

For the off state, the DC magnetic field is $-\mathbf{H}_0$. For the inverse direction of magnetization, the parameter g changes its sign, i.e., it is equal to -0.21. The calculated frequency responses are shown in Fig. 13(a). As can be seen, at the central frequency $\omega a/2\pi c = 0.30318$, ports 2 and 3 are not excited and most of the input signal is absorbed by an ideally matched load connected on port 4. In Fig. 13(b), one can see the AC magnetic field component H_z for this regime at the central frequency $\omega a/2\pi c = 0.30318$.

(a)

(b)

Fig. 11 Multifunctional component operating in regime 1 (on state), under the influence of parasitic reflections originated in port 2. (a) Frequency response. (b) H_z distribution at central frequency.

(a)

(b)

Fig. 12 Multifunctional component operating in regime 1, on state, under the influence of parasitic reflections originated in port 3. (a) Frequency response. (b) H_z distribution at central frequency.
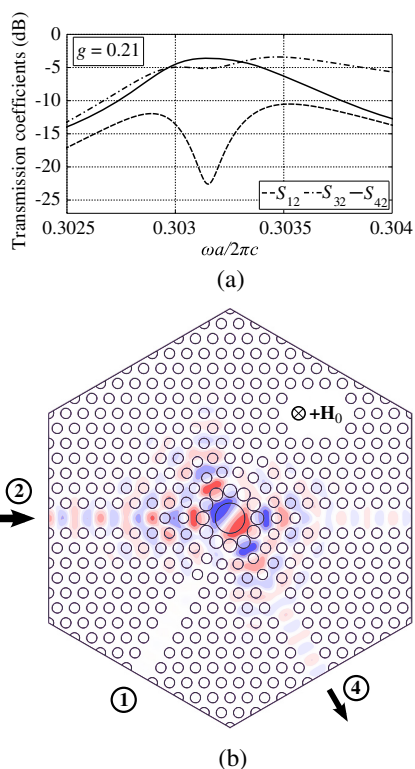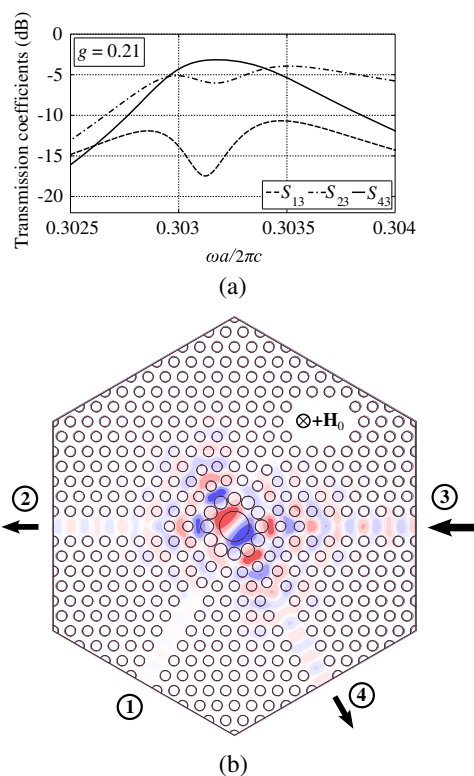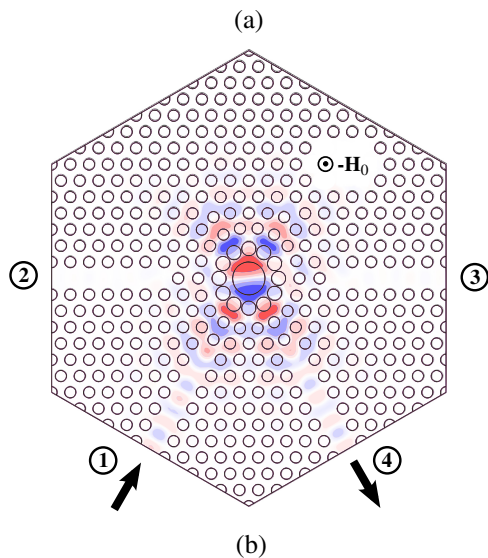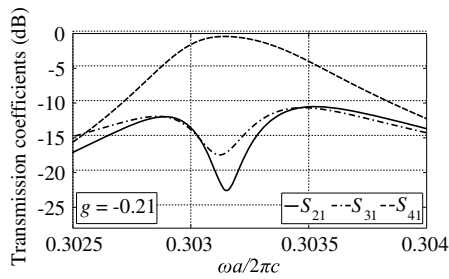
Fig. 13 Multifunctional component operating in regime 1, off state, for excitation at port 1. (a) Frequency response. (b) H_z distribution at central frequency.

Fig. 14 Multifunctional component operating in regime 2, on state, under the influence of parasitic reflections originated in port 4. (a) Frequency response. (b) H_z distribution at central frequency.

7.3 *Regime 2, 120 deg Bending-Switch*

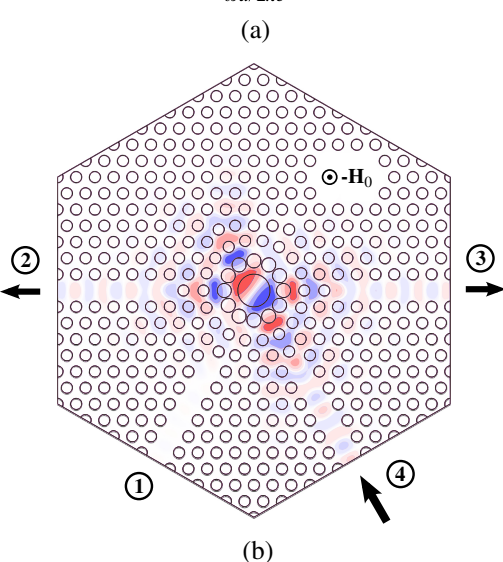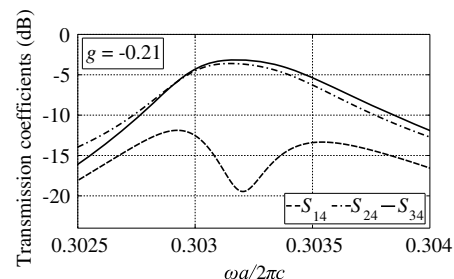#### 7.3.1 *On state*

In this regime, $-\mathbf{H}_0$ is the applied DC magnetic field and the parameter g is -0.21. The input signal is bent by 120 deg and most of the input power is coupled to the output port. The frequency response of the device is shown in Fig. 13(a) and the AC magnetic field component H_z is shown in Fig. 13(b). At the central frequency $\omega a/2\pi c = 0.30318$, the transmission coefficients are $S_{41} = -0.45$ dB, $S_{21} = -21$ dB, and $S_{31} = -17$ dB. The frequency band, defined at the level -15 dB of the isolation curves, is about 113 GHz.

Parasitic reflections from unmatched elements connected in the output port are absorbed by two matched loads connected to ports 2 and 3. Therefore, the signal source connected to port 1 is protected from harmful reflections. By exciting the device through port 4, one can see this property, as shown in Figs. 14(a) and 14(b).

7.3.2 *Off state*

The applied DC magnetic field in this case is $+\mathbf{H}_0$. Consequently, the output port is not excited and the input power is redirected to ports 2 and 3. The frequency response of the device, operating on this regime, is shown in Fig. 10(a), while the AC magnetic field component H_z is shown in Fig. 10(b).

7.4 *Regime 3, Three-Way Divider*

In this regime, the DC magnetic field is $+\mathbf{H}_1$ and the parameter g is 0.07. The parameter g is approximately proportional to the DC magnetic field, therefore, the field $+\mathbf{H}_1$ is approximately three times lower than the field $+\mathbf{H}_0$. The input signal in port 1 is almost equally divided between the three output ports 2, 3, and 4. This can be seen in Fig. 6.

Around the central frequency $\omega a/2\pi c = 0.30309$, the division levels of the input power are around -5.24 dB, while the frequency band defined at the level -6 dB of the three-way division curves is about 110 GHz. In this band, the variation of the division levels between the three output ports is (-5.24 ± 0.76) dB. The frequency response of the device in this regime is shown in Fig. 15(a), and in Fig. 15(b), the AC magnetic field component H_z at the central frequency is shown.

8 Conclusions

The inplane dimensions of our component are defined by the MO resonator and are approximately $10a \times 10a$, where a is the lattice parameter. One such component can substitute for two or three conventional elements (for example, switch, isolator, and divider connected in series), reducing the occupied area at least three times. Taking into account the necessary connecting waveguides between the conventional elements, the benefit of such a substitution can be much higher. Another advantage of the investigated device is a considerable reduction of insertion losses in comparison to the sum of

(a)

(b)
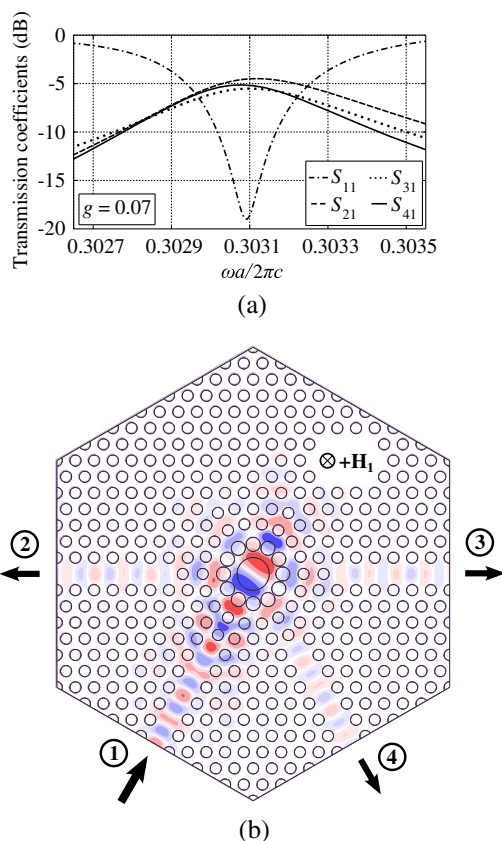
Fig. 15 Multifunctional component operating in regime 3 for excitation at port 1. (a) Frequency response. (b) H_z distribution at central frequency.

the losses of the three conventional elements. These two advantages are very important in highly integrated PhC circuits where there are severe restrictions on the dimensions and on the power dissipation. We believe that the component with the projected characteristics can be realized at telecom frequencies ($\lambda = 1.55$ μm) and at lower ones. For higher

frequencies, technological problems of fabrication and low values of the parameter g can restrict feasibility.

Summarizing, we have demonstrated theoretically and by numerical simulations the feasibility of a component which can fulfill different functions, namely division to two channels, division to three channels, isolation, switching, and waveguide bending.

Appendix: Details of Resonator Design

The details of the geometry of the proposed multifunctional device are shown in Fig. 16.

The white holes are related to the periodic structure of the employed PhC and each of them has a radius equal to $0.3a$, where a is the lattice constant. For $\lambda = 1.55$ μm, $a = 480$ nm.

The central hole (hole No. 0) has an elliptical shape and its major and minor semiaxes are oriented along the y- and x-axes, respectively. Its semimajor axis is equal to $0.8775a$, while its semiminor axis is equal to $0.8625a$. The radii of the 12 holes of the first ring (holes No. 1) are $0.38a$ and they form the ring with radius $R_1 = 1.58a$. The radii of the 18 holes of the second ring (holes No. 2) are $0.3a$, and they form the ring with radius $R_2 = 2.69a$. Last, the radii of the six holes of the third ring (holes No. 3) are $0.3a$ and they form the ring with radius $R_3 = 3.76a$.

We have used in our calculus the values of an abstract MO material. One can encounter different values of the parameter g of the MO tensor used for analysis of optical nonreciprocal devices. For example, for calculations of a circulator, the authors of Ref. 8 used $g = 0.1$. For an optical isolator in Ref. 6, the value $g = 0.41$ was chosen by the authors. In our theoretical calculations, we used $g = 0.21$ and a typical value of $\epsilon_r = 6.25$. The Voigt parameter in this case is $g/\epsilon_r = 0.033$ which is close to that of the existing MO materials, e.g., magnetic semiconductors. Our component can be projected with lower Voigt parameter g/ϵ_r, but this will proportionally reduce the bandwidth of the component. The
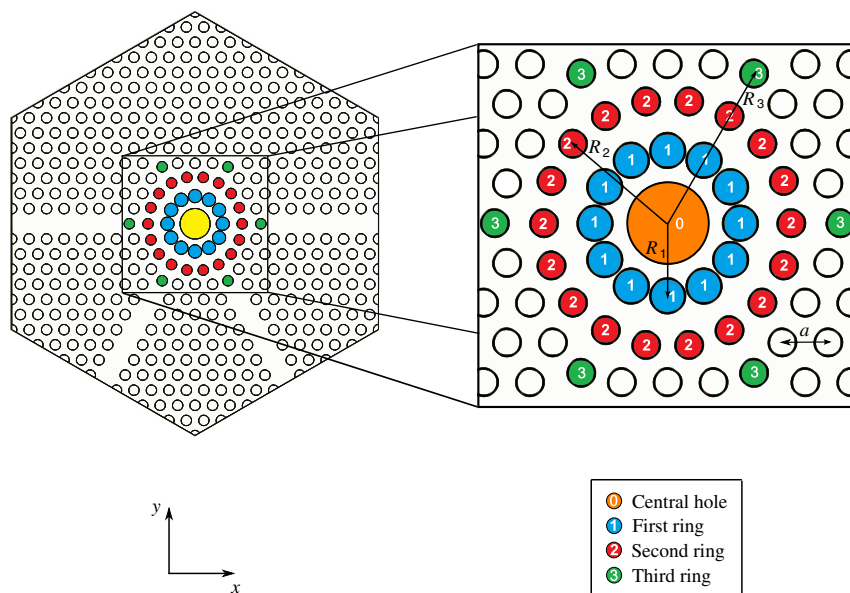
Fig. 16 Schematic of the design.

parameters of real MO material are presented in different literature sources (see, e.g., Refs. 13–16).

Acknowledgments

References

1. J. D. Joannopoulos et al., *Photonic Crystals: Molding the Flow of Light*, 2nd ed., Princeton University Press, New Jersey (2008).
2. V. Dmitriev, M. Kawakatsu, and G. Portela, "Compact optical switch based on 2d photonic crystal and magneto-optical cavity," *Opt. Letters* **38**, 1016–1018 (2013).
3. V. Dmitriev and M. Kawakatsu, "Nonreciprocal optical divider based on 2D photonic crystal and magneto-optical cavity," *Appl. Opt.* **51**, 5917–5920 (2012).
4. V. Dmitriev and G. Portela, "Optical component: nonreciprocal three-way divider based on magneto-optical resonator," *Appl. Opt.* **52**, 6657–6662 (2013).
5. L. Frandsen et al., "Broadband photonic crystal waveguide 60 degrees bend obtained utilizing topology optimization," *Opt. Express* **12**, 5916–5921 (2004).
6. H. Takeda and S. John, "Compact optical one-way waveguide isolators for photonic-band-gap microchips," *Phys. Rev. A* **78**, 023804 (2008).
7. V. Dmitriev, M. Kawakatsu, and F. Souza, "Compact three-port optical 2D photonic crystal-based circulator of W-format," *Opt. Lett.* **37**, 3192–3194 (2012).
8. W. Smigaj et al., "Magneto-optical circulator designed for operation in a uniform external magnetic field," *Opt. Lett.* **35**, 568–570 (2010).
9. Z. Wang and S. Fan, "Optical circulators in two-dimensional magneto-optical photonic crystal," *Opt. Lett.* **30**, 1989–1991 (2005).
10. A. A. Barybin and V. Dmitriev, *Modern Electrodynamics and Coupled-Mode Theory: Application to Guided-Wave Optics*, Rinton Press, Princeton, New Jersey (2002).
11. J. L. Altman, *Microwave Circuits*, Van Nostrand, New York (1964).
12. COMSOL, www.comsol.com.
13. M. C. Sekhar et al., "Giant faraday rotation in $Bi_xCe_{3-x}Fe_5O_{12}$ epitaxial garnet films," *Opt. Express* **20**, 9624–9639 (2012).
14. E. L. Nagaev, "Ferromagnetic and antiferromagnetic semiconductors," *Sov. Phys. Usp.* **18**, 863–892 (1975).
15. S. Methfessel and D. C. Mattis, "Magnetic semiconductors," in *Handbuch der Physik*, Springer Verlag, Berlin (1968).
16. A. K. Zvezdin and V. A. Khotov, *Modern Magneto-Optics and Magneto-Optical Materials*, IOP, Bristol (1997).

Victor Dmitriev received the MEng and PhD degrees in electrical engineering from the Bauman Moscow State University, Moscow, Russia, in 1971 and 1977, respectively. His research interest includes group theoretical methods in electromagnetic theory, propagation of electromagnetic waves in complex media, metamaterials, antennas and nanoantennas, photonic crystals, nanoelectronics, and nanophotonics. He has published more than 200 conference papers, 90 journal papers, two books, and six book chapters.

Gianni Portela is a PhD student at the Federal University of Para. He received his BS degree in mathematics from the Para State University in 2006 and the BS and MS degrees in electrical engineering from the Federal University of Para in 2007 and 2008, respectively. He is an author of four journal papers and five patent grant requests related to passive devices based on photonic crystals. His current research interests include photonic crystals-based devices.

CONSIDERAÇÕES FINAIS

Ao longo dos meses de atividades que originaram este trabalho, foram desenvolvidos oito dispositivos passivos inéditos baseados em cristais fotônicos magneto-ópticos bidimensionais. Foram desenvolvidos cinco chaves, um circulador, um divisor de potência e um dispositivo multifuncional, com características de desempenho ótimas e dimensões reduzidas, que os tornam adequados para utilização em sistemas de comunicações ópticas com alta densidade de componentes.

Em sistemas de comunicações ópticas com canais de largura igual a 20 GHz (valor típico), vários canais podem ser transmitidos pelos dispositivos apresentados, pois os mesmos apresentam grande largura de banda de operação. A utilização de dispositivos com grande largura de banda possibilita, entre outros, a redução de perdas e a diminuição de gastos, pois menos dispositivos são necessários para a transmissão de vários canais de comunicações.

Além disso, os dispositivos projetados possuem dimensões reduzidas. A constante de rede do cristal fotônico empregado no projeto dos dispositivos é igual a 480 nm e os mesmos podem ser facilmente incorporados a sistemas totalmente ópticos com alta densidade de integração de componentes. Nestes sistemas não há necessidade de conversão de sinais elétricos em ópticos e vice-versa, portanto, o desempenho deles é muito superior quando comparados a sistemas tradicionalmente empregados, onde tais conversões são necessárias.

Também vale ressaltar que o problema de dobramento de um sinal eletromagnético pode ser superado com a utilização de alguns dos dispositivos projetados. Em fibras ópticas, o ângulo de dobramento não pode ser abrupto, de modo que a mudança de direção precisa ser suave e a curva precisa ser feita ao longo de uma grande área. Caso contrário, as perdas do sinal serão significativas.

Os dispositivos apresentados que possuem a função de dobramento incorporada são uma alternativa para a solução deste problema. Eles permitem a mudança de direção de propagação de um sinal pelos mais variados ângulos e as curvas não necessitam de grandes áreas.

Merece destaque também o fato de que alguns dispositivos apresentados são capazes de realizar, em uma única estrutura de cristal fotônico, mais de uma função. Em sistemas ópticos integrados, a utilização de tais dispositivos permite o projeto de

sistemas com dimensões cada vez mais reduzidas. Além disso, a utilização de dispositivos multifuncionais permite a redução das perdas e o barateamento no projeto destes sistemas.

A combinação entre análises teóricas, baseadas na Teoria de Grupos, e simulações computacionais, baseadas na utilização do método dos elementos finitos implementado no software COMSOL Multiphysics, se mostrou muito eficiente no projeto dos dispositivos passivos baseados em cristais fotônicos apresentados neste trabalho. Esta estratégia provavelmente continuará a ser aplicada quando do projeto de novos dispositivos.

Deste modo, foi possível a publicação dos seis artigos científicos que servem como base para esta tese de doutorado, escrita a partir da agregação dos mesmos. Além disso, sete pedidos de patente de invenção nacionais e cinco pedidos de patente de invenção internacionais foram realizados, bem como quatro trabalhos foram apresentados em eventos científicos.

Também vale ressaltar que, além dos oito dispositivos passivos para utilização em sistemas de comunicações ópticas, mencionados nos seis artigos que fundamentaram esta tese de doutorado, outros dispositivos foram desenvolvidos. Dois novos circuladores e três novas chaves, para utilização em sistemas de comunicações em terahertz, foram projetados. Os resultados das pesquisas que deram origem a estes outros dispositivos ainda serão divulgados em periódicos e eventos científicos da área, bem como serão realizados os pedidos de patente de invenção relacionados aos mesmos.

Com base no exposto, pode-se concluir que os objetivos pretendidos foram alcançados, contribuindo para com o desenvolvimento de novos sistemas ópticos integrados.

Ao longo dos próximos meses, serão realizadas as seguintes atividades relacionadas ao projeto de novos dispositivos passivos baseados em cristais fotônicos:

- Investigação sobre o uso de modos localizados com formato de vórtice em cavidades ressonantes baseadas em cristais fotônicos (em andamento);
- Estudo sobre a aplicação da técnica de conexão de cavidades ressonantes em cascata (em andamento);
- Pesquisas sobre o efeito de estados de superfície em guias de ondas unidirecionais baseados em cristais fotônicos (em andamento);

- Realização de simulações computacionais a partir da utilização de Redes Neurais e de algoritmos de otimização bio-inspirados, como o *Particle Swarm Optimization* (PSO) (em andamento);

- Modelagens tridimensionais dos dispositivos a serem projetados (em andamento);

- Construção de protótipos, com medição de características de desempenho.

PRODUÇÃO CIENTÍFICA E TECNOLÓGICA

A seguir será listada toda a produção científica e tecnológica que está diretamente associada a esta tese de doutorado, ou seja, aos oito dispositivos abordados nos seis artigos científicos apresentados anteriormente:

Artigos publicados em periódicos

- DMITRIEV, Victor; PORTELA, Gianni; MARTINS, Leno. Three-port circulators with low symmetry based on photonic crystals and magneto-optical resonators. *Photonic Network Communications* (versão eletrônica, 12 de Julho de 2015);

- DMITRIEV, Victor; PORTELA, Gianni. Multifunctional 2D photonic crystal optical component based on magneto-optical resonator: nonreciprocal two-way divider-switch, nonreciprocal 120° bending-switch and three-way divider. *Optical Engineering*, v. 53, 115102, 2014;

- DMITRIEV, Victor; PORTELA, Gianni; BATISTA, Raphael. Magneto-optical resonator switches in two-dimensional photonic crystals: geometry, symmetry, scattering matrices, and two examples. *Applied Optics*, v. 53, p. 4460-4467, 2014;

- DMITRIEV, Victor; PORTELA, Gianni; ZIMMER, Daimam. Possible mechanisms of switching in symmetrical two-ports based on 2D photonic crystals with magneto-optical resonators. *Optics Letters*, v. 38, p. 4040-4043, 2013;

- DMITRIEV, Victor; PORTELA, Gianni. Optical component: nonreciprocal three-way divider based on magneto-optical resonator. *Applied Optics*, v. 52, p. 6657-6662, 2013;

- DMITRIEV, Victor; KAWAKATSU, Marcelo; PORTELA, Gianni. Compact optical switch based on 2D photonic crystal and magneto-optical cavity. *Optics Letters*, v. 38, p. 1016-1018, 2013.

Pedidos de patente de invenção nacionais

- DMITRIEV, Victor; PORTELA, Gianni; MARTINS, Leno. Circulador óptico de três portas em formato de garfo baseado em um cristal fotônico bidimensional com rede triangular (patente pendente). 2015, Brasil. Patente: Privilégio de Inovação. Número do registro: BR1020150109610, data de depósito: 13/05/2015, Instituição de registro: INPI - Instituto Nacional da Propriedade Industrial;

- DMITRIEV, Victor; PORTELA, Gianni. Dispositivo óptico multifuncional baseado em um cristal fotônico bidimensional e em um ressoador magneto-óptico (patente pendente). 2014, Brasil. Patente: Privilégio de Inovação. Número do registro: BR1020140250751, data de depósito: 08/10/2014, Instituição de registro: INPI - Instituto Nacional da Propriedade Industrial;

- DMITRIEV, Victor; PORTELA, Gianni; BATISTA, Raphael. Chave óptica compacta baseada em um cristal fotônico bidimensional com dobramento de 60 graus (patente pendente). 2014, Brasil. Patente: Privilégio de Inovação. Número do registro: BR1020140165479, data de depósito: 22/05/2014, Instituição de registro: INPI - Instituto Nacional da Propriedade Industrial;

- DMITRIEV, Victor; PORTELA, Gianni; BATISTA, Raphael. Chave óptica compacta baseada em um cristal fotônico bidimensional com dobramento de 120 graus (patente pendente). 2014, Brasil. Patente: Privilégio de Inovação. Número do registro: BR1020140165495, data de depósito: 22/05/2014, Instituição de registro: INPI - Instituto Nacional da Propriedade Industrial;

- DMITRIEV, Victor; PORTELA, Gianni; ZIMMER, Daimam. Chave óptica compacta baseada em um cristal fotônico bidimensional e em guias de onda lateralmente acoplados a um ressoador magneto-óptico (patente pendente). 2013, Brasil. Patente: Privilégio de Inovação. Número do registro: BR1020130306231, data de depósito: 07/11/2013, Instituição de registro: INPI - Instituto Nacional da Propriedade Industrial;

- DMITRIEV, Victor; PORTELA, Gianni; ZIMMER, Daimam. Chave óptica compacta baseada em um cristal fotônico bidimensional com guias de onda frontalmente acoplados a um ressoador magneto-óptico (patente pendente). 2013, Brasil. Patente: Privilégio de Inovação. Número do registro:

BR1020130306240, data de depósito: 07/11/2013, Instituição de registro: INPI - Instituto Nacional da Propriedade Industrial;

- DMITRIEV, Victor; PORTELA, Gianni. Divisor por três não recíproco baseado em um ressoador magneto-óptico (patente pendente). 2013, Brasil. Patente: Privilégio de Inovação. Número do registro: BR1020130188697, data de depósito: 25/06/2013, Instituição de registro: INPI - Instituto Nacional da Propriedade Industrial.

Pedidos de patente de invenção internacionais

- DMITRIEV, Victor; PORTELA, Gianni; BATISTA, Raphael. Compact optical switch based on a two-dimensional photonic crystal with 60 degree bending. Número do registro: PCT/BR2015/050062, data de depósito: 22/05/2015, PCT (Patent Cooperation Treaty);

- DMITRIEV, Victor; PORTELA, Gianni; BATISTA, Raphael. Compact optical switch based on a two-dimensional photonic crystal with 120 degree bending. Número do registro: PCT/BR2015/050061, data de depósito: 22/05/2015, PCT (Patent Cooperation Treaty);

- DMITRIEV, Victor; PORTELA, Gianni; ZIMMER, Daimam. Compact optical switch based on a two-dimensional photonic crystal and on waveguides side-coupled to a magneto-optical resonator. Número do registro: PCT/BR2014/000407, data de depósito: 13/11/2014, PCT (Patent Cooperation Treaty);

- DMITRIEV, Victor; PORTELA, Gianni; ZIMMER, Daimam. Compact optical switch based on a two-dimensional photonic crystal with waveguides front-coupled to a magneto-optical resonator. Número do registro: PCT/BR2014/000429, data de depósito: 13/11/2014, PCT (Patent Cooperation Treaty);

- DMITRIEV, Victor; PORTELA, Gianni. Nonreciprocal three-way divider based on a magneto-optical resonator. Número do registro: PCT/BR2014/000210, data de depósito: 26/06/2014, PCT (Patent Cooperation Treaty).

Trabalhos apresentados em conferências

- DMITRIEV, Victor; PORTELA, Gianni; BATISTA, Raphael. Magneto-optical resonator switches in 2D photonic crystals: geometry, symmetry, scattering matrices and two examples. In: MOMAG 2014 - 16º SBMO - SIMPÓSIO BRASILEIRO DE MICRO-ONDAS E OPTOELETRÔNICA E 11º CBMAG - CONGRESSO BRASILEIRO DE ELETROMAGNETISMO, 2014, Curitiba;

- DMITRIEV, Victor; PORTELA, Gianni; BATISTA, Raphael. Photonic Crystal Based Magneto-Optical Switches With 60º And 120º Bends. In: WORKINNOVA 2013, 2013, Campinas;

- DMITRIEV, Victor; PORTELA, Gianni. A new optical component: nonreciprocal three-way divider based on magneto-optical resonator. In: 2013 SBMO/IEEE MTT-S INTERNATIONAL MICROWAVE AND OPTOELECTRONICS CONFERENCE (IMOC), 2013, Rio de Janeiro;

- DMITRIEV, Victor; PORTELA, Gianni; ZIMMER, Daimam. Possible mechanisms of switching in two-ports based on 2D photonic crystals with magneto-optical resonators. In: 2013 SBMO/IEEE MTT-S INTERNATIONAL MICROWAVE AND OPTOELECTRONICS CONFERENCE (IMOC), 2013, Rio de Janeiro.

Além destes trabalhos, merecem destaque os trabalhos listados a seguir. Eles ainda não foram publicados ou, apesar de terem relação com a tecnologia de cristais fotônicos e contarem com a participação do autor desta tese de doutorado, não possuem relação direta com os seis artigos científicos que fundamentaram esta tese:

Outros trabalhos

- DMITRIEV, Victor; ZIMMER, Daimam; PORTELA, Gianni. Wideband compact 2D photonic crystal switch based on ferrite resonator in square lattice with 90° bending. Microwave and Optical Technology Letters, 2015 (aceito para publicação);

- DMITRIEV, Victor; PORTELA, Gianni; MARTINS, Leno. Magneto-optical photonic crystal-based circulators with three and four ports. Photonic Network Communications, 2015 (em processo de *peer review*);

- DMITRIEV, Victor; PORTELA, Gianni; MARTINS, Leno. Magneto-optical photonic crystal-based three-port circulators with low symmetry. In: 2015 SBMO/IEEE MTT-S INTERNATIONAL MICROWAVE AND OPTOELECTRONICS CONFERENCE (IMOC), 2015, Porto de Galinhas (aceito para inclusão no programa final);

- DMITRIEV, Victor; ZIMMER, Daimam; PORTELA, Gianni. Photonic crystal magneto-optical switch. In: 2015 SBMO/IEEE MTT-S INTERNATIONAL MICROWAVE AND OPTOELECTRONICS CONFERENCE (IMOC), 2015, Porto de Galinhas (aceito para inclusão no programa final);

- DMITRIEV, Victor; SOUZA, Daniel; PORTELA, Gianni; BATISTA, Raphael. Design and optimization of new sub-THz compact switch based on 2D photonic crystal with quadrupole resonance in ferrite resonator. In: 2015 SBMO/IEEE MTT-S INTERNATIONAL MICROWAVE AND OPTOELECTRONICS CONFERENCE (IMOC), 2015, Porto de Galinhas (aceito para inclusão no programa final);

- DMITRIEV, Victor; PORTELA, Gianni; MARTINS, Leno. Circulador T baseado em um cristal fotônico bidimensional com rede quadrada (patente pendente). 2015, Brasil. Patente: Privilégio de Inovação. Número do registro: BR1020150109644, data de depósito: 13/05/2015, Instituição de registro: INPI - Instituto Nacional da Propriedade Industrial;

- DMITRIEV, Victor; PORTELA, Gianni; MARTINS, Leno. Design and Optimization of T-shaped Circulator Based on Magneto-Optical Resonator in 2D-Photonic Crystals. In: ADVCOMP 2015: THE NINTH INTERNATIONAL CONFERENCE ON ADVANCED ENGINEERING COMPUTING AND APPLICATIONS IN SCIENCES, 2015, Nice;

- DMITRIEV, Victor; PORTELA, Gianni; BATISTA, Raphael. Compact optical switches based on 2D photonic crystals. In: II PHYSICS MEETING IN AMAZONIA, 2014, Belém;

- DMITRIEV, Victor; ZIMMER, Daimam; PORTELA, Gianni. Switch based on a photonic crystal 2-D network square with ferrite resonator and waveguides forming angle of 90º operating in sub-terahertz range. In: II PHYSICS MEETING IN AMAZONIA, 2014, Belém.

REFERÊNCIAS BIBLIOGRÁFICAS

As referências utilizadas durante a escrita desta tese de doutorado são citadas logo abaixo. Por outro lado, as referências utilizadas durante a escrita dos seis artigos científicos em que esta tese se baseia podem ser consultadas a partir da leitura dos mesmos.

[1] INOUE, Kuon; OHTAKA, Kazuo. Photonic Crystals: Physics, Fabrication and Applications. Nova York: Springer Verlag, 2004;

[2] HO, K.; CHAN, C.; SOUKOULIS, C. Existence of a photonic gap in periodic dielectric structures. *Physical Review Letters*, v. 65, p. 3152-3155, 1990;

[3] JOANNOPOULOS, John et al. Photonic Crystals – Molding the Flow of Light. 2 ed. Nova Jersey: Princeton University Press, 2008;

[4] WU, Zhuoyuan et al. Gyrotropic photonic crystal waveguide switches. *Applied Physics Letters*, v. 96, 051125, 2010;

[5] JIN, Xin et al. Highly Compact Circulators in Square-Lattice Photonic Crystal Waveguides. *PLoS ONE*, v. 9(11), e113508, 2014;

[6] ESMAIELI, Ali; GHAYOUR, Rahim. Magneto-optical photonic crystal 1×3 switchable power divider. *Photonics and Nanostructures – Fundamentals and Applications*, v. 10, p. 131–139, 2012;

[7] SMIGAJ, Wojciech et al. Magneto-optical circulator designed for operation in a uniform external magnetic field. *Optics Letters*, v. 35, p. 568-570, 2010;

[8] BARYBIN, Anatoly; DMITRIEV, Victor. Modern electrodynamics and coupled-mode theory: application to guided-wave optics. Nova Jersey: Rinton Press, 2002;

[9] http://www.comsol.com

[10] http://ab-initio.mit.edu/mpb/